Amyloid Amplification Assays for the Sensitive Detection of Protein Aggregates

---

Dissertation

zur

Erlangung der naturwissenschaftlichen Doktorwürde
(Dr. sc. nat.)

vorgelegt der

Mathematisch-naturwissenschaftlichen Fakultät

der

Universität Zürich

von

Manuela Christine Pfammatter

von

Naters VS

Promotionskommission

Prof. Dr. Adriano Aguzzi (Vorsitz und Leitung der Dissertation)

PD Dr. Simone Hornemann (Leitung der Dissertation)

Prof. Dr. Ben Schuler

Prof. Dr. Tuomas Knowles

Zürich, 2018

University of Zurich

University Hospital Zurich

PhD Thesis

Amyloid Amplification Assays for the Sensitive Detection of Protein Aggregates

Manuela Pfammatter

Thesis Committee

Adriano Aguzzi
Institute of Neuropathology, University of Zurich

Simone Hornemann
Institute of Neuropathology, University of Zurich

Ben Schuler
Institute of Biochemistry, University of Zurich

Tuomas Knowles
Department of Chemistry, University of Cambridge

Zurich, 2018

Manuela Pfammatter

Amyloid Amplification Assays for the Sensitive Detection of Protein Aggregates

PhD Thesis, Zurich, 2018

University of Zurich
Institute of Neuropathology
University Hospital Zurich
Schmelzbergstrasse 12
CH-8091 Zurich

Summary

Protein misfolding and aggregation diseases such as Alzheimer's, Parkinson's or prion diseases are devastating neurodegenerative disorders that strongly affect the ageing population. Prolonged life expectancy and the fact that age represents a crucial risk factor for these disorders will exacerbate the problem in the future. As a consequence, there is an urgent need for diagnostic tests that allow early and reliable diagnosis of these diseases. The main pathological hallmark of protein misfolding and aggregation diseases is the accumulation of proteins as amyloid aggregates. Recently developed biochemical assays aim to amplify and detect small amounts of protein aggregates for disease diagnosis. These assays are based on the self-replication properties of amyloid aggregates, which enable the amplification and detection of minute amounts of amyloid aggregates.

My thesis focuses on the development of innovative amyloid amplification assays that enable not only the sensitive detection but also the absolute quantification of amyloid aggregates. I have developed amyloid amplification assays for three different amyloidogenic proteins including insulin, prion protein, and α-synuclein.

In the first part of this thesis, I describe the development of a digital amyloid amplification assay for the sensitive detection and absolute quantification of insulin amyloid aggregates. I used droplet-based microfluidics to encapsulate thousands of individual amplification reactions into small, uniform reaction compartments. Parallel, template-catalysed amplification led to the formation of large aggregates in droplets that initially encapsulated amyloid propagons. The number of propagons in the analyte was calculated from the fraction of aggregate-positive droplets of different dilutions of the analyte. The high number of replicate reactions yielded large, highly accurate data sets for rapid digital analysis using low reagent volumes. The assay proved to be a reliable and precise tool for the detection of single amyloid propagons, and for the absolute quantification of propagon numbers.

The second part of my thesis focuses on the establishment and application of the real-time quaking-induced conversion (RT-QuIC) assay, an amyloid amplification assay for prion protein. RT-QuIC allows the detection of small amounts of the scrapie prion protein through seeded conversion of the cellular prion protein. In the first step,

I implemented and validated the diagnostic RT-QuIC on cerebrospinal fluid samples from patients with suspected Creutzfeldt-Jakob disease. Samples from suspected cases were analysed by RT-QuIC, and the results were confirmed with autopsy results. Furthermore, I adapted the RT-QuIC assay to assess inactivation of prions adsorbed to surgical steel surfaces. Inactivation of prions adsorbed to surgical steel is crucial to reduce the potential risk of iatrogenic transmission of prion infectivity. A new formulation composed of hypochlorite, phosphate, silicate and phosphonate was identified as a potential decontaminant for prions bound to surgical steel. Finally, the assay was used to investigate prion self-replication in cerebellar organotypic cultured slices treated with neurotoxic anti-prion antibodies. The results showed that neurotoxic anti-prion antibodies do not induce self-replication of prions, but rather act downstream of prion self-replication.

In the last part of my thesis, I describe the development of an α-synuclein amyloid amplification assay that can detect minimal amounts of α-synuclein aggregates. The assay has been used to investigate the inactivation of α-synuclein aggregates bound to stainless steel. Treatment with formic acid and sodium hypochlorite achieved efficient inactivation of α-synuclein propagons. Furthermore, the α-synuclein amyloid amplification assay was adapted to detect pathological aggregates in blood samples of affected patients. Different pretreatments were tested to enrich low-abundance aggregates in blood. Immunoprecipitation with specific anti-α-synuclein antibodies was the most efficient treatment. Applying this treatment, I could demonstrate that samples from Parkinson's disease patients showed low-level propagation activity in the amplification assay.

The highly sensitive amyloid amplification assays developed in my thesis enabled the detection of minute amounts of pathological protein aggregates. A digital droplet-based amplification assay further allowed the determination of the absolute number of amyloid propagons in an analyte and the detection of single propagation units. These assays hold great potential for the early diagnosis of protein misfolding and aggregation diseases. In addition, the assays will help us to gain a more profound understanding of the molecular mechanisms underlying neurodegeneration.

Zusammenfassung

Neurodegenerative Erkrankungen wie Alzheimer, Parkinson oder Prionenerkrankungen gehören zu den verheerendsten Krankheiten im Alter. Da die Häufigkeit der Erkrankungen mit steigendem Alter zunimmt, stellen neurodegenerative Krankheiten eine grosse Herausforderung für die alternde Gesellschaft mit stetig steigender Lebenserwartung dar. Entsprechend hoch ist das Bedürfnis nach verlässlichen Methoden zum Nachweis dieser Erkrankungen. Neurodegenerative Erkrankungen sind durch die Ablagerung von fehlgefalteten Proteinen in sogenannten Amyloidaggregaten gekennzeichnet. Kürzlich entwickelte, biochemische Verfahren zur Diagnose von Proteinfehlfaltungserkrankungen zielen darauf ab, kleinste Mengen von Amyloidaggregaten zu vervielfältigen und so deren Detektion zu ermöglichen. Diese Verfahren beruhen auf der Fähigkeit zur Selbstreplikation von Amyloidaggregaten, bei welcher Keime von fehlgefalteten Proteinen die Umwandlung von natürlich gefalteten Proteinen in wachsende Amyloidaggregate verursachen.

In meiner Dissertation habe ich mich mit der Entwicklung von innovativen Tests zur Vervielfältigung von Amyloidaggregaten, die neben dem empfindlichen Nachweis von Aggregaten auch deren Quantifizierung ermöglichen, beschäftigt.

Im ersten Teil beschreibe ich die Entwicklung eines Tests zur Quantifizierung von einzelnen Insulinaggregaten. Tausende mikroskopisch kleine Tröpfchen dienten als Reaktionsbehälter für die Nachweisreaktionen von Amyloidaggregaten. In jedem dieser Tröpfchen fand eine einzelne Vervielfältigungsreaktion statt, so dass zu Reaktionsende all jene Tröpfchen, die zu Beginn ein Aggregat enthielten, grosse, deutlich erkennbare Aggregate umschlossen. Aus dem Anteil der Tröpfchen mit neu gebildeten Aggregaten liess sich mittels digitaler Analyse die Anzahl ursprünglicher Aggregate in der Analytlösung berechnen. Durch die grosse Anzahl paralleler Reaktionen in den Mikrotröpfchen war es möglich, einzelne Amyloidaggregate nachzuweisen und präzise zu zählen.

Im zweiten Teil beschreibe ich verschiedene Anwendungen des 'Real-Time Quaking-Induced Conversion' (RT-QuIC) Verfahrens, einer Nachweismethode für Prionaggregate. Der Nachweis basiert auf der Umwandlung des zellulären Prionproteins in fehlgefaltetes Prionprotein durch die Zugabe von Keimen des fehlgefal-

teten Prionproteins. Zunächst habe ich die Methode zur Diagnose von Gehirn-Rückenmarksflüssigkeit bei Patienten mit Verdacht auf Creutzfeldt-Jakob-Krankheit eingeführt und validiert. Verdachtsfälle wurden mit der RT-QuIC Methode analysiert und die Resultate mittels Autopsiedaten bestätigt. In einem weiteren Schritt habe ich die RT-QuIC Methode verwendet, um die Inaktivierung von Prionen auf Oberflächen aus chirurgischem Stahl zu untersuchen. Die besten Dekontaminierungsergebnisse erzielte eine Formulierung aus Hypochlorit, Phosphat, Silikat und Phosphonat. In einer weiteren Anwendung habe ich mittels RT-QuIC untersucht, ob neurotoxische Anti-Prion-Antikörper zur Neubildung von fehlgefalteten Prionaggregaten führen können. Die Untersuchung von behandelten organotypischen Kleinhirnschnitten zeigte, dass die Antikörper keine Selbstreplikation von Prionen auslösen, sondern vielmehr auf nachfolgende Prozesse wirken.

Im dritten Teil beschreibe ich die Entwicklung eines Tests zur Vervielfältigung minimaler Mengen von α-Synukleinaggregaten. Mithilfe dieses Tests habe ich die Inaktivierung von α-Synukleinaggregaten auf Oberflächen aus chirurgischem Stahl untersucht. Ameisensäure und Natriumhypochlorit waren die wirksamsten der getesteten Dekontaminierungsmittel. Des Weiteren habe ich den Test für den Nachweis von pathologischen α-Synukleinaggregaten in Blutproben angepasst. Dazu habe ich verschiedene Vorbehandlungsmethoden zur Anreicherung der Aggregate getestet. Die Fällung von Aggregaten mittels spezifischer Antikörper erwies sich am erfolgreichsten, so dass in Proben von Parkinson-Patienten geringfügige Aggregat-Vervielfältigung nachgewiesen werden konnten.

Die empfindlichen Nachweisverfahren für Amyloidaggregate, die ich entwickelt habe, ermöglichen den Nachweis von kleinsten Mengen an pathologischen Proteinaggregaten. Basierend auf Tropfen-Mikrofluidik konnte der Nachweis von einzelnen Aggregaten und die Bestimmung der exakten Anzahl von Aggregationseinheiten erzielt werden. Die in dieser Dissertation beschriebenen Verfahren haben daher grosses Potenzial zur diagnostischen Früherkennung von Proteinfehlfaltungserkrankungen. Ausserdem erwarte ich, dass sie zu einem besseren Verständnis der molekularen Mechanismen von neurodegenerativen Erkrankungen beitragen werden.

Abbreviations

aa	amino acid
Ab	antibody
Aβ	amyloid β
AD	Alzheimer's disease
AFM	atomic force microscopy
ASA	amyloid seeding assay
aSyn	α-synuclein
CC	charge cluster
CD	circular dichroism
CJD	Creutzfeldt-Jakob disease
COCS	cerebellar organotypic cultured slices
CSF	cerebrospinal fluid
CSF RT-QuIC	real-time quaking-induced conversion assay with cerebrospinal fluid
d-AQuA	digital amyloid quantification assay
ddH_2O	deionised water
ddPCR	droplet digital polymerase chain reaction
DLB	dementia with Lewy bodies
DLS	dynamic light scattering
DNA	deoxyribonucleic acid
ε_{280}	molar extinction coefficient ($M^{-1}cm^{-1}$)
E. coli	*Escherichia coli*
EDTA	ethylenediaminetetraacetic acid
ESI-MS	electrospray ionisation mass spectrometry
FFI	fatal familial insomnia
FTIR	Fourier transform infra-red
gCJD	genetic Creutzfeldt-Jakob disease
GdmCl	guanidinium chloride
GSS	Gerstmann-Sträussler-Scheinker disease
HaPrP	hamster prion protein
HCl	hydrochloric acid
HD	hydrophobic domain
HCOOH	formic acid
iCJD	iatrogenic Creutzfeldt-Jakob disease
ID	identifier
IEC	ion exchange chromatography
LAG3	lymphocyte-activation gene 3
MSA	multiple system atrophy
MW	molecular weight
m/z	mass-to-charge ratio

NAC	non-amyloid component
NaCl	sodium chloride
NaH_2PO_4	sodium dihydrogen phosphate
NaOAc	sodium acetate
NaOCl	sodium hypochlorite
NaOH	sodium hydroxide
NaPTA	sodium phosphotungstic acid
NBH	non-infectious brain homogenate
NCJDRSU	National CJD Research & Surveillance Unit, Edinburgh, United Kingdom
Ni-NTA	Ni^{2+}-nitrilotriacetic acid
NMR	nuclear magnetic resonance
OR	octapeptide repeat
PBS	phosphate buffered saline
PCR	polymerase chain reaction
PD	Parkinson's disease
PDMS	poly(dimethylsiloxane)
PFF	preformed fibril
pH	-log[H^+], measure of hydrogen ion concentration
PK	proteinase K
PMCA	protein misfolding cyclic amplification
PMSF	phenylmethylsulfonylfluorid
PRNP	gene encoding human prion protein
PrP	prion protein
PrP^{C}	cellular prion protein
PrP^{res}	protease-resistant prion protein
PrP^{Sc}	scrapie prion protein
recPrP	recombinant prion protein (bacterially expressed)
RML	Rocky Mountain Laboratory strain scrapie prions
RT-QuIC	real-time quaking-induced conversion
scFv	single chain variable fragment
sCJD	sporadic Creutzfeldt-Jakob disease
SD	standard deviation
SD_{50}	seeding dose giving 50% positive replicate reactions
SDS	sodium dodecyl sulfate
SDS-PAGE	sodium dodecyl sulfate polyacrylamide gel electrophoresis
SEC	size exclusion chromatography
SNCA	gene encoding human α-synuclein
SOFIA	surround optical fibre immunoassay
TB	Terrific Broth
ThT	thioflavin T
Tris	tris(hydroxymethyl)aminomethane
vCJD	variant Creutzfeldt-Jakob disease
WHO	World Health Organization

Declaration

I declare that all the work included in this PhD thesis entitled **"Amyloid Amplification Assays for the Sensitive Detection of Protein Aggregates"** is original work of the author, unless referenced to other sources.

Some passages are reproduced or quoted verbatim from the following sources:

Absolute Quantification of Amyloid Propagons by Digital Microfluidics
Manuela Pfammatter, Maria Andreasen, Georg Meisl, Christopher G. Taylor, Jozef Adamcik, Sreenath Bolisetty, Antoni Sanchez-Ferrer, David Klenerman, Christopher M. Dobson, Raffaele Mezzenga, Tuomas P. J. Knowles, Adriano Aguzzi, and Simone Hornemann
doi: 10.1021/acs.analchem.7b03279

Neurotoxic Antibodies against the Prion Protein Do Not Trigger Prion Replication
Karl Frontzek, Manuela Pfammatter, Silvia Sorce, Assunta Senatore, Petra Schwarz, Rita Moos, Katrin Frauenknecht, Simone Hornemann, Adriano Aguzzi
doi: 10.1371/journal.pone.0163601

α-Synuclein Amyloid Amplification Assay for the Absolute Quantification of α-Synuclein Propagons
Manuela Pfammatter, Daniel Heinzer, Rita Moos, Lisa Caflisch, Adriano Aguzzi, and Simone Hornemann
manuscript in preparation

Zurich, 2018

Manuela Pfammatter

Contents

1 Introduction

1.1 Amyloid State of Proteins

1.1.1 Amyloid Structure

Protein aggregation is a widespread phenomenon in living organisms with both physiological and deleterious functions. Over the last decades, there has been growing interest in protein aggregation, mainly due to the association of protein aggregation with a range of neurodegenerative disorders. Protein aggregation involves self-association of soluble proteins to form insoluble, highly ordered fibrillar aggregates referred to as 'amyloid' (Chiti and Dobson, 2006; Eisenberg and Jucker, 2012). The term 'amyloid' was introduced in the medical scientific literature by the German pathologist Rudolf Virchow (1821-1902) to describe cerebral corpora amylacea reacting with iodine-sulphuric acid, a stain conventionally used to detect starch in plants. Virchow was convinced to have found structures made of starch, and named them amyloid, referring to starch-like (Virchow, 1854). The name remained, even though soon after its discovery, the main constituent of amyloid was shown to be proteinaceous (Friedreich and Kekule, 1859).

Early structural studies used Congo red staining to identify the well-ordered, repetitive structure of protein fibrils (Bennhold, 1922). Reactivity to the aniline dye Congo red was a traditional criterion for amyloid, which has now been refined by structure-related criteria mainly derived from X-ray crystallography (Eanes and Glenner, 1968; Geddes et al., 1968). Amyloid fibrils are long, unbranched protein filaments (Cohen and Calkins, 1959) with a typical cross-β spine architecture (**Fig. 1.1**). The basic repeating unit of amyloid fibrils are β-strands that are stacked perpendicular to the fibril axis and connected laterally by hydrogen bonds to form β-sheets in parallel to

the axis. The β-sheets are usually aligned 'in register', which means that identical side chains of consecutive peptides are placed on top of each other along the fibril (Nelson et al., 2005). The continuous β-sheets constitute protofilaments, which assemble into mature fibrils (Jiménez et al., 2002).

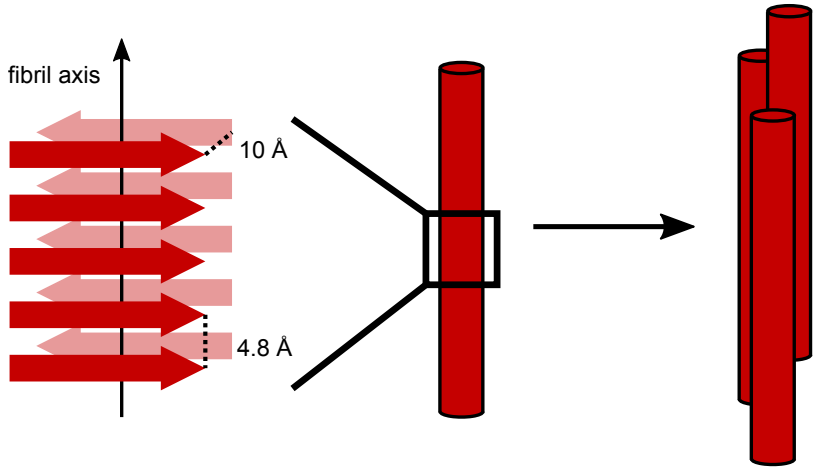

Fig. 1.1.: Architecture of amyloid fibrils (adapted from Serpell, 2014). Mature amyloid fibrils (*right*) are composed of protofilaments (*centre*) intertwining due to hydrophobic interactions. Each protofilament is made up of β-strands stacked perpendicular to the fibril axis forming two β-sheets running parallel to the axis (*left*). Interstrand distances of 4.8 Å and intersheet distances of 10 Å are characteristic for amyloid fibrils (Nelson et al., 2005; Eisenberg and Jucker, 2012).

1.1.2 Models of Protein Misfolding and Amyloid Aggregation

Thermodynamics of Amyloid Formation

One of the unique properties of amyloid fibrils is their remarkably high level of thermodynamic stability. The high stability makes the fibrillation process virtually irreversible in the conditions under which the fibrils form. The main reason for the great stability are strong intermolecular interactions (Nelson et al., 2005; Makin et al., 2005; Knowles et al., 2007). Accordingly, the stability of the amyloid state is dependent on the protein concentration. The stability of the monomeric, native state, however, is independent of the protein concentration. Therefore, above a critical concentration, the amyloid state is thermodynamically favoured over the native state (Gazit, 2002; Knowles et al., 2014). The free energy of the amyloid state is lower than the free energy of the native state (**Fig. 1.2**). The two states are separated by an energy barrier, the activation energy, E_a. If the energy barrier is high enough, the transition into the more stable amyloid state is prevented, and the protein remains kinetically trapped in the native state. If the transition state is easily reached, the native state spontaneously converts to the amyloid state.

Even though the native state is highly stable and thermodynamically favoured over the unfolded state, in contrast to what was postulated by Anfinsen (Anfinsen, 1973), the native state is a local minimum rather than the global minimum in the folding energy landscape for a large number of proteins. The global minimum with the lowest free energy is represented by the amyloid state. The native state is a metastable state with respect to the amyloid state, a local minimum separated from the global minimum by an energy barrier (Gazit, 2002; Baldwin et al., 2011).

Under physiological conditions, the concentration of many amyloidogenic proteins was found to be higher than the critical concentration (Baldwin et al., 2011), and hence, the amyloid state is thermodynamically favoured over the native state. And yet, native proteins do not constantly convert into aggregates. The relative stability of the native state with respect to the amyloid state is therefore due to a kinetic barrier, which prevents the uncontrolled formation of amyloid (Baldwin et al., 2011).

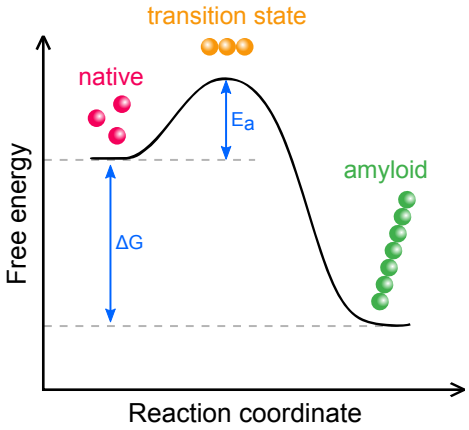

Fig. 1.2.: Thermodynamic energy profile of amyloid formation. The difference of free energy between a protein in the native state and in the amyloid state is the Gibbs free energy change, ΔG, of amyloid formation. The transition from the native state to the amyloid state requires the activation energy, E_a, which represents an energy barrier to the high-energy transition state.

Kinetics of Amyloid Formation

The conversion of native proteins into amyloid aggregates is a complex, multistep process with diverse intermediate states of interconverting species with different polymerisation states. The underlying mechanistic pathways of amyloid assembly have been unravelled with the help of chemical kinetics. Early kinetic studies investigating the polymerisation of proteins showed that polymer assembly can be described by a two-step process (Oosawa and Kasai, 1962). The process involves a nucleation step in which small growth-competent aggregates are formed from monomeric proteins, and an elongation step in which monomeric protein is added to the ends of a growing polymer (**Fig. 1.3a**). The integrated rate law formulated by Oosawa and Kasai, 1962 describes the time evolution of the polymerisation process considering the underlying processes of nucleation and elongation.

The nucleation-polymerisation model was further extended with two additional processes responsible for the observed autocatalysis: heterogeneous nucleation (Ferrone et al., 1980; Bishop and Ferrone, 1984; Ferrone et al., 1985) and polymer fragmentation (Wegner, 1982; Bishop and Ferrone, 1984). In both processes, existing polymers are involved in the generation of new polymers. In secondary nucleation processes, new polymers nucleate on the surface of existing filaments, and fragmentation processes generate new growth-competent polymer ends by

breaking existing filaments into smaller pieces (**Fig. 1.3a**). These early studies comprehensively presented the microscopic processes of polymerisation, which were subsequently used to describe protein aggregation and amyloid formation (Ferrone, 1999; Collins et al., 2004; Tanaka et al., 2006).

To determine the relative contribution of the microscopic processes, the non-linear rate equations underlying the aggregation process need to be solved. Knowles and colleagues presented a general analytical solution to the master equation describing the kinetics of amyloid formation (Knowles et al., 2009; Cohen et al., 2011; Cohen et al., 2012). Macroscopically, amyloid formation typically follows a sigmoidal curve with an initial lag phase followed by an exponential growth phase and a plateau phase (**Fig. 1.3b**). Comparing this theoretical kinetic description with experimental

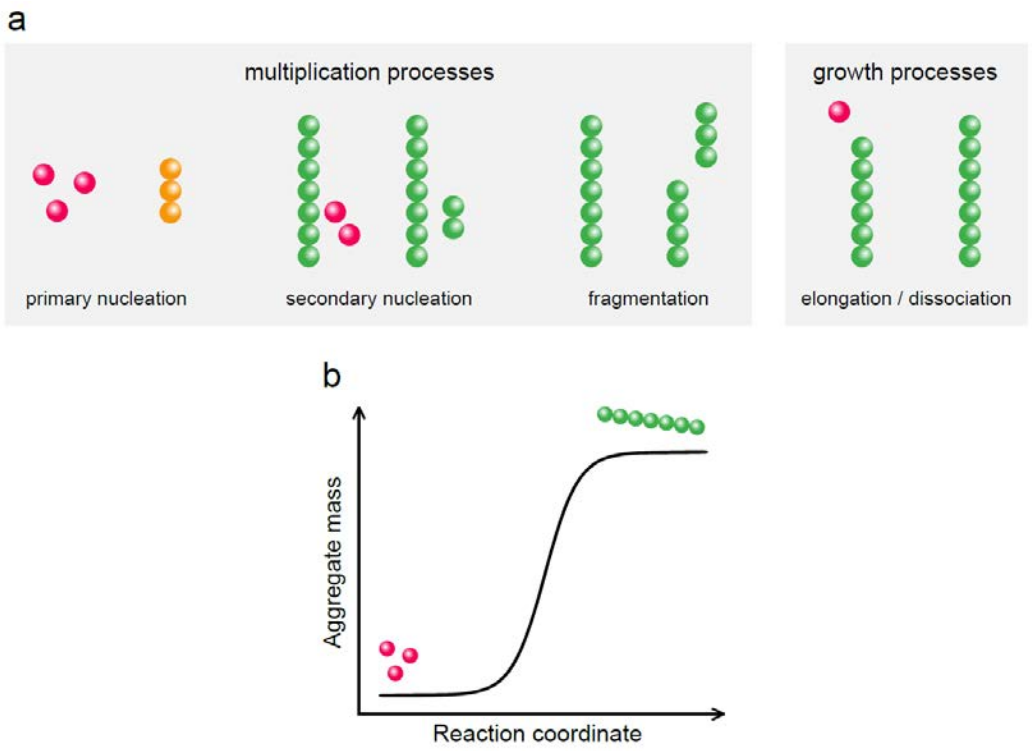

Fig. 1.3.: (a) Microscopic processes underlying amyloid fibrillation (adapted from Cohen et al., 2011). The microscopic processes can be categorised into multiplication processes and growth processes. Multiplication processes lead to an increase in the number of fibrils, and therefore to an increase in the number of growth-competent ends. Growth processes generate new fibril mass (Meisl et al., 2017). Multiplication processes can be primary processes depending on the concentration of monomeric species (primary nucleation) or secondary processes depending on the concentration of preexisting fibrils (secondary nucleation, fragmentation). (b) Sigmoidal function describing the macroscopic time course of amyloid formation. The curve is typically described by an initial lag phase followed by an exponential growth phase, which ends in a plateau phase upon substrate depletion.

data allows one to unravel the relative importance of the underlying microscopic processes.

The use of chemical kinetics to decipher molecular mechanisms of amyloid aggregation has been applied to a variety of amyloidogenic proteins. Examples include the study of the aggregation kinetics of Aβ_{40} and Aβ_{42} (Cohen et al., 2013; Meisl et al., 2014), α-synuclein (Galvagnion et al., 2015; Flagmeier et al., 2016) and insulin (Meisl et al., 2017). Moreover, the approach has enabled studies investigating the effect of aggregation inhibitors such as molecular chaperones. Using the kinetic approach, the microscopic polymerisation events inhibited by a chaperone were identified (Cohen et al., 2015; Arosio et al., 2016). Every microscopic process was found to be individually targetable by specific molecular chaperones, which opens up new perspectives for the rational design of aggregation inhibitors to interfere with the molecular mechanisms of amyloid aggregation (Arosio et al., 2016).

From a functional perspective, the term 'propagon' was introduced to describe species capable of self-replication through conversion of monomeric proteins into amyloid in a template-catalysed way (Cox et al., 2003; Aguzzi et al., 2013). The term encompasses the totality of all propagation-active species. In this respect, it differs from the term 'nucleus', which describes a merely kinetic rather than functional entity.

1.1.3 Protein Misfolding and Aggregation Diseases

The aggregation of proteins into amyloid fibrils and the accumulation of the fibrillar aggregates are the underlying principles of many neurodegenerative and systemic disorders. The common denominator of all of these diseases is the conversion of a soluble, physiologically functional protein into fibrillar amyloid aggregates (Knowles et al., 2014). The conversion of soluble protein into amyloid aggregates might promote disease by a loss of function of the physiological form of the protein, or by a gain of function of the aggregated form. Each protein misfolding disease is characterised by a specific protein undergoing misfolding and aggregation.

To date, more than 40 diseases have been described that are associated with protein misfolding and amyloid fibrillation (Chiti and Dobson, 2006). A selection of some of the most common disorders is listed in **Figure 1.4**. The diseases are concep-

Disease	Aggregating protein	Location of aggregation
Neurodegenerative diseases		
prion diseases (CJD, GSS, FFI, kuru)	prion protein	cortex, thalamus, brain stem, cerebellum, other areas
Alzheimer's disease	amyloid β, tau	cortex, hippocampus, basal forebrain, brain stem
Parkinson's disease	α-synuclein	substantia nigra, cortex, locus ceruleus, other areas
dementia with Lewy bodies	α-synuclein	frontal cortex, brain stem, other areas
multiple system atrophy	α-synuclein	striatum, substantia nigra, cerebellum, inferior olives
frontotemporal dementia	tau, FUS	frontal and temporal cortex, hippocampus
amyotrophic lateral sclerosis	TDP-43, FUS, SOD1	spinal motor neurons, motor cortex
Huntington's disease	Huntingtin	striatum, basal ganglia, cortex, other areas
familial amyloidotic polyneuropathy	transthyretin (mutant)	peripheral nervous system
Non-neurodegenerative diseases		
AL amyloidosis	immunoglobulin light chains	all organs except CNS
AA amyloidosis	serum amyloid A protein	all organs except CNS
transthyretin amyloidosis, ATTR	transthyretin (wild-type)	heart, ligaments, carpal tunnel
haemodialysis-related amyloidosis	β_2-microglobulin	musculoskeletal system
lysozyme amyloidosis	lysozyme	kidney, liver
apolipoprotein amyloidosis	Apo A-I, A-II, A-IV, C-II, C-III	kidney, heart, liver
type II diabetes	islet amyloid polypeptide	islets of Langerhans in the pancreas (β-cells)
cataracts	crystallins	ocular lens
injection-localised amyloidosis	insulin	subcutaneous sites of medication injection

adapted from Ross & Poirier, 2004; Chiti & Dobson, 2006; Sipe et al., 2016

Fig. 1.4.: Examples of human diseases associated with protein misfolding and amyloid aggregation. Partial list of neurodegenerative and non-neurodegenerative diseases associated with amyloid formation including the aggregating protein and the location of aggregate deposition. Table adapted from Ross and Poirier, 2004; Chiti and Dobson, 2006; Sipe et al., 2016.

tually split into neurodegenerative and non-neurodegenerative disorders. Amyloid deposits in neurodegenerative diseases are primarily found in the central nervous system mainly in the brain, while in non-neurodegenerative amyloidoses, protein deposits accumulate in peripheral organs (Chiti and Dobson, 2006).

The disorders, which are particularly relevant for this thesis include prion diseases, mainly Creutzfeldt-Jakob disease (CJD), α-synucleinopathies, and injection-localised amyloidosis associated with insulin. A brief overview is given in the following sections.

Human Prion Diseases and Their Diagnosis

Human prion diseases. Human prion diseases, also known as human transmissible spongiform encephalopathies, are a group of neurodegenerative disorders, which result from the misfolding and accumulation of the cellular prion protein (PrP^{C}). The diseases are clinically characterised by a rapidly progressive dementia accompanied by movement disorders, ataxia and myoclonus (Aguzzi et al., 2008). The main neuropathological hallmarks of prion diseases include vacuolation or spongiform change, neuronal cell loss, reactive astrogliosis, and microglia activation (Budka et al., 1995; Aguzzi and Zhu, 2017).

Human prion diseases are aetiologically classified into sporadic, inherited and acquired forms (Collinge, 2001). Sporadic prion diseases, including sporadic Creutzfeldt-Jakob disease (sCJD) and rarely sporadic fatal familial insomnia, account for the majority of cases ($\sim$85%). The cause of sporadic prion diseases is unknown (Collinge, 2001). Inherited or genetic prion diseases are associated with inherited, pathologic germline mutations in the prion protein gene (*PRNP*) and account for approximately 15% of cases (Collinge, 2001). Genetic forms of prion diseases include genetic Creutzfeldt-Jakob disease (gCJD), Gerstmann-Sträussler-Scheinker disease (GSS), and fatal familial insomnia (FFI). Acquired forms, including iatrogenic Creutzfeldt-Jakob disease (iCJD), variant Creutzfeldt-Jakob disease (vCJD) and kuru, are caused by the transmission of infectivity. These latter disease types, however, are very rare (Will, 2003).

Diagnosis of prion diseases. Human prion diseases are definitely diagnosed by post mortem histological or biochemical detection of the misfolded scrapie prion protein (PrP^{Sc}) in brain tissue. However, a set of diagnostic criteria for the ante mortem diagnosis of CJD has been proposed by the World Health Organisation (WHO, 1998). According to the WHO criteria, probable CJD is diagnosed in patients if presenting with progressive dementia accompanied by two of the typical clinical symptoms including myoclonus, visual or cerebellar disturbance, pyramidal/extrapyramidal dysfunction, akinetic mutism, and a positive result in one of the approved diagnostic tests (WHO, 1998). Diagnostic tests include a typical pattern in electroencephalography (Steinhoff et al., 2004) and magnetic resonance imaging (Zerr et al., 2009) or the detection of the biomarker 14-3-3 protein in the cerebrospinal fluid (CSF; Collins et al., 2000). These tests, however, are not specific to CJD, and definitive diagnosis requires post mortem analysis of brain tissue. Recently developed biochemical assays exploiting the self-propagation activity of pathological prions, such as the RT-QuIC assay (see '1.1.5 Amyloid Amplification Assays, Assays for the in vitro Replication of Prions'), have the potential to be more accurate tools for the specific diagnosis of CJD (Groveman et al., 2017), and might eventually be included in the WHO diagnostic criteria for CJD.

α-Synucleinopathies and Their Diagnosis

α-Synucleinopathies. α-Synucleinopathies comprise a group of neurodegenerative disorders that are characterised by the misfolding and accumulation of pathologic α-synuclein. The three main α-synucleinopathies include Parkinson's disease (PD), dementia with Lewy bodies (DLB), and multiple system atrophy (MSA). Common clinical disease symptoms include progressive decline in motor, cognitive and autonomic functions and behavioural changes (Martí et al., 2003). However, symptoms vary across the different diseases and are dependent on the affected brain areas and structures. PD is mainly characterised by motor dysfunction with the three cardinal symptoms resting tremor, bradykinesia and rigidity (Jankovic, 2008). Early lesions primarily involve the accumulation of α-synuclein aggregates in the form of Lewy bodies in dopaminergic neurons of the substantia nigra in the brainstem (Braak et al.,

2003b). DLB patients present with cognitive impairment, dementia, hallucinations and Parkinson-like symptoms (McKeith et al., 2005). Lewy bodies are predominantly found across subcortical, paralimbic, and neocortical structures (Gomez-Tortosa et al., 1999). MSA clinical symptoms include autonomic dysfunction, cerebellar ataxia, corticospinal dysfunction and parkinsonism (Gilman et al., 1999). Early lesions affect brainstem, striatum, basal ganglia and cerebellum (Jellinger et al., 2005). While in PD and DLB α-synuclein inclusions are found in neurons (Baba et al., 1998), in MSA they are predominantly found as glial cytoplasmic inclusions (Spillantini et al., 1998).

Diagnosis of α-synucleinopathies. α-Synucleinopathies are routinely diagnosed based on clinical criteria. However, autopsy examination is required for neuropathological confirmation of the diagnosis. The confirmation criterion at autopsy is the histopathological detection of α-synuclein inclusions in brain tissue (Gelb et al., 1999). In practice, the clinical diagnosis of PD is based on the recognition of the cardinal symptoms and responsiveness to levodopa (Gelb et al., 1999). In addition to the clinical data, structural and functional neuroimaging has proven useful to detect changes specific for α-synucleinopathies (Pyatigorskaya et al., 2014). In advanced stages, classical cases of PD are diagnosed rather confidently. However, the large heterogeneity in clinical presentation and the overlap in clinical symptoms makes the differential diagnosis of the various α-synucleinopathies very challenging, particularly at early disease stages (Tolosa et al., 2006). Due to the inherent limitations of clinical diagnostics, research has been directed towards the development of novel diagnostic tools such as new biomarkers or biochemical assays. Very recently, amplification assays for the detection of small quantities of α-synuclein aggregates have been developed. Analogous to the amplification assays described for the diagnosis of prion diseases, the self-propagation activity of α-synuclein was used to amplify α-synuclein aggregates from brain tissue or CSF samples in these assays (Fairfoul et al., 2016; Shahnawaz et al., 2017; Sano et al., 2017). Due to their high sensitivity and specificity, these assays hold great potential for a more accurate and reliable diagnosis of α-synucleinopathies.

Iatrogenic Insulin-Associated Amyloidosis

Therapeutic insulin, used to treat diabetes patients, is conventionally administered by subcutaneous injections or pump-regulated infusions (Matteucci et al., 2015). In some patients, extracellular amyloid deposits consisting of aggregated insulin were found at the site of injection. First reports of insulin amyloidosis described the formation of amyloid formation following therapeutic insulin administration in diabetes patients (Störkel et al., 1983; Dische et al., 1988). The aggregated protein was identified as insulin by immunohistochemistry and amino acid sequencing (Dische et al., 1988). Since the initial reports of injection-localised insulin amyloidosis, an increasing number of case reports have recently been published in the specialised literature (Nilsson, 2016).

The main clinical implication of insulin-derived amyloidosis is poor blood glucose control caused by an impairment of insulin absorption. The absorption at an affected injection site is two-thirds lower than at a normal, unaffected site (Nagase et al., 2014). Accordingly, the administered insulin dose is too low to reduce blood glucose levels, and hyperglycaemia can occur. Injection-localised amyloidosis is treated by surgical ablation of amyloidomas and by avoiding further injections at the site of amyloidosis (Gupta et al., 2015).

1.1.4 Amyloid Proteins

Prion Protein and the Prion Hypothesis

Structure and function. The cellular human prion protein is a small, glycosylphosphatidylinositol anchored cell-surface protein encoded by the *PRNP* gene on chromosome 20 (Sparkes et al., 1986). The protein is synthesised from a precursor protein with an N-terminal signal sequence directing the protein to the endoplasmic reticulum (Kretzschmar et al., 1986). The mature protein consists of 208 amino acids (residues 23-230), which constitute two structurally and functionally distinct moieties (Riek et al., 1997; Zahn et al., 2000): the N-terminal flexible tail (aa 23-124) and the C-terminal globular domain (aa 125-230). The structurally disordered flexible tail contains five tandem repeats of an octapeptide (octapeptide repeat, OR) flanked by positively charged clusters (charge clusters 1 and 2, CC1 and CC2) on both sides, and a hydrophobic region separating the flexible tail from the C-terminal globular domain (**Fig. 1.5a**). The globular domain is structurally well ordered (**Fig. 1.5b**) and consists of two β-strands and three α-helices connected by loop regions (Riek et al., 1996; Zahn et al., 2000).
Despite extensive research efforts, the physiological function of the cellular prion protein is still not fully understood. Recent studies have shown that PrP^{C} plays a central role in peripheral myelin maintenance (Bremer et al., 2010). The N-terminal flexible tail of PrP^{C} was found to interact specifically with the G-protein coupled receptor Gpr126 on Schwann cells, thereby promoting nerve myelin maintenance (Küffer et al., 2016). Many other functions in neuroprotection, development, memory formation, circadian rhythm and others have been proposed and need to be revisited in the future (Wulf et al., 2017).

Protein-only hypothesis. In 1982 Prusiner isolated the infectious agent suspected of causing transmissible spongiform encephalopathies. He suggested that the infectious particle consists only of protein and proposed the term 'prion' to describe the proteinaceous infectious particle (Prusiner et al., 1982). The scrapie-associated form of the prion protein (PrP^{Sc}) was found to be particularly resistant to proteinase

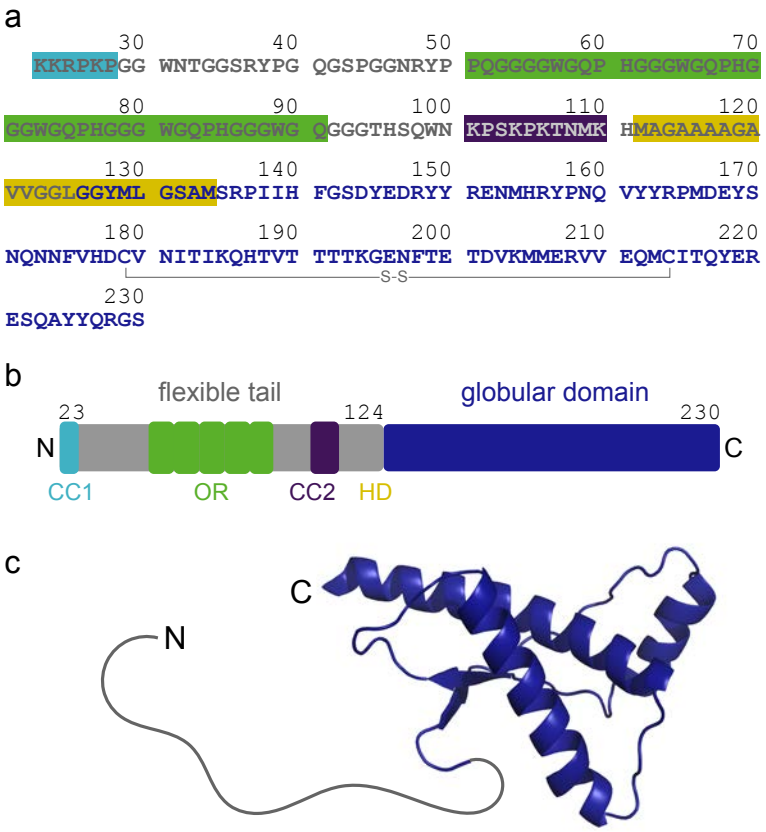

Fig. 1.5.: Sequence and structure of the human cellular prion protein. (a) Primary amino acid sequence. Residues of the charge cluster 1 (CC1, *turquoise*), the octapeptide repeat (OR, *green*), the charge cluster 2 (CC2, *purple*), and the hydrophobic domain (HD, *yellow*) are highlighted (Béland and Roucou, 2012). (b) Schematic representation of the domain structure. The protein consists of an N-terminal flexible tail (*grey*, residues 23-124) and a C-terminal globular domain (*dark blue*, residues 125-230). CC1, OR, CC2, and HD are indicated. (c) NMR structure of the cellular prion protein (PDB: 1QLX, Zahn et al., 2000). The N-terminal domain is largely unstructured (*grey line*, modelled), whereas the C-terminal domain adopts a globular fold (*dark blue*).

K (PK) digestion (Bolton et al., 1982) and to bind the amyloid specific dye Congo red (Prusiner et al., 1983). The identification of a single gene encoding both the prion protein extracted from healthy animals as well as the scrapie-associated PrP^{Sc} provided evidence for the existence of two conformational isoforms with the same primary sequence: the cellular PrP^{C} and the scrapie PrP^{Sc} (Basler et al., 1986). PrP^{Sc} was shown to multiply through conversion of endogenous PrP^{C} into the scrapie isoform (Prusiner et al., 1990). Compelling evidence for the 'protein-only hypothesis' was provided by Büeler and coworkers, who showed that mice lacking the cellular isoform PrP^{C} are resistant to scrapie infection and do not show disease symptoms. They concluded that the scrapie pathology strictly depends on the presence of PrP^{C}

(Büeler et al., 1993). The final proof for the 'protein-only hypothesis' was provided by studies in which recombinantly produced PrP was converted into infectious PrP^{Sc} in vitro (Diaz-Espinoza and Soto, 2010). Inoculation with synthetic PrP aggregates led to neurologic dysfunction in transgenic mice (Legname et al., 2004) and wild-type hamsters (Castilla et al., 2005b). These results showed that infectious prion agents can be produced from pure recombinant protein.

The term 'prion' refers strictly to infectious agents, which are transmissible to susceptible hosts through serial passages (Prusiner et al., 1982; Aguzzi, 2009). In contrast, the term 'prionoid' has been introduced for protein aggregates with prion-like properties for which infectivity has not been demonstrated (Aguzzi, 2009). Prionoids can self-propagate and spread transcellularly, but they are not transmitted from one host to another (Aguzzi and Rajendran, 2009).

α-Synuclein - a Prion-Like Protein

Structure and function. Human α-synuclein is a 140-amino acid small, acidic protein encoded by the *SNCA* gene on chromosome 4 (Spillantini et al., 1995). The protein was first described in 1988 as a neuron-specific protein localised to the presynapse and the nucleus of nerve cells (Maroteaux et al., 1988). Its primary sequence is subdivided into three domains: (1) the highly conserved N-terminus containing imperfect repeats of the hexameric 'KTKEGV' motif, (2) the central hydrophobic, highly amyloidogenic NAC (non-amyloid-β component of Alzheimer's disease amyloid, historically named by Uéda et al., 1993) domain, and (3) the C-terminal domain enriched in acidic residues and prolines (**Fig. 1.6a,b**). In its soluble, monomeric form, α-synuclein is intrinsically disordered and primarily composed of random coils (Eliezer et al., 2001), while upon interaction with lipids the protein acquires some secondary structure (**Fig. 1.6c**). Upon interaction with lipids, the N-terminal repeat domain shifts to an amphipathic α-helix, which mediates binding to negatively charged phospholipids in vesicles and membranes (Davidson et al., 1998). The central, hydrophobic NAC domain is essential for aggregation and mediates the conversion of α-synuclein from the native state to β-sheet rich amyloid aggregates (Giasson et al., 2001). The largely unstructured C-terminal domain interacts with

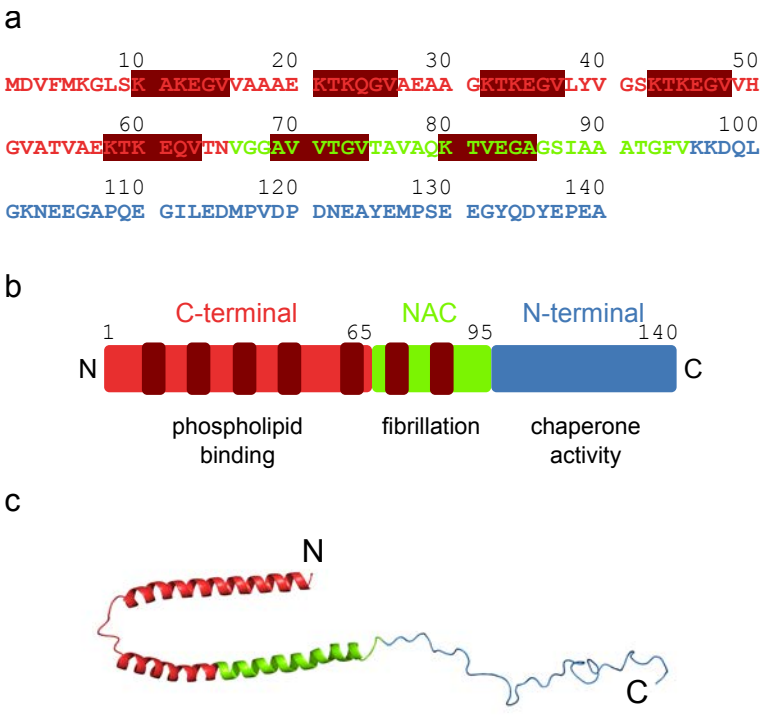

Fig. 1.6.: Sequence and structure of human α-synuclein. (a) Primary amino acid sequence. The residues of the N-terminal, imperfect hexameric repeat region are highlighted. The C-terminal region mainly consists of negatively charged amino acids. (b) Schematic representation of the domain structure. The protein consists of the N-terminal repeat domain (*red*, residues 1-65; repeats marked in *bordeaux*), the central NAC domain (*green*, residues 66-95) and the acidic C-terminal domain (*blue*, residues 96-140). (c) Crystal structure of lipid-bound human α-synuclein (PDB: 1XQ8, Ulmer et al., 2005). The N-terminal region adopts an amphipathic, α-helical conformation. The highly amyloidogenic, central NAC domain forms a helix, and the C-terminus is largely unstructured.

both proteins and small molecules through its highly charged residues and is thought to be crucial for chaperone-like activities of α-synuclein (Souza et al., 2000).

Although substantial efforts have been made to investigate the role of α-synuclein, its exact physiological function is not yet fully understood. The localisation to presynaptic nerve terminals and the association with synaptic vesicles (Maroteaux et al., 1988) suggest a role in vesicle transport and neurotransmitter release. α-Synuclein was shown to stimulate synaptic activity by promoting soluble N-ethylmaleimide-sensitive factor attachment protein receptor (SNARE) complex assembly for neurotransmitter release in a chaperone-like manner (Burré et al., 2010). More recently, α-synuclein has been described to stimulate the dilation of the exocytic fusion pore, thereby promoting the fusion of secretory vesicles with the membrane and the release of

neurotransmitters through exocytosis (Logan et al., 2017). An impairment of this function in neurotransmitter release would affect synaptic function and neuronal communication.

Prion-like spreading of α-synuclein pathology. Emerging evidence indicates that a prion-like mechanism underlies α-synuclein pathology involving cell-to-cell spreading through self-propagation of pathological aggregates. The first report of in vivo transmission of α-synucleinopathies was described in a study in which brain homogenates of affected animals were intracerebrally inoculated into healthy transgenic α-synuclein mice. The inoculation of mice expressing aggregation prone A53T mutated α-synuclein led to significant acceleration of the α-synuclein pathology (Mougenot et al., 2012; Luk et al., 2012a). Similar findings were reported for inoculations with synthetic α-synuclein fibrils assembled from recombinant human α-synuclein (Luk et al., 2012a). Furthermore, cell-to-cell transmission of α-synuclein pathology was observed following intracerebral inoculation of synthetic α-synuclein fibrils (Luk et al., 2012b) or insoluble α-synuclein from DLB patient brains (Masuda-Suzukake et al., 2013) in wild-type nontransgenic mice. Animals infected with pathological α-synuclein aggregates showed accumulation of endogenous α-synuclein inclusions and developed clinical symptoms reminiscent of α-synucleinopathies (Luk et al., 2012b; Masuda-Suzukake et al., 2013). In vivo imaging of individual neurons revealed selective cell-death of neurons bearing α-synuclein inclusions, which indicates a correlation between inclusion formation and cytotoxicity (Osterberg et al., 2015). Recently, a molecular mechanism for cell-to-cell transmission and toxicity of pathologic α-synuclein aggregates through receptor-mediated endocytosis has been proposed. According to this mechanism, α-synuclein aggregates are bound by lymphocyte-activation gene 3 (LAG3) and internalised through endocytosis (Mao et al., 2016). These recently published studies add to a growing body of evidence suggesting that prion-like propagation of α-synuclein aggregates, and possibly even other amyloidogenic proteins, might cause infectivity in neurodegenerative disorders (Aguzzi and Rajendran, 2009). Accordingly, α-synuclein is the prionoid most likely to be reclassified as a *bona fide* prion.

Insulin - a Model Protein for Amyloid Aggregation

Structure and function. Insulin is a small peptide hormone of 51 amino acids synthesised from the biologically inactive precursor preproinsulin produced in the β-cells in the pancreas (Chan et al., 1976). Preproinsulin is converted into proinsulin (Steiner et al., 1967) and finally into insulin by proteolytic cleavage. Biologically active insulin consists of two polypeptide chains. The two chains, the 21-aa long A chain and the 30-aa long B chain are linked by two disulfide bridges (**Fig. 1.7a**). Both chains contain ordered secondary structure elements that pack around a hydrophobic core (Hua et al., 1995). In solution, insulin exists in a dynamic equilibrium of monomers, dimers, tetramers, and hexamers (Jeffrey and Coates, 1966). Apart from associating into higher-order assemblies under native conditions, insulin was found to assemble into fibrils in acidic conditions or at elevated temperatures (Waugh, 1944; Waugh, 1946). The fibrils are formed from a partially unfolded intermediate conformation derived from monomeric protein (Nielsen et al., 2001). Characterisation of the fibrils revealed a cross-β structure characteristic for amyloid fibrils (Burke and Rougvie, 1972), which makes insulin a good model system to study amyloid formation.

Insulin is a key regulator of blood glucose levels. In response to elevated blood glucose levels, insulin is secreted from β-cells in the pancreas to increase glucose uptake and storage by muscle and fat, and to inhibit glucose production by the liver

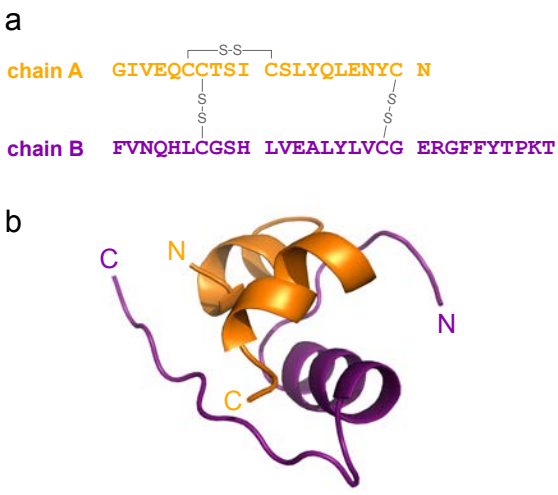

Fig. 1.7.: Sequence and structure of human insulin. (a) Primary amino acid sequence with disulfide bridges (A7-B7, A20-B19, A6-A11) indicated. (b) NMR structure of human insulin (PDB: 2HIU, Hua et al., 1995).

(Saltiel and Kahn, 2001). Glucose uptake is mediated by the glucose transporter GLUT4, which is translocated from the intracellular space to the cell surface upon insulin signalling (Huang and Czech, 2007). Defects in insulin signalling lead to diabetes mellitus, one of the leading causes of death in many developed countries (ADA, 2010). Diabetes mellitus is a group of metabolic diseases characterised by abnormally high levels of blood glucose - hyperglycaemia. The two main forms of diabetes are classified as type 1 and type 2 diabetes. While type 1 diabetes results from defects in insulin production, type 2 diabetes is caused by insulin resistance through impaired insulin signalling (ADA, 2010).

According to the WHO, diabetes can be treated by subcutaneous administration of recombinant insulin (WHO, 2013). Therapeutic human insulin was the first pharmaceutical product produced by recombinant DNA technology (Johnson, 1983). Today it is one of the best characterised therapeutic proteins. Along with an increasing number of insulin analogues designed to improve pharmacokinetics, insulin is still widely used in the treatment of diabetes mellitus patients.

1.1.5 Amyloid Amplification Assays

Basic Principle of Amyloid Amplification Assays

The molecular organisation of amyloid fibrils builds the structural basis for the self-propagating properties of amyloid fibrils (Baskakov, 2009). The cross-β structure of amyloid fibrils acts as a template for fibril elongation through monomer addition to both fibril ends. In this way, preexisting fibrils propagate their fibrillar conformation to monomeric protein, which leads to the conversion of monomer into amyloid and ultimately to amyloid growth. The combination of amyloid growth and multiplication of the amyloid template leads to highly efficient amyloid amplification (**Fig. 1.8**). Amyloid amplification assays exploit the autocatalytic amplification cycle to detect minute levels of amyloid aggregates. Traces of amyloid aggregates propagate their fibrillar conformation to monomeric substrate protein, which leads to a growth of fibril mass at the expense of the monomeric substrate. The growing fibrils are subsequently fragmented into smaller additional propagation units, each of which

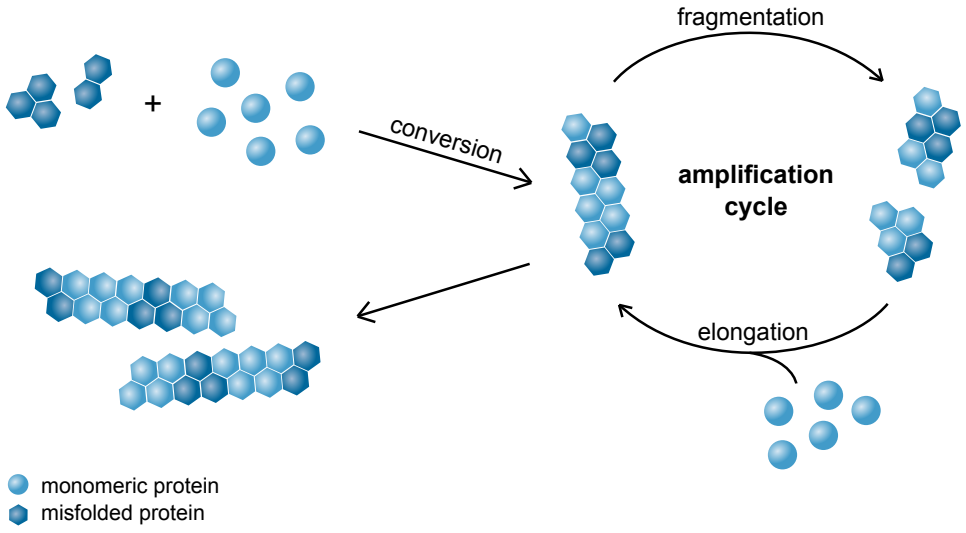

Fig. 1.8.: Autocatalytic amplification cycle of amyloid proteins. When incubated with monomeric protein (*light blue spheres*), amyloid aggregates (*dark blue hexagons*) self-propagate into larger aggregates by incorporating the monomeric protein in a template-catalysed way. Large amyloid aggregates can be broken into a higher number of smaller aggregates by fragmentation. The newly formed aggregates constitute new reactive units or propagons, which promote further self-replication of amyloid aggregates.

can again grow into larger fibrils. Consecutive repetition of the cycle enables the amplification of undetectably small amounts of amyloid aggregates to detectable levels of fibrillar aggregates.

The same basic principle of amplification underlies many different assays that have been described so far (Saborio et al., 2001; Colby et al., 2007; Wilham et al., 2010). Early progress was made mainly in the field of prion replication, and subsequently transferred to other amyloidogenic proteins. Adaptations of the experimental mechanism of fragmentation, the conditions for optimal elongation, and the monomeric substrate protein have recently led to a stepwise improvement in the development of amyloid amplification assays. In the following sections, the main achievements are outlined.

Assays for the in vitro Replication of Prions

In vitro replication of prions. To recapitulate in vitro the mechanisms underlying prion propagation observed in vivo, first attempts to convert the cellular prion protein PrP^{C} into the protease-resistant scrapie isoform PrP^{Sc} in cell-free systems were described in the 1990s (Raeber et al., 1992; Kocisko et al., 1994; Caughey et al., 1995). The first evidence for in vitro conversion of PrP^{C} into PrP^{Sc} came from experiments with radiolabelled PrP^{C} incubated with a large excess of PrP^{Sc}. After incubation of recombinant hamster ^{35}S-PrP^{C} with PrP^{Sc} purified from hamster brains for two days, a form of ^{35}S-radiolabelled, PK-resistant PrP was detected suggesting the conversion of ^{35}S-PrP^{C} into a ^{35}S-PrP^{Sc}-like form (Kocisko et al., 1994). The PrP^{Sc}-like form displayed biochemical properties indistinguishable from brain derived PrP^{Sc}. However, the PrP^{Sc}-like form generated in vitro did not propagate infectivity in a mouse bioassay (Hill et al., 1999). The low conversion efficiency was shown to depend on the incubation time as well as on the initial concentrations of PrP^{Sc} and ^{35}S-PrP^{C} (Caughey et al., 1995). Despite the reduced conversion efficiency and infectivity transmission, these initial experiments demonstrated prion self-replication in vitro and provided evidence for the 'protein-only' hypothesis of prion formation.

Protein misfolding cyclic amplification. Based on the self-replication principle, a more efficient assay for in vitro replication of prions has been described a few years later by Soto and colleagues (Saborio et al., 2001). The protein misfolding cyclic amplification (PMCA) assay consists of alternated cycles of sonication multiplying the number of PrP^{Sc} aggregates through fragmentation, followed by an incubation phase in which the aggregates grow by recruiting more PrP^{C} molecules. Conceptually analogous to DNA amplification by polymerase chain reaction (PCR), PMCA drastically amplifies the levels of PK-resistant prion protein (PrP^{res}) starting from small amounts of template PrP^{Sc} purified from prion-infected hamster brains and substrate PrP^{C} from brain homogenates of healthy animals. Newly formed PrP^{res} is detected by immunoblotting following PK digestion of residual PrP^{C} (Saborio et al., 2001). The in vitro synthesised PrP aggregates have similar biochemical and structural properties as PrP^{Sc} derived from prion-infected brains and have been shown to propagate prion infectivity in a hamster bioassay (Castilla et al., 2005b).
Since its first description, the PMCA assay has constantly been adapted and improved to detect PrP^{Sc} in tissue samples of different species. In one of the early applications of the assay, Soto and colleagues adapted the assay to demonstrate the presence of PrP^{res} in brain tissue (Soto et al., 2005) and in blood (Castilla et al., 2005a) of prion-infected hamsters. They were able to distinguish healthy animals from intracerebrally prion-inoculated, sick animals even at very early, presymptomatic stages of the disease (Soto et al., 2005; Saá et al., 2006a) using the PMCA technology. Later, the assay was used to amplify PK-resistant PrP^{res} from urine of prion-infected hamsters (Gonzalez-Romero et al., 2008) and from whole blood of presymptomatic, prion-infected mice (Tattum et al., 2010). It was further refined to quantify concentrations of misfolded prion protein in brain, spleen, blood and urine of prion-infected hamsters from the number of PMCA cycles required for detection (Chen et al., 2010). More recently, the PMCA assay has been adapted for the detection of prions in human tissues and body fluids. Especially remarkable was the detection of prions in the blood of patients suffering from vCJD (Lacroux et al., 2014; Concha-Marambio et al., 2016; Bougard et al., 2016).
At the same time, the assay has also undergone various technological modifications

and improvements. The assay was improved by automation (Castilla et al., 2005a; Saá et al., 2006b), and the efficiency of the assay was further enhanced through improved amplification and a more sensitive readout. In PMCAb, the PrP^{C} to PrP^{Sc} conversion is increased tenfold through the introduction of teflon beads in the PMCA reaction (Gonzalez-Montalban et al., 2011). In another approach, PrP^{Sc} is enriched with super-paramagnetic nanoparticles prior to amplification (Miller and Supattapone, 2011). Concentrating PrP^{Sc} templates before amplification allowed a more rapid amplification. To improve the readout of the PMCA assay, Rubenstein and colleagues combined the assay with a surround optical fibre immunoassay (SOFIA). SOFIA uses specific monoclonal antibodies with a fibre optics-based fluorescence detection system, which enables a more sensitive detection of PrP^{res} after fewer rounds of PMCA (Rubenstein et al., 2010).

However, the method has several disadvantages such as impractical sonication steps, and tedious immunoblot readouts, and requires the use of tissue homogenates as source of substrate protein. To overcome these shortcomings, the method was further optimised.

Real-time quaking-induced conversion. A major breakthrough in prion amplification assays was achieved by the use of recombinantly expressed prion protein as a substrate and the change to automated tube shaking to induce multiplication of PrP^{Sc}. The use of recombinant hamster PrP in the rPrP-PMCA allowed the detection of PrP^{res} in the CSF of prion-infected hamsters in 2-3 days (Atarashi et al., 2007), and the substitution of automated shaking for sonication in the quaking-induced conversion (QuIC) assay further decreased the assay duration to a single day (Atarashi et al., 2008). This new method allowed the discrimination between healthy and scrapie-affected hamsters in less time with higher sensitivity and efficiency (Atarashi et al., 2008).

Another important development was the introduction of the amyloid-specific dye thioflavin T (ThT) for the readout of newly formed amyloid aggregates instead of immunodetection. ThT staining in combination with amplification inside microplates, as described in the amyloid seeding assay (ASA), dramatically facilitated the con-

version assays by automating both the amplification process as well as the readout (Colby et al., 2007). This idea was taken up by Caughey and colleagues, who combined it with the previously described quaking-induced conversion method. The resulting assay, termed real-time quaking-induced conversion (RT-QuIC), is a rapid high-throughput assay, which has been adopted to quantify propagation activity of prions (Wilham et al., 2010). The propagation or seeding activity is determined from a series of dilutions of the original prion-containing sample. The seeding dose (SD_{50}) refers to the concentration at which 50% of replicate reactions are positive. To validate the assay, prion infectivity was determined in brain tissue, CSF and blood of prion-infected hamsters, sheep and deer (Wilham et al., 2010; Elder et al., 2013). Apart from its quantitative measure, the RT-QuIC assay has been shown to outperform other assays with respect to sensitivity and specificity, as well as with a reduced number of spontaneously aggregating, false positive reactions (Wilham et al., 2010).

Similar as described for the PMCA, the RT-QuIC technology has been constantly refined and adapted to prions isolated from various tissues of different host organisms. Most crucial was the adaptation of the assay to human patient samples, which enables the use of the assay as a tool for diagnosis of CJD.

Diagnostic application of the RT-QuIC. The first diagnostic application of the RT-QuIC was described in 2011 (Atarashi et al., 2011). In a proof-of-concept study, CSF samples from 18 definite sCJD patients and 35 control patients were correctly diagnosed with an improved version of the RT-QuIC (CSF RT-QuIC). Additional 185 samples were tested in a blinded study. The assay achieved a sensitivity of more than 80% and a specificity of 100% (Atarashi et al., 2011). These results were confirmed by many subsequent, independent studies conducted in different laboratories around the world (McGuire et al., 2012; Orrú et al., 2015; Park et al., 2016). The correct diagnosis of hundreds of sCJD cases and controls with RT-QuIC indicate that the assay is a powerful tool for antemortem diagnosis of sCJD. The reproducibility of the assay for diagnosing human prion diseases was further assessed in multi-centered, international ringtrial studies (McGuire et al., 2016; Cramm et al.,

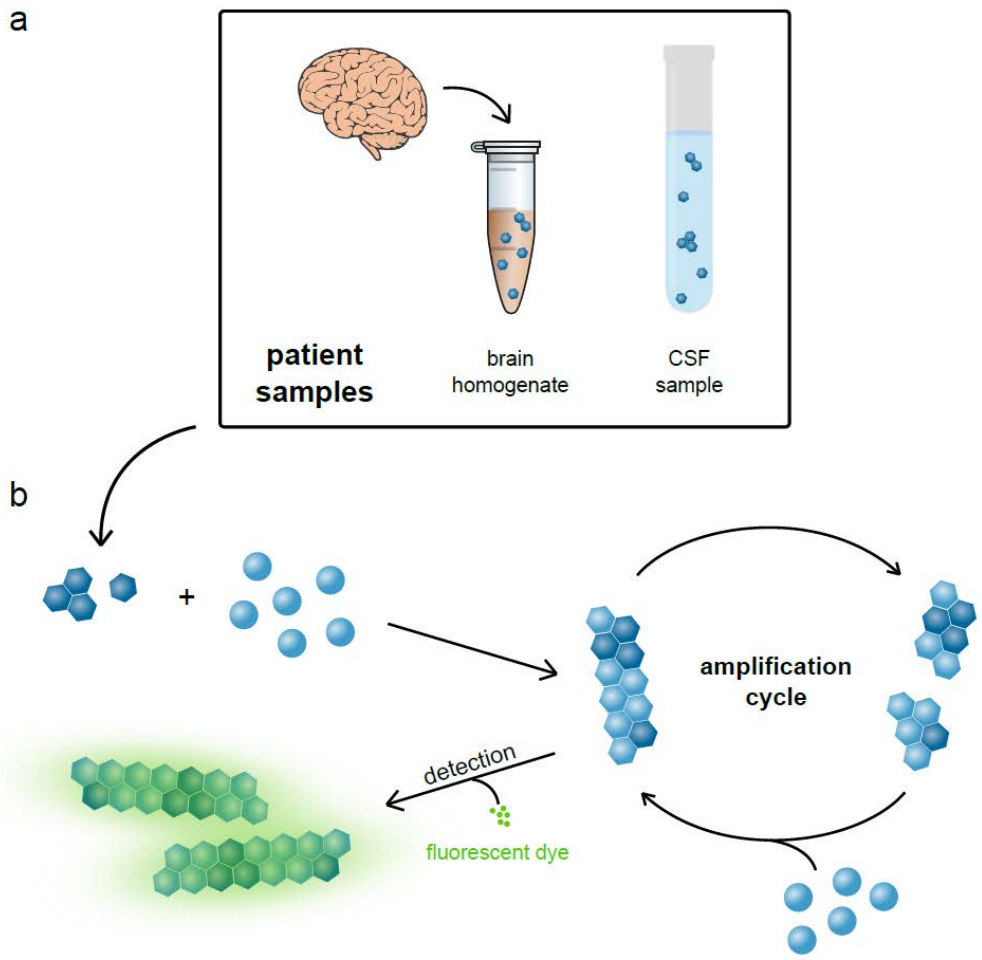

Fig. 1.9.: Principle of diagnostic amyloid amplification assays. (a) Samples are collected from patients suspected of suffering from a neurodegenerative disorder linked to protein aggregation. These include brain homogenates prepared from brain biopsies and CSF samples from lumbar puncture. (b) Patient samples are used to seed the amyloid amplification reaction. Samples containing amyloid aggregates cause amplification of aggregates, which can be detected using conventional amyloid dyes, such as ThT. Fluorescence-positive samples indicate samples positive for the disease.

2016). Taken together, CSF samples of sCJD patients and control CSF samples were analysed by RT-QuIC at 14 different study centres spread around the world. Even though the involved laboratories used partly different recombinant substrate proteins and different instrumentation, the results of all participants were in almost perfect agreement. The complete inter-laboratory concordance of the RT-QuIC results proves the diagnostic applicability of the assay.

The diagnostic RT-QuIC has further been optimised and refined over the past years. The long assay duration (approximately 5 days), which is the main practical limitation

of the conventional CSF RT-QuIC assay, was shortened in a refined version of the assay (Orrú et al., 2015). Truncated hamster HaPrP$_{90-231}$ substrate, an increased incubation temperature, and the addition of trace amounts of SDS increased the speed of the RT-QuIC conversion reaction by approximately one third. In addition, the diagnostic sensitivity and specificity were enhanced to 95% and 100%, respectively (Orrú et al., 2015). The improved assay with the truncated hamster substrate was validated in a study with a larger panel of CSF samples and was directly compared to the conventional CSF RT-QuIC. The study included 113 CJD patients and 64 control patients and demonstrated the advantages of the adapted assay such as faster kinetics, shorter assay time and increased assay sensitivity (Groveman et al., 2017). Furthermore, the RT-QuIC assay was adapted to detecting prions in the olfactory epithelium collected from nasal brushings. Nasal brushings from 31 patients suffering from sCJD were accurately diagnosed with a sensitivity of 97% and a specificity of 100% (Orrú et al., 2014). As nasal brushings are minimally invasive, this assay has a great potential to further enhance CJD diagnostics. In view of the recent technological advances and the high reliability, specificity and sensitivity of the RT-QuIC assay, the diagnostic criteria of the WHO might be adapted to include RT-QuIC for the diagnosis of CJD in the future.

Amplification Assays for Other Amyloidogenic Proteins

The active progress in the development of amyloid amplification assays in the prion field and the emerging concept of prion-like propagation of various disease-associated proteins have promoted the development of conceptually similar amplification assays for a variety of different proteins. Most relevant are amplification assays described for both Alzheimer's disease (AD) linked proteins, amyloid β and tau, and for α-synuclein, the protein aggregating in Parkinson's disease.

Amyloid β (Aβ) and tau amplification assays. The first report of an Aβ amplification assay described a significantly faster aggregation time course for aggregation reactions spiked with brain homogenates from an AD mouse model compared to reactions spiked with wild-type mouse brain homogenate (Du et al., 2011). A few

years later, Soto and colleagues established conditions for an Aβ amplification assay (Salvadores et al., 2014) that was able to detect Aβ oligomers in the CSF of AD patients. The different aggregation kinetics of reactions spiked with CSF samples containing pathologic Aβ oligomers and samples devoid of Aβ oligomers allowed the discrimination of samples of AD patients from healthy patient samples (Salvadores et al., 2014). Further development of the Aβ amplification assay enabled the detection of Aβ oligomers in peripheral blood of AD transgenic mice and its application in screening of drug candidates for their therapeutic effects (Estrada et al., 2016). Tau amplification assays have been used for the detection of misfolded tau aggregates in brain homogenates from human AD patients (Meyer et al., 2014; Saijo et al., 2017) and in CSF samples from patients suffering from Pick's disease (Saijo et al., 2017).

α-Synuclein amplification assays. The first described amyloid amplification assay for α-synuclein made use of synthetic α-synuclein fibrils to seed the conversion of monomeric α-synuclein (Herva et al., 2014). Aggregates formed by the assay were found to have biochemical and biophysical properties similar to in vivo α-synuclein aggregates. Herva et al., 2014 applied the assay to screen different anti-amyloid compounds and their effect on the template-catalysed conversion of monomeric α-synuclein. Later adaptations mainly aimed at the diagnostic detection of α-synuclein aggregates in tissues and body fluids from patients suffering from α-synucleinopathies. Recent studies have reported the detection of pathologic aggregates in the brain and CSF of PD, DLB and MSA patients with sensitivities of around 90% and specificities of roughly 95% (Fairfoul et al., 2016; Shahnawaz et al., 2017; Sano et al., 2017). The kinetic parameters measured in the amplification assays indicated a negative correlation between aggregation onset in the assay and disease severity and progression (Shahnawaz et al., 2017). α-Synuclein amplification has also been used to address the question of different strains of α-synuclein fibrillar conformations. The conformations of α-synuclein fibrils from two different transgenic mouse strains were shown to faithfully propagate in the amplification assay (Jung et al., 2017).

1.2 Digital Microfluidics

Microfluidics, the science of manipulating small volume fluids inside micron-scale channels, has emerged as a powerful platform for biochemical and medicinal analyses. Miniaturisation provides the advantages of low analyte volumes, short analysis times, and a high sensitivity (Whitesides, 2006). One of the main applications is droplet-based or digital microfluidics, in which discrete droplets generated from immiscible phases (mostly water-in-oil emulsions) serve as reaction compartments. Highly monodisperse droplets with nanometer to micrometer diameter are generated at kilohertz frequencies, and the reactions inside individual droplets can be analysed independently (Guo et al., 2012). The large number of droplets allows parallel processing and analysis of droplets, yielding large data sets required for digital data analysis. Digital microfluidics, therefore, offers great potential for parallelisation and high-throughput (Guo et al., 2012).

The use of digital microfluidics has revolutionised biochemical and biomedical analytics by enabling qualitative and quantitative analysis of droplet content (Guo et al., 2012; Basova and Foret, 2015). Digital microfluidics has mainly been applied for nucleic acid research such as digital PCR (Beer et al., 2007; Kiss et al., 2008), next generation sequencing (Lan et al., 2016), or microarray technology (Wang et al., 2003; Situma et al., 2006). More recently, it has also been used for protein analysis including biomarker detection studies (Mok et al., 2014), crystallisation (Zhu et al., 2014), or studies on amyloid growth (Knowles et al., 2011).

Amongst the most powerful applications of digital microfluidics is droplet digital polymerase chain reaction (ddPCR), a technique allowing the absolute quantification of DNA molecules (Hindson et al., 2011). In ddPCR, a target DNA sample is partitioned into a large number of discrete microdroplets representing individual reaction compartments, and the droplets are subjected to parallel PCR amplification. After endpoint amplification, droplets containing a target DNA molecule are counted based on a target-specific fluorescence readout. Since target DNA molecules are distributed randomly in the analyte, the number of molecules per reaction compartment is described by the Poisson distribution (Collins et al., 2015). Accordingly,

Poisson statistics is applied to calculate the DNA copy number in the analyte solution without the use of a calibration curve. The quantification of target DNA molecules using ddPCR is highly precise and sensitive, therefore representing a new tool for accurate molecular diagnostics (Huggett et al., 2015).

1.3 Motivation and Aims of the Thesis

Protein aggregation diseases are among the most significant disorders in the ageing population. Despite the high prevalence of these diseases, early and reliable diagnostic tests remain still elusive. Over the last decade, assays for the amplification and detection of small quantities of prion aggregates have been developed, and successfully applied to prion diagnostics. However, these assays are mainly restricted to the prion protein, and limited in throughput, robustness, and precision. This thesis aims to advance the amyloid amplification assays of three different amyloid proteins including insulin, prion protein and α-synuclein. For each protein an amplification assay was developed and applied to detect minute amounts of amyloid aggregates.

My first aim was to establish a robust and precise assay for the quantitative analysis of insulin amyloid aggregates. A few attempts to quantify propagation activity of amyloid aggregates using amplification assays have been reported previously (Shi et al., 2013; Henderson et al., 2015; Takatsuki et al., 2015). However, in all of these studies the propagation activity has been quantified relative to a known standard sample. The objective of this thesis was therefore to develop a sensitive assay capable of quantifying amyloid propagons in absolute numbers. To achieve this objective, I developed an insulin amyloid amplification assay with digital readout using droplet-based microfluidics.

In a second project, I aimed to implement and optimise the RT-QuIC assay for prion diagnostics and biomedical applications. This included (1) the application of the assay to detect PrP^{Sc} in human body fluids and tissues for CJD diagnosis, (2) the adaptation of the assay to study the inactivation of prions bound to surgical steel, and (3) the assessment of prion self-replication in cerebellar organotypic cultured slices treated with neurotoxic anti-prion antibodies. The above aims required the adaptation of the RT-QuIC to detect PrP aggregates in samples different from the commonly used brain homogenates or CSF samples.

In the third part of this thesis, I aimed at extending the principle of amyloid amplification to α-synuclein. α-Synuclein has been shown to self-propagate in a prion-like fashion (Luk et al., 2012b; Masuda-Suzukake et al., 2013). This property can be exploited to amplify α-synuclein aggregates in a template-catalysed manner. The main aim was to establish conditions for the specific amplification of low amounts of α-synuclein propagons, and to investigate possibilities to detect α-synuclein aggregates in patient blood samples. Furthermore, the assay was used to investigate several decontamination agents for their potential to inactivate the propagation properties of α-synuclein aggregates.

2

Digital Insulin Amyloid Amplification Assay

2.1 Introduction

Biochemical assays for the sensitive detection of protein aggregates are crucial for basic research and diagnostics. The detection of minute quantities of amyloid aggregates enables the identification of early steps in the aggregation cascade, which is instrumental to prevent further propagation of the aggregation reaction. In this chapter I describe the development of a digital amyloid quantification assay (d-AQuA) for the detection of single amyloid propagons. The assay combines the self-propagation properties of amyloid fibrils with the power of digital droplet microfluidics, which enables the precise quantification of amyloid propagons at low concentrations.

Parts of this chapter are reproduced or quoted verbatim from the following article published by Analytical Chemistry on November 21, 2017:

Absolute Quantification of Amyloid Propagons by Digital Microfluidics

Manuela Pfammatter, Maria Andreasen, Georg Meisl, Christopher G. Taylor, Jozef Adamcik, Sreenath Bolisetty, Antoni Sanchez-Ferrer, David Klenerman, Christopher M. Dobson, Raffaele Mezzenga, Tuomas P. J. Knowles, Adriano Aguzzi, and Simone Hornemann

doi: 10.1021/acs.analchem.7b03279, https://pubs.acs.org/doi/10.1021/acs.analchem.7b03279

2.2 Results

2.2.1 Basic Principle of D-AQuA

To address the challenges mentioned above, I established a digital amyloid amplification assay, d-AQuA. D-AQuA is a digital amyloid amplification assay used to quantify amyloid propagons, minute amounts of amyloid protein seeds. The assay exploits the power of digital droplet microfluidics by partitioning amyloid propagons into discrete droplets (**Fig. 2.1, *i***) prior to template-catalysed amyloid amplification. Similarly to droplet digital PCR, amplification of limited dilutions of template amyloid propagons is performed within individual droplets in a highly parallel manner (**Fig. 2.1, *ii***). This provides the data volumes required for digital analysis and absolute quantification of propagons in the input sample (**Fig. 2.1, *iii***).

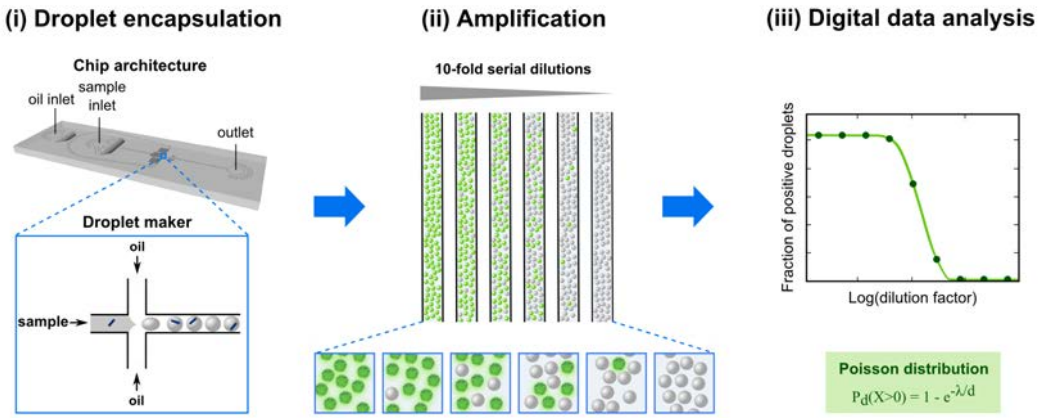

Fig. 2.1.: D-AQuA workflow. (i) Samples containing 10-fold serial dilutions of the standard fibril sample (*blue dashes*) are mixed with soluble substrate protein and ThT. The mixtures are partitioned into several thousand pL-droplets using a microfluidic flow-focusing device. (ii) Microdroplets are collected into glass capillaries for endpoint amplification and detection by ThT fluorescence (*green*). (iii) ThT-positive droplets are counted and the absolute number of propagons in the standard fibril sample is quantified by Poisson statistics. Reprinted with permission from Pfammatter et al., 2017.

To generate uniform droplet compartments for highly parallel amplification of single propagons, a microfluidic chip with flow focusing geometry is used (**Fig. 2.2a**). Both oil phase and analyte are floated through the flow focusing junction to form water-in-oil emulsion droplets at kilohertz frequency (**Fig. 2.2a-c**). Stable droplets encapsulating soluble substrate protein, Thioflavin T and serial 10-fold dilutions of

propagon-containing input sample are generated. The droplets are collected into glass capillaries (**Fig. 2.2d**), and the capillaries are sealed and aligned on a glass slide (**Fig. 2.2e**). The glass slide with the capillaries is covered with a hotplate heated to 65 °C to initiate the amplification reaction and mounted on an automated motorised stage of a fluorescent laser microscope for imaging.

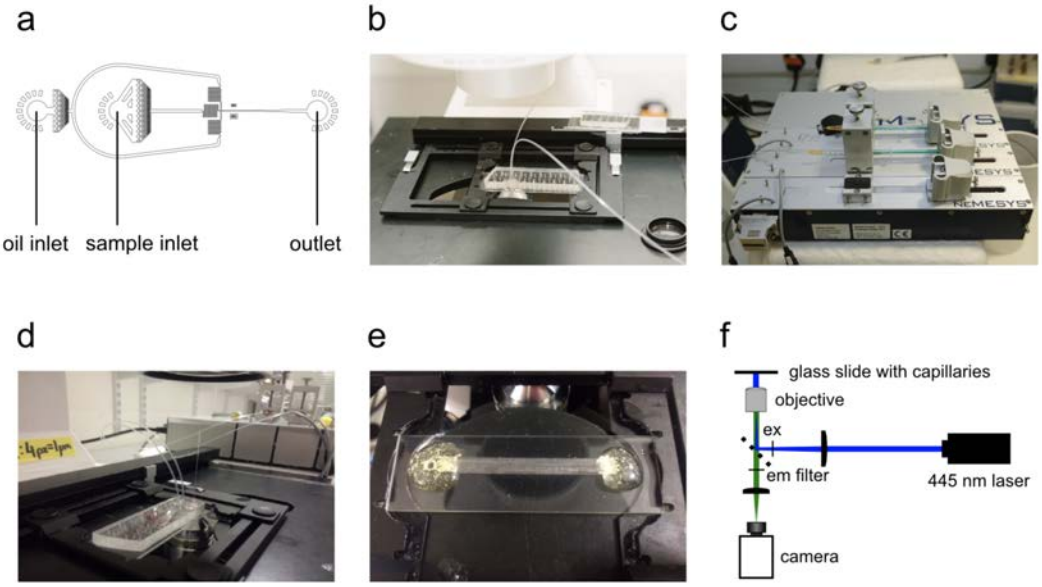

Fig. 2.2.: Experimental setup of d-AQuA. (a) Design of the microfluidic flow focusing device for droplet generation with oil and sample inlets as well as outlet labelled. (b) Injection of oil and sample phase. (c) Flow rates are precisely controlled with a syringe pump to form microdroplets at the flow focusing junction. (d) Droplet collection into glass capillaries. (e) Assembly of capillaries containing droplets with different fibril dilutions. (f) Schematic illustration of the laser setup used for monitoring the fluorescence intensity of the microdroplets. Reprinted with permission from Pfammatter et al., 2017.

Template-catalysed amplification of propagons leads to the formation of large amyloid aggregates specifically in propagon-encapsulating droplets. Depending on the dilution of the input sample, a certain fraction of droplets contains propagons, which are amplified to large aggregates. No amplification takes place in the droplets that do not contain propagons. At the endpoint, droplets containing amplified aggregates are detected by their positive ThT fluorescence signals. The number of positive and negative droplets at every dilution factor is counted. The Poisson distribution model is applied to determine the absolute number of propagons in the input sample. The high number of parallel reactions enables a digital interpretation of the data and allows for a reliable measurement of propagon numbers with high accuracy. (Pfammatter et al., 2017)

2.2.2 Insulin Standard Fibril Sample

For the development and validation of d-AQuA, I used human insulin as a model system. Insulin readily forms amyloid aggregates through mechanistic pathways analogous to the fibrillation of disease-related amyloidogenic proteins (Jiménez et al., 2002), and is therefore widely used as an experimental model to study amyloid formation (Nettleton et al., 2000; Bouchard et al., 2000; Ivanova et al., 2009). I generated a standard sample of preformed insulin fibrils with reproducible propagation properties, which was used to establish and validate the d-AQuA method.

Insulin fibrils were reconstituted in vitro by incubating human insulin at a concentration of 1 mM in hydrochloric acid (HCl, pH 2.0) at 65 °C and agitation at 600 rpm for 72 h. Residual monomeric protein was removed by intensive washing with HCl (pH 2.0) (Nilsson and Dobson, 2003). The remaining fibrils were lyophilised and stored at -20 °C. Before usage, fibrils were diluted to a concentration of 400 µM (monomer equivalents) to yield the standard fibril sample. In collaboration with Raffaele Mezzenga and coworkers (Laboratory of Food and Soft Materials, ETH Zurich) morphological and biophysical characteristics as well as self-propagation activity of the standard fibril sample were analysed (**Fig. 2.3**). Dynamic light scattering (DLS) measurements showed that the fibrils have a mean hydrodynamic radius of 85 nm (**Fig. 2.3a**). Furthermore, both Fourier transform infrared (FTIR) and circular dichroism (CD) spectra indicated a high β-sheet content (about 86%), which is characteristic of amyloid fibrils (Bouchard et al., 2000; Nelson et al., 2005) (**Fig. 2.3b,c**). To assess the propagation activity of the sample, the kinetics of fibril formation by monomeric insulin in the presence of preformed fibrils from the standard sample were monitored by optical density at OD_{370nm} (**Fig. 2.3d**). Increasing concentrations of preformed fibrils (1, 2 and 5% of total protein concentration) were found to shorten the lag phase of the aggregation reaction gradually (**Fig. 2.3e**), as expected for a nucleated self-assembly process. These results indicate that the standard fibril sample exhibits the typical biophysical characteristics of amyloid fibrils. (Pfammatter et al., 2017)

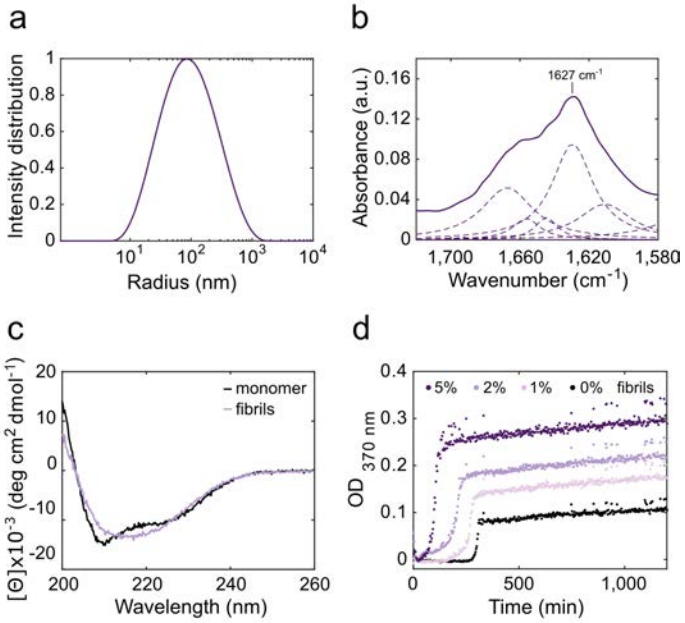

Fig. 2.3.: Characterisation of the standard fibril sample. The standard fibril sample was characterised by DLS (a), FTIR spectroscopy (b, shown are the whole spectrum as a solid line and its deconvoluted peaks as dashed lines), far-UV CD spectroscopy (c) and the self-propagation activity assay (d). Reprinted with permission from Pfammatter et al., 2017.

2.2.3 Development of D-AQuA

Next, I established the experimental conditions for d-AQuA. 400 µM insulin in HCl (pH 2.0), 0.1 M guanidinium chloride (GdmCl) and 40 µM ThT were encapsulated inside microdroplets together with serial 10-fold dilutions ranging from 10^2 to 10^8 of the standard fibril sample (in monomer equivalents). I found that the use of a high concentration of the substrate and the addition of low amounts of GdmCl, which accelerates aggregation by inducing partial unfolding of the monomeric species (Ahmad et al., 2003), were important for efficient amplification. Droplets with different dilutions of preformed fibrils were collected in separate capillaries, mounted on a microscope slide and heated to 65 °C to accelerate the growth and proliferation of the propagons. Fluorescence images were taken every 15 min to follow the amplification process in the individual droplets over 24 h (**Fig. 2.4a,b**). For the absolute quantification of the number of propagons, I analysed between 500 and 1400 droplets per dilution and digitised the readout by grouping the fluorescence endpoint signals into positive and negative outcomes by thresholding (see Materials

and Methods for details). A Poisson distribution was fitted to the number of fluorescence positive (i.e. propagon containing) droplets for each dilution factor at the assay endpoint. The best fits yielded an average number of $2.1 \cdot 10^{11}$ propagons per µL (accurate to within a factor of 1.1, n=2) in the standard fibril sample (**Fig. 2.4c**). Moreover, under these conditions I obtained a very low average false positive rate of only ∼0.4% spontaneously aggregating reactions in a total of about 700 droplets of the unseeded control. Because of the high level of conformity of the data to the Poisson distribution model, I concluded that the assay is capable of amplifying single propagons in pL droplets and allows the precise quantification of absolute numbers of propagons at low femtomolar concentrations. (Pfammatter et al., 2017)

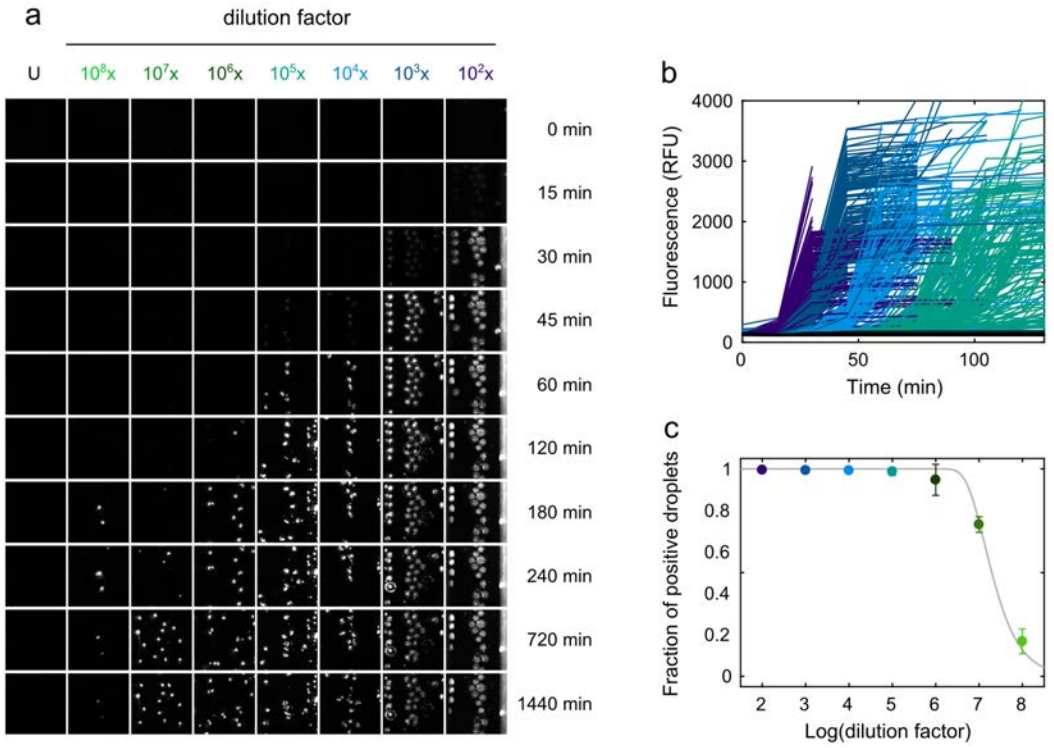

Fig. 2.4.: D-AQuA for single propagon quantification. (a) Representative fluorescence images of the capillaries containing microdroplets with 10-fold serial dilutions of the standard fibril sample. Droplets containing newly formed aggregates appeared as ThT fluorescence positive, whereas droplets without preformed fibrils were fluorescence negative. U: unseeded control. (b) Time courses of insulin fibril formation inside microdroplets for different fibril dilutions (*coloured*; unseeded control in *black*) monitored by ThT fluorescence. 200 representative reactions are shown per dilution. (c) Fraction of fluorescence-positive droplets as a function of the logarithm of the dilution factor. Every data point represents the mean ± SD from two independent experiments of d-AQuA. A Poisson distribution was fitted to the data (*grey line*) to quantify the number of propagons in the standard fibril sample. Reprinted with permission from Pfammatter et al., 2017.

2.2.4 Microplate Digital Amyloid Quantification Assay

Microplate-based amyloid amplification assays in 96-well plate formats with an analogue readout are the current standard assays for detecting amyloid aggregates in biological samples (Salvadores et al., 2014; Shahnawaz et al., 2017; McGuire et al., 2016). To enable a direct comparison between the sensitivity of this method with d-AQuA, I developed an amyloid amplification assay for insulin in a microplate with a digital readout (**Fig. 2.5**). As the precision of digital readouts increases with the number of replicate reactions, I established the assay in a 384-well format. I also adapted the experimental conditions to account for the higher volumes and larger surface areas used in the microplate assay. A range of experimental parameters including substrate protein concentration, temperature, shaking cycles, pH value, buffer conditions and additives were systematically screened and optimised for best assay performance. Especially crucial was the addition of D-mannitol, which has recently been reported to suppress spontaneous nucleation of insulin by stabilisation of the monomer, while enhancing the growth rate of existing fibrils (Saha et al., 2016). Formic acid (HCOOH) at pH 3.0 was chosen as the solvent, because of its reported ability to reduce spontaneous aggregation of monomeric insulin (Brange et al., 1997). Finally, I identified a concentration of 2 µM soluble substrate protein in 0.75 M D-mannitol, 1 M GdmCl, 10 µM ThT, HCOOH (pH 3.0) with cyclic agitation (1 min at 300 rpm, 2 min quiescent) at 30 °C as optimal assay conditions. These conditions resulted in an efficient reduction of spontaneous aggregation to a false positive rate of 1–2% in 384 replicates over the course of the experiment (24 h), while yielding highly reproducible aggregation kinetics of the propagon-catalysed reactions (**Fig. 2.5a**).

For digital quantification of the propagon number in our standard fibril sample, I again performed serial 10-fold dilutions of the standard fibril sample (10^4- to 10^{15}-fold dilutions in monomer equivalents) using 16 replicates per dilution. The aggregation time course was monitored by real-time ThT fluorescence over 24 h (**Fig. 2.5a**). At low dilutions (10^4- to 10^9-fold), I observed lag times of approximately 8 h, which gradually increased with higher dilutions of preformed fibrils. Endpoint fluorescence

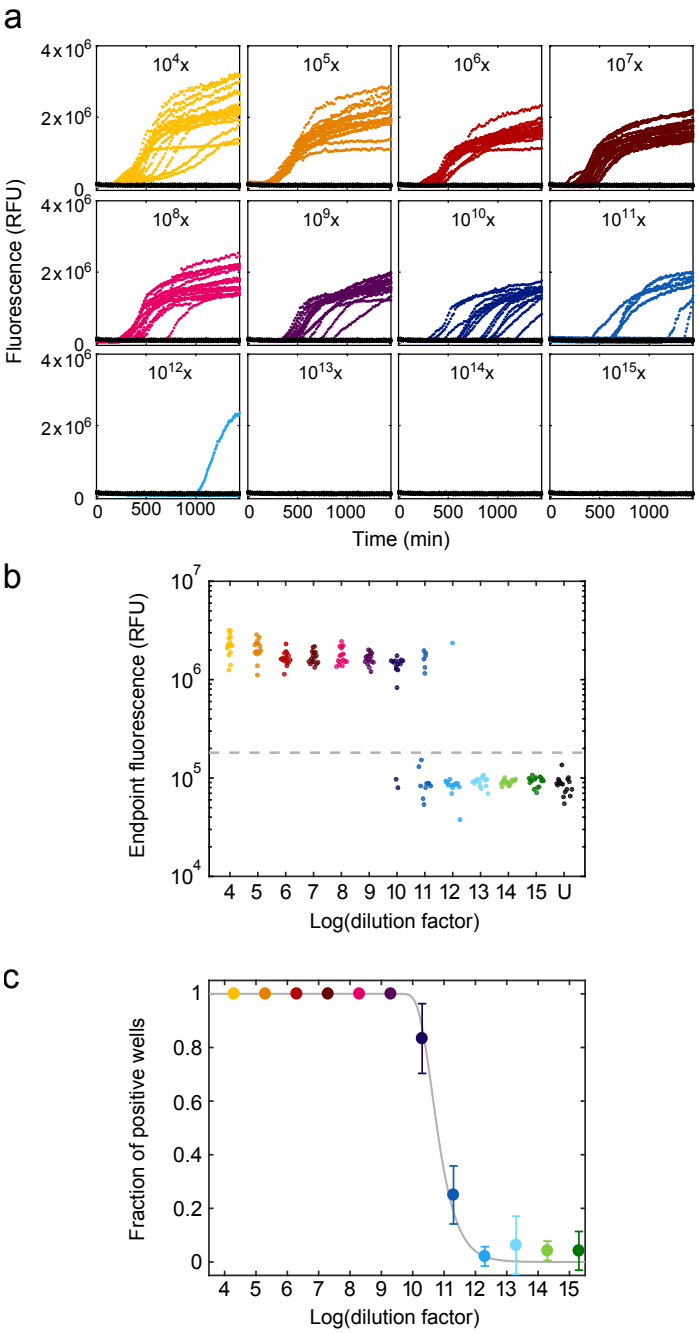

Fig. 2.5.: Microplate amyloid amplification assay. (a) Real-time ThT fluorescence time courses of insulin fibril formation with 10-fold serial dilutions from 10^4 to 10^{15} of the standard fibril sample on a microplate (*coloured*; unseeded controls in *black*). All reactions and the control reaction were performed in 16 technical replicates. (b) Fluorescence endpoint signals at different fibril dilution factors (*coloured*; unseeded controls in *black*, U). The grey dashed line shows the threshold ($\bar{x}_0 + 5\sigma_0$) used for the positive/negative scoring of the signals. (c) Fraction of positive wells as a function of the logarithm of the dilution factor. Data represent the mean $\pm$ SD from three independent experiments. A Poisson distribution was fitted to the data (*grey line*) to quantify the number of propagons in the standard fibril sample. Reprinted with permission from Pfammatter et al., 2017.

signals of reactions with low dilution factors ($\leq 10^9$-fold) of preformed fibrils were all positive, whereas at higher dilutions only fractions of the replicate reactions appeared positive (14, 6 and 1 out of 16 replicates for 10^{10}-, 10^{11}- and 10^{12}-fold dilutions, respectively). All reactions at dilution factors $\geq 10^{13}$-fold, as well as the control (without preformed fibrils) were scored negative (**Fig. 2.5b**). The fraction of positive signals was correlated with the dilution factors, and a Poisson distribution was fitted to the data (**Fig. 2.5c**). The best fit yielded an average number of $1.4 \cdot 10^9$ propagons μL^{-1} (accurate to within a factor of 1.2, n=3) in the standard fibril sample. These data show that the microplate assay ($1.4 \cdot 10^9$ propagons μL^{-1}) is also capable of detecting individual propagons. However, compared to d-AQuA ($2.1 \cdot 10^{11}$ propagons μL^{-1}) two orders of magnitude less propagons were detected with the microplate assay.

The detection of a lower number of active propagons might be due to a loss of fibrils to various solid surfaces during the extensive pipetting steps or due to their adherence to the microplate surface. The absence of solid contact surfaces in the microdroplets or the small droplet sizes, associated with higher effective concentrations (Guo et al., 2012), might result in a higher number of effective propagons. High losses of propagons, however, significantly impair the sensitivity and reproducibility of the microplate assay. Compared to the microplate assay, d-AQuA also exhibited a greatly reduced average false positive rate of unspecific amplification reactions in the unseeded control ($\sim$0.4% compared to 1-2%) and decreased assay time ($\sim$8 h compared to 24 h). (Pfammatter et al., 2017)

2.2.5 Validation With Quantitative Atomic Force Microscopy

To complement the data obtained by d-AQuA with an alternative method, I used atomic force microscopy (AFM), measured in collaboration with Raffaele Mezzenga and coworkers (Laboratory of Food and Soft Materials, ETH Zurich). This allowed me to estimate the dimensions and physical number of fibrillar aggregates present in the standard fibril sample (**Fig. 2.6a**). The average contour length of the fibrils was (50 ± 35) nm (**Fig. 2.6b**) and the height was (5.3 ± 1.7) nm (**Fig. 2.6c**). I used these

dimensions and mass conservation to calculate the physical number of fibrils per unit volume of the standard fibril sample (see 'Fibril Quantification by AFM' in Materials and Methods section for details). The calculations yielded an average number of $1.1 \cdot 10^{12}$ µL^{-1} fibrils. This number is very similar (less than an order of magnitude, i.e. within a factor of ∼5) to the number of propagons determined by d-AQuA ($2.1 \cdot 10^{11}$ propagons µL^{-1}). A possible explanation for the small difference between these numbers might be that not all fibrillar aggregates detected by AFM also act as active propagons in d-AQuA. I therefore concluded that the active propagons detected by d-AQuA are identical to a fraction of morphologically defined fibrillar aggregates. (Pfammatter et al., 2017)

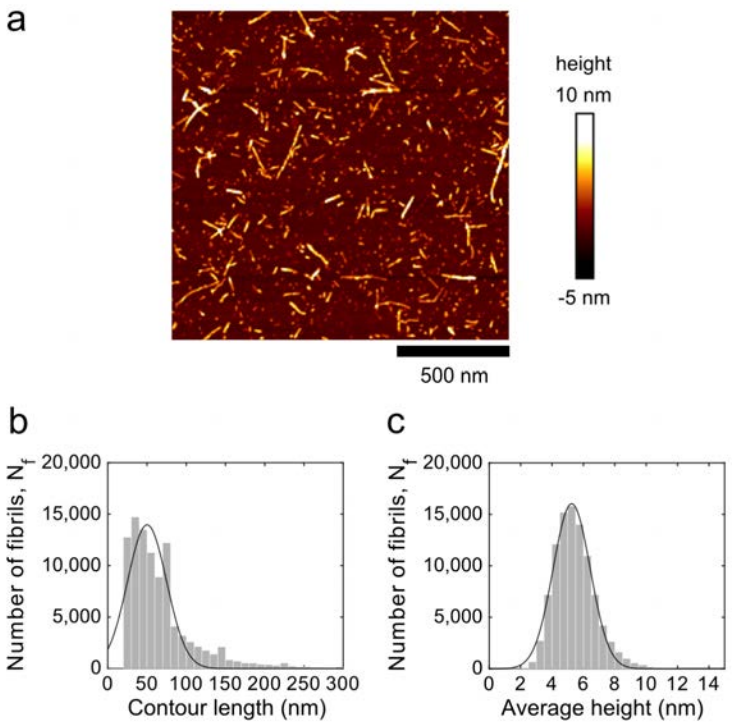

Fig. 2.6.: Quantitative AFM measurements. (a) AFM height image of preformed insulin fibrils. (b) Histogram of the fibril contour length distribution of preformed insulin fibrils. (c) Histogram of the average height distribution of the preformed insulin fibrils. Data were fitted to a Gaussian distribution (*solid line*) to obtain the mean ± SD of the contour length and the fibril heights. Reprinted with permission from Pfammatter et al., 2017.

2.3 Discussion and Outlook

In this chapter, I described d-AQuA, a digital amyloid amplification assay in which the power of digital microfluidics was exploited for the sensitive detection and quantification of amyloid propagons. In d-AQuA, individual amplification reactions were encapsulated inside microdroplets and amplified in a template-catalysed way. The encapsulation allowed the parallel amplification of thousands of reactions in pL volumes for highly accurate and precise digital data analysis. The presented results showed that d-AQuA enables the measurement of the activity of single propagons and the digital quantification of the absolute number of propagons present in a sample. With the capability to detect single propagons, the assay reached the ultimate sensitivity limit of detection.

Compared to the microplate assay, which also reached the ultimate level of sensitivity, d-AQuA was shown to be the more rapid and precise method and to have a higher recovery rate of low-abundance propagons. The microfluidic assay offers several important advantages over the most commonly used amyloid amplification assays, PMCA (Saborio et al., 2001) and RT-QuIC (Wilham et al., 2010; Orru et al., 2012). First, the large numbers of replicate measurements in d-AQuA (up to 1400 compared to typically 3 to 8 in PMCA (Saborio et al., 2001) and RT-QuIC (Wilham et al., 2010; Orru et al., 2012)) yielded highly precise data sets through more powerful statistical analysis of the data. D-AQuA enables the detection of single propagons and absolute propagon quantification, whereas in PMCA and RT-QuIC, propagons were typically quantified either in gram or mol or given as amyloid seeding activity or tissue dilutions (Saborio et al., 2001; Wilham et al., 2010; Orru et al., 2012). Compared to PMCA (Saborio et al., 2001), d-AQuA also provides a simpler and faster readout by using ThT fluorescence instead of detection by immunoblotting. In experiments described in this study, d-AQuA also required a significantly decreased assay time ($\sim$8 h compared to typically 1-3 days in PMCA (Saborio et al., 2001; Orru et al., 2012) and RT-QuIC (Orru et al., 2012)), reduced labor-intensive and time-consuming pipetting steps and associated errors. Moreover, the use of pL-droplets instead of µL-volumes significantly reduced the consumption of reagents

and, in particular, of the analyte. This is crucial, when precious clinical samples with a low concentration of propagons need to be analysed. Hence, d-AQuA offers a major improvement over the microplate assays in determining exact numbers of propagons, a result that is of major importance in the context of ultrasensitive detection and precise quantification of the number of low-abundance propagons in a given sample. (Pfammatter et al., 2017)

The most important innovation of d-AQuA is the precise, absolute quantification of amyloid propagons without the need of a standard curve. The idea to quantify amyloid propagons based on their seeding or propagation activity has already been described for the PMCA assay (Chen et al., 2010) and for the RT-QuIC assay (Wilham et al., 2010; Shi et al., 2013; Henderson et al., 2015; Takatsuki et al., 2015). In these studies, the amounts of PrP^{Sc} seeds was correlated either to the number of PMCA rounds required for the immunodetection of amplified PrP^{Sc} (Chen et al., 2010), to the seeding dose (SD_{50}, the dilution at with 50% of RT-QuIC reactions are positive (Wilham et al., 2010)), or to the lag time of the conversion reaction (Shi et al., 2013) for quantification. However, in all previous studies, PrP^{Sc} has been quantified by interpolation of the unknown sample on a standard calibration curve derived from a reference sample with known amounts of PrP^{Sc}. The absolute PrP^{Sc} quantities in the reference sample were determined by independent methodologies such as immunoassays. By contrast, d-AQuA enables absolute quantification directly from the number of propagation-positive replicates without the need for a standard curve. Individual propagons are counted directly, which greatly increases the accuracy of quantification.

The sensitive detection and absolute quantification of propagating amyloid aggregates offer the possibility for multiple applications. The detection and quantification of small traces of insulin propagons, which are not detectable with conventional analytical methods, might be relevant to the pharmaceutical production of insulin. Recombinantly produced insulin for the treatment of diabetes patients was shown to be prone to aggregation (Waugh, 1944; Waugh, 1946), which can cause problems in drug formulation, stability and pharmacokinetics (Brange et al., 1997). Aggregation of pharmaceutical proteins can affect product quality through impeding deliverability

and absorption or through eliciting undesired immunogenicity in patients (Roberts, 2014). Identification of early protein aggregation in pharmaceutical products is inevitable to guarantee product quality and stability. D-AQuA could serve as a quality control assay for pharmaceutical insulin products. The detection of early aggregated states during different stages of the manufacturing process would help to optimise manufacturing and to prevent biotechnical and biomedical problems arising from insulin aggregation. As a result, product quality and stability could be improved.
Finally, d-AQuA represents a proof-of-concept assay for amyloid amplification, which could be adapted to a range of different amyloidogenic protein systems. The assay holds great potential for ultrasensitive and rapid diagnosis of protein aggregation diseases such as prion diseases, α-synucleinopathies, and Alzheimer's disease. Through the detection of minimal quantities of early pathological aggregates, the method might be sensitive enough for preclinical diagnosis. In particular, a small-volume, single-use disposable chip with the ability to diagnose protein aggregation diseases accurately from body fluids in a point-of-care manner holds great promise for novel automated diagnostic approaches.

2.4 Materials and Methods

2.4.1 Materials

Human insulin was purchased from Sigma-Aldrich (SAFC Biosciences) and used without further purification. All chemicals unless otherwise specified were purchased from Sigma-Aldrich.

2.4.2 Standard Fibril Sample Preparation

Fibrils were assembled in vitro by incubating 1 mM monomeric human insulin in a 10 mM HCl water solution at pH 2.0 (HCl, pH 2.0) at 65 °C and agitation at 600 rpm for 72 h. Residual monomeric species were removed by intense washing with HCl (pH 2.0) using Amicon centrifugal filters with a molecular weight cut-off of 100 kDa (Nilsson and Dobson, 2003). Fibrils were lyophilised and stored at -20 °C until usage. The sample was diluted to a concentration of 400 µM (monomer equivalents) to yield the standard fibril sample.

2.4.3 Atomic Force Microscopy

A droplet of 20 µL of insulin fibril solution (1 µM in HCl, pH 2.0) was deposited on freshly cleaved mica substrate, incubated for 2 min at room temperature, rinsed with deionised water to remove unbound fibrils, and dried with compressed air flow. The samples were scanned on a MultiMode VIII Scanning Probe Microscope (Bruker) covered with an acoustic hood to minimise vibrational noise. The AFM was operated in tapping mode under ambient conditions using commercial silicon nitride cantilevers. The AFM images were acquired with a scan rate of 0.1 Hz and a resolution of 5120 x 5120 pixels per image. All images were flattened to remove background curvature using the Bruker Nanoscope 8.10 software. No further image processing was carried out. The contour lengths and the average height distributions were extracted from >95,000 individually traced fibrils using FiberApp (Usov and

Mezzenga, 2015), an open-source tracking and analysis software written in Matlab (The MathWorks, USA).

2.4.4 Dynamic Light Scattering

DLS spectra of a 100 µM insulin fibril solution in HCl (pH 2.0) were recorded using a 3D cross-correlation dynamic light scattering spectrometer (LS instruments) equipped with a He-Ne-Laser emitting polarised light at a wavelength of 632.8 nm. Dynamic light scattering measurements were performed at room temperature at a fixed scattering angle of 90°. The spectrum represents the average of three independent measurements of 600 s each. Time correlation functions of the scattered intensity were analysed using the CONTIN analysis algorithm (Provencher, 1982).

2.4.5 Fourier Transform Infrared Spectroscopy

FTIR spectra of lyophilised insulin fibrils were obtained by using a Varian 640 FTIR spectrometer (Varian Inc.) equipped with a Specac Diamond ATR Golden Gate single attenuated total reflection (ATR) system. Samples were scanned at room temperature over the range of 4000 to 600 cm^{-1} with a resolution of 2 cm^{-1}, averaged over 64 scans, and baseline corrected. The amide region was normalised, resolved by second-derivative analysis, and peak deconvoluted using Igor Pro 6.3.4.1 software.

2.4.6 Far-UV Circular Dichroism Spectroscopy

CD spectra were obtained on a Jasco J-815 spectropolarimeter (Jasco Inc.) at 25 °C using an insulin concentration of 20 µM in HCl (pH 2.0). Far-UV CD spectra were recorded in a 0.1 cm precision quartz cuvette (Hellma) from 200 to 260 nm with a data pitch of 0.2 nm, a bandwidth of 2 nm and a scanning speed of 20 nm min^{-1}.

Spectra were background subtracted and averaged over 10 scans. The molar mean residue ellipticity θ_{mrw} was calculated as

$$\theta_{mrw} = \frac{\theta}{d \cdot c \cdot n_{aa}} \tag{2.1}$$

where θ is the measured ellipticity, d the thickness of the cuvette, c the concentration and n_{aa} the number of residues of insulin.

2.4.7 Self-Propagation Activity Assay

The self-propagation activity of the preformed insulin fibrils was assessed in a seeded aggregation experiment. 400 µM monomeric insulin was mixed with 0, 1, 2 and 5% (related to the monomer concentration) preformed fibrils and incubated in HCl (pH 2.0) at 45 °C and 300 rpm continuous agitation in 96-well polystyrene microplates (Corning, Prod.No. 3880). The aggregation time course was monitored by following the absorbance at 370 nm using a Spectramax Paradigm microplate reader (Molecular Devices). Triplicate measurements of all conditions were performed and averaged to calculate mean and standard deviations of the lag phases.

2.4.8 Microdroplet Device Fabrication

Microfluidic flow focusing devices (**Fig. 2.2a**) were fabricated using standard soft-lithography techniques (McDonald et al., 2000). Briefly, the device design was patterned on a silicon wafer using SU-8 negative photoresist (MicroChem) to produce a negative mold. Microfluidic channels were cast into poly(dimethylsiloxane) (PDMS; Dow Corning Sylgard 184 Silicone Elastomer) on the silicon mold, and the PDMS stamp was cured at 65 °C for 150 min before peeling off the mold. Channel inlets and outlets were punched into the PDMS stamp before oxygen plasma bonding it to a glass slide to seal the channels. To make channel walls hydrophobic, the device was flushed with the water repellent agent Aquapel (PPG Industries) for 30 min before washing with isopropanol and then blow-dried with a nitrogen stream.

2.4.9 D-AQuA Assay

Lyophilised insulin was dissolved in HCl (pH 2.0) at a concentration of 6 mg mL^{-1} and filtered (50 kDa Amicon centrifugal filters; Millipore UFC505096) to remove higher molecular weight species. The protein was dissolved to a final assay concentration of 400 µM in HCl (pH 2.0) containing 0.1 M GdmCl and 40 µM Thioflavin T (ThT). Serial 10-fold dilutions of the standard fibril sample were prepared in HCl (pH 2.0) and added to the reaction mixture immediately before encapsulating the mixture into microdroplets. Negative controls were incubated with the same volume of HCl (pH 2.0) instead of fibrils. Amplification reactions were encapsulated into water-in-oil emulsions using a microfluidic device with flow focusing geometry. The sample containing monomeric substrate, fibrils and ThT was injected into the middle inlet on the chip at a flow rate of 200 µL h^{-1}. The carrier oil phase made of fluorinated FC-40 (Sigma) with 4% (w/v) triblock co-polymer (ABA) surfactant (where A is a perfluorinated poly(propylene oxide) block and B a poly(ethylene oxide) block, synthesised as previously described (Holtze et al., 2008)) was injected into the outer inlet at a flow rate of 300 µL h^{-1} to generate droplets with a radius of $\sim$25 µm (volume $\sim$65 pL). Flow rates were controlled with a Cetoni neMESYS syringe pump (Cetoni GmbH). Between 500 and 1400 replicate droplets were collected per dilution at the outlet into Rectangular Borosilicate capillaries (CM Scientific), and the capillaries were sealed with wax plugs to prevent sample evaporation. Before imaging the capillaries containing samples at different fibril dilutions, capillaries were aligned on a glass slide for amplification and imaging. The aligned capillaries were placed on the automated motorised stage of a custom-built epifluorescence laser microscope (**Fig. 2.2f**) and covered with a hotplate heated to 65 °C to induce amplification. To track aggregate formation inside the droplets, fluorescent images were acquired every 15 min for approximately 24 h using laser excitation at 445 nm (diode laser (MLD445, Cobolt)). Individual droplets were identified manually, and the average intensity of the droplet area was extracted for all frames. The brightness of the images of the 10^2 capillary in Figure 2.4a was adjusted to account for minor differences in brightness arising from imaging on different frames of the automated

stage laser. Fluorescent traces in Figure 2.4b were considered complete once the plateau region was obtained.

2.4.10 Microplate Amyloid Amplification Assay

Lyophilised insulin was dissolved in HCOOH (pH 3.0) at a concentration of 6 mg mL^{-1} and filtered using 50 kDa Amicon Ultra centrifugal filters (Millipore, Prod. No. UFC505096). The protein was dissolved to a final concentration of 2 µM in 0.75 M D-mannitol, 1 M GdmCl, 10 µM ThT, HCOOH (pH 3.0) in a reaction volume of 28.5 µL per well. To each reaction either 1.5 µL of serial 10-fold dilutions from 10^4 to 10^{15} of the standard fibril sample (dissolved in HCOOH, pH 3.0) or HCOOH (pH 3.0, negative control) was added. Each dilution and the control were performed in sixteen technical replicates on black 384-well polystyrene microplates (Corning, Prod. No. 3540) covered with sealing tape (Sarstedt, Prod. No. 95.1999). Microplates were incubated at a constant temperature of 30 °C with cyclic agitation (1 min at 300 rpm followed by 2 min quiescent) on a SpectraMax Paradigm microplate reader (Molecular Devices). To monitor the aggregation kinetics, ThT fluorescence was measured at 482 nm following excitation at 440 nm every 3 min using bottom read. The error of the assay was calculated from three independent replicate measurements of the microplate assay.

2.4.11 Digital Data Analysis

To digitise the assay readout for absolute propagon quantification, fluorescence endpoint values of the amplification reactions were transformed into positive and negative signals by thresholding. For the microplate assay, the threshold was set to five standard deviations above the mean of the unseeded negative control reactions ($\bar{x}_0 + 5\sigma_0$). Any signal above the threshold was regarded as positive signal. For d-AQuA, droplets which showed positive ThT fluorescence at the endpoint were scored positive. The fraction of positive droplets at every dilution was then calculated from the number of positive droplets and the total number of droplets counted in

the corresponding brightfield images. The absolute number of propagons in both assays was calculated using the Poisson distribution model. The probability of finding k propagons in a reaction compartment if the average number of propagons per reaction compartment is λ, is described by the Poisson distribution

$$P(X = k) = \frac{\lambda^k e^{-\lambda}}{k!} \tag{2.2}$$

The probability of having one or more propagons per reaction compartment (the probability of a positive signal) is given by

$$P(X > 0) = 1 - P(X = 0) = 1 - e^{-\lambda} \tag{2.3}$$

where $P(X = 0)$ is the probability of not having any propagons in the reaction compartment (the probability of a negative signal). For the different dilution factors d, the probability of having one or more propagons per compartment can be described as

$$P_d(X > 0) = 1 - e^{-\lambda/d} \tag{2.4}$$

where λ is the average number of propagons in the original sample and d is the dilution factor. The fraction of positive signals can be related to the dilution factors using equation 2.4, and therefore the absolute number of propagons in the original sample λ can be calculated. All data analysis was carried out using Matlab (The MathWorks, USA).

2.4.12 Fibril Quantification by AFM

The number of fibrils per unit volume of the standard fibril sample was estimated from AFM length distribution and mass conservation. The distribution of fibrils $N_i(L)$ as a function of the contour length measured by AFM is shown in Figure 2.6b. This distribution is essentially the same distribution of fibrils per unit volume, differing by a mere normalisation constant α, so that the distribution of fibrils per unit volume is simply $\alpha N_i(L)$. The constant α can be obtained from the total mass per unit volume,

which is obtained from the initial molar concentration of monomer c_m, i.e. $c_m MW$. Therefore, by mass conservation this results in

$$\sum \alpha N_i(L) \cdot L_i \pi r^2 \rho = c_m MW, \tag{2.5}$$

where ρ is the density of the monomer and the fibril, that are assumed here to be identical. This then gives $\alpha = \frac{c_m MW}{\sum N_i(L) \cdot L_i \pi r^2 \rho}$, since all the terms on the right hand are known.

The total number of fibrils per unit volume, $\frac{N_f}{V}$, is then

$$\frac{N_f}{V} = \sum \alpha N_i(L) = \alpha \sum N_i(L) = \frac{c_m MW}{\pi r^2 \rho \sum N_i(L) \cdot L_i} \sum N_i(L), \tag{2.6}$$

where both $\sum N_i(L) \cdot L_i$ and $N_i(L)$ are known from the distribution of fibrils as a function of the contour length in Figure 2.6b.

3 Real-Time Quaking-Induced Conversion Assay

3.1 Introduction

The real-time quaking-induced conversion (RT-QuIC) assay is a sensitive assay for the detection of the misfolded form of the prion protein (PrP^{Sc}). It is based on the self-propagation properties of PrP^{Sc}, which stimulates the conversion of PrP^{C} into PrP^{Sc}. Monomeric full-length hamster prion protein ($HaPrP_{23-231}$) as a substrate of the amplification reaction is converted into large aggregates through PrP^{Sc}. The PrP^{Sc} aggregates are amplified through cyclic shaking, which fragments the aggregates into smaller propagons and catalyses the conversion of monomeric PrP.
In this thesis I describe the establishment and different applications of the RT-QuIC assay to detect PrP^{Sc} in human brain tissues and cerebrospinal fluid (CSF) for CJD diagnostics, in murine cerebellar organotypic slice cultures, and on the metal surface of PrP^{Sc}-coated steel beads.

Parts of this chapter (section on RT-QuIC with cerebellar organotypic cultured slices) are reproduced or quoted verbatim from the following article published by PLoS One on September 29, 2016:
Neurotoxic Antibodies against the Prion Protein Do Not Trigger Prion Replication
Karl Frontzek, Manuela Pfammatter, Silvia Sorce, Assunta Senatore, Petra Schwarz, Rita Moos, Katrin Frauenknecht, Simone Hornemann, Adriano Aguzzi
doi: 10.1371/journal.pone.0163601, https://doi.org/10.1371/journal.pone.0163601

3.2 Results

3.2.1 Expression and Purification of Hamster Prion Protein

A prerequisite for the RT-QuIC assay is the high purity of the substrate protein needed for conversion. Towards this goal a gene block encoding the hamster (*Mesocricetus auratus*) prion protein gene was cloned into the pRSET A expression vector using the NdeI and EcoRI restriction sites. The protein was overexpressed in *E. coli*, and the purification protocol was optimised for high production yields. Briefly, the protein was isolated from inclusion bodies and purified by Ni^{2+}-nitriloacetic acid (Ni-NTA) affinity chromatography (**Fig. 3.1a**, see Materials and Methods for more details). The identity of the purified protein was confirmed by electrospray ionisation mass spectrometry (ESI-MS; **Fig. 3.1b**). The peak at m/z 23,102 corresponded to the molecular mass of $HaPrP_{23-231}$ (expected MW: 22,973 Da, + 131 Da for methionine, - 2 Da oxidation of cysteines = 23,102 Da). The purity of the sample was analysed by SDS-PAGE (**Fig. 3.1c**). The average purification yield was 50 mg of highly pure $HaPrP_{23-231}$ per litre of bacterial culture.

3.2.2 Diagnostic RT-QuIC

The highly specific and sensitive amplification of PrP^{Sc} makes the RT-QuIC a useful tool for the reliable and accurate diagnosis of Creutzfeldt-Jakob disease (CJD). The methodology was adapted to test patient samples such as brain tissue or CSF for the presence of PrP^{Sc}. In the CSF RT-QuIC small amounts of PrP^{Sc} in patient CSF convert monomeric PrP into detectable PrP^{Sc} aggregates. It therefore allows the discrimination of CSF samples from sCJD patients containing pathological PrP^{Sc} aggregates from CSF samples from healthy donors.

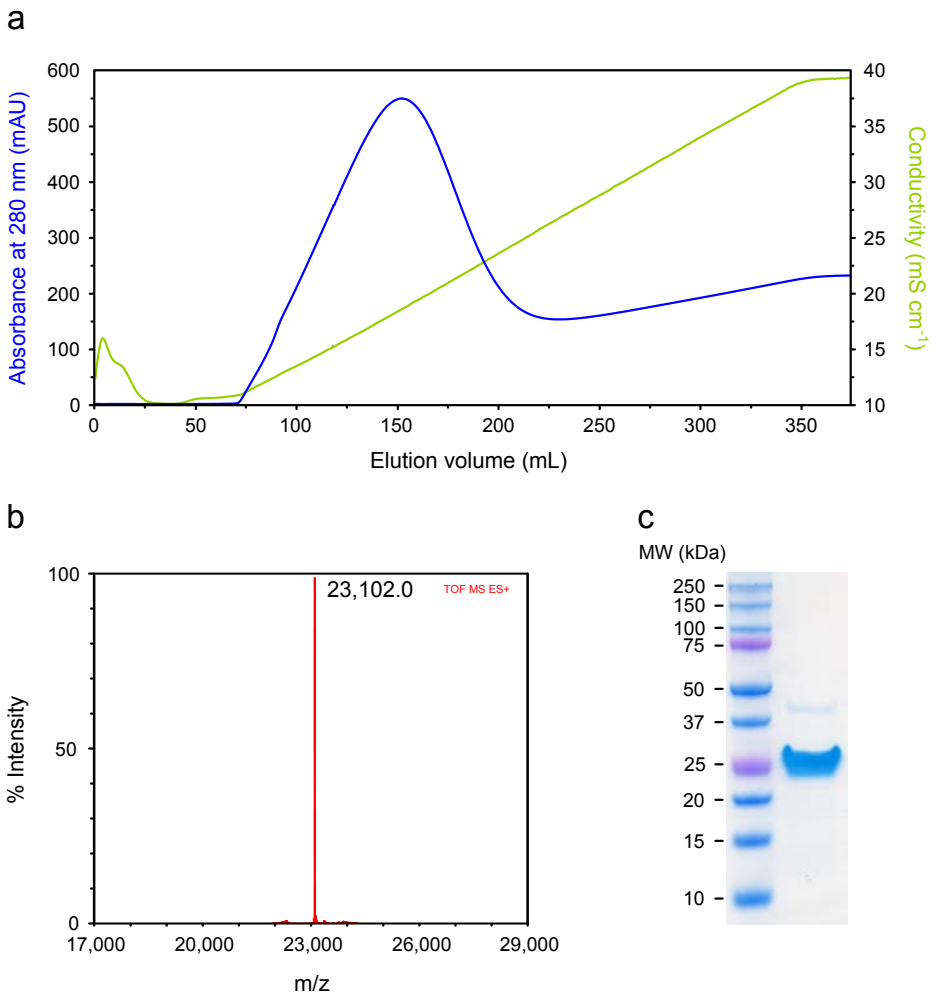

Fig. 3.1.: Production and characterisation of HaPrP$_{23-231}$. (a) Elution profile of Ni-NTA affinity purification. (b) ESI-MS of purified HaPrP$_{23-231}$ (expected molecular weight 22,973 Da + 131 Da - 2 Da = 23,102 Da). (c) SDS-PAGE purity analysis of HaPrP$_{23-231}$. The gel was stained with Coomassie protein stain (InstantBlue, Expedeon).

Ring Trial Validation

The RT-QuIC was initially validated with human CSF samples provided by the National CJD Research & Surveillance Unit (NCJDRSU), Edinburgh, UK. Similar as in the international ring trial conducted by the NCJDRSU previously, ten blinded CSF samples were analysed by RT-QuIC (**Fig. 3.2**) using experimental and instrumental parameters as published by the NCJDRSU (McGuire et al., 2016). All samples were analysed using both the substrate HaPrP$_{23-231}$ provided by the NCJDRSU as well as with in-house produced HaPrP$_{23-231}$. CSF samples with 3 or 4 positive RT-QuIC responses out of 4 replicate reactions were diagnosed as RT-QuIC positive. Out of

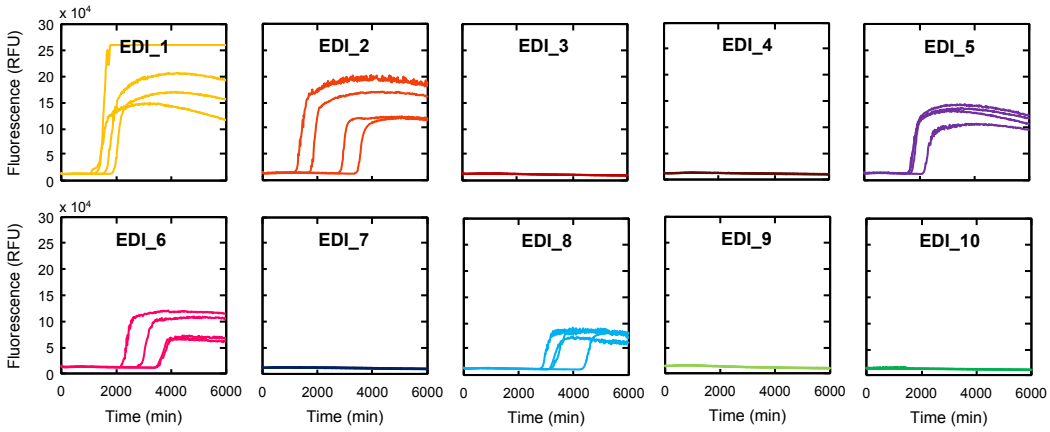

Fig. 3.2.: RT-QuIC analysis of human CSF samples from the NCJDRSU ring trial. Real-time ThT fluorescence time courses of RT-QuIC reactions seeded with of human CSF samples provided by the NCJDRSU. All reactions were seeded with 30 µL of CSF and performed in quadruplicate.

ten blinded samples, five were found to be RT-QuIC positive (EDI_1, 2, 5, 6, 8) and five were RT-QuIC negative (EDI_3, 4, 7, 9, 10). All samples were unambiguously positive (4/4 replicates positive) or negative (0/4 replicates positive). The RT-QuIC results were compared to the clinical diagnoses provided by the NCJDRSU (**Tab. 3.1**). All samples coincided with the corresponding clinical diagnosis. This validation experiment showed that the RT-QuIC assay was successfully transferred to our laboratory, and that the method can be used to accurately and reliably diagnose sCJD from CSF samples.

Patient ID	Gender	Age	Diagnosis	RT-QuIC Result
EDI_1	f	67	probable sCJD	positive
EDI_2	f	70	probable sCJD	positive
EDI_3	m	73	not CJD	negative
EDI_4	m	82	not CJD	negative
EDI_5	m	75	probable sCJD	positive
EDI_6	m	68	confirmed sCJD	positive
EDI_7	m	72	not CJD	negative
EDI_8	f	64	probable sCJD	positive
EDI_9	f	44	not CJD	negative
EDI_10	m	61	not CJD	negative

Tab. 3.1.: Demographic data, clinical diagnosis and results of the RT-QuIC analysis of CSF samples from ring trial. Samples were provided by the National CJD Research & Surveillance Unit, Edinburgh, United Kingdom.

sCJD Diagnostics

The CSF 14-3-3 protein is a surrogate marker for neuronal degeneration. Although widely used for the premortem clinical diagnosis of CJD, it is not entirely specific (Collins et al., 2000; Zerr et al., 2009). To complement this lack in specificity, the CSF RT-QuIC was implemented as a tool for diagnosing CJD. The assay was further validated by testing autopsy-confirmed brain tissue and CSF samples of our brain biobank (**Fig. 3.3**). All RT-QuIC test results were consistent with the neuropathological, definite diagnoses, and the CSF RT-QuIC assay has since been included in the diagnosis of suspected CJD cases.

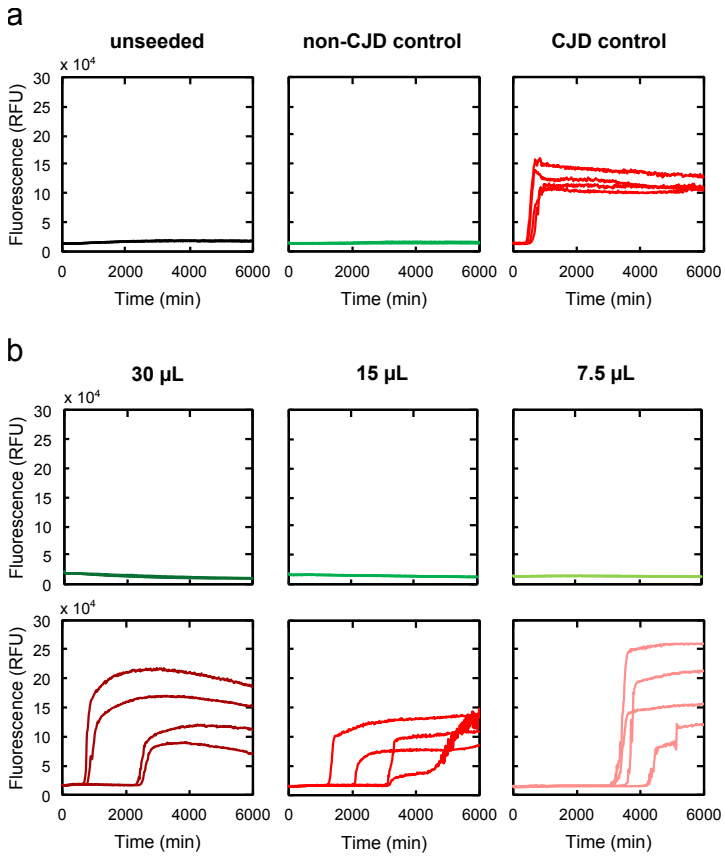

Fig. 3.3.: Example results of diagnostic CSF RT-QuIC. (a) Plate controls included on every RT-QuIC experiment. Unseeded RT-QuIC reaction (*black*), brain homogenate of a patient with CJD diagnosis excluded (*green*), brain homogenate of a patient with confirmed CJD (*red*). (b) RT-QuIC results of a CJD-negative patient (*upper panel, green*) and a CJD-positive patient (*lower panel, red*). All CSF samples were tested in quadruplicate using three different volumes (30, 15, 7.5 µL) of CSF in the reaction mixture.

3.2.3 Steel Beads RT-QuIC

Prions are highly resistant to conventional decontamination and sterilisation procedures (Taylor, 2000). Additionally, prions strongly adsorb to stainless steel surfaces and can transmit infectivity via steel surfaces (Zobeley et al., 1999; Flechsig et al., 2001). These properties increase the risk of iatrogenic prion transmission from contaminated surgical stainless steel instruments. To date, there are no effective and practical decontamination treatments for surgical steel surfaces. Daniel Heinzer and colleagues (Institute of Neuropathology, University Hospital Zurich) have been testing new prion decontaminating formulations developed for the inactivation of pathological prions on medical instruments in collaboration with Borer Chemie AG (Zuchwil). Stainless steel beads coated with mouse prions were used to study the effect of different decontamination formulations on prion infectivity. Daniel Heinzer and colleagues developed a cell-based prion infectivity assay to assess the decontamination efficiency of the new formulations. In addition, I adapted the RT-QuIC assay to test propagation activity of steel surface-bound prions inactivated with decontamination reagents.

Development of a Steel Beads RT-QuIC

Introducing prion-coated steel beads in the RT-QuIC reaction might affect the conversion reaction in various ways. The beads might cause false positive aggregation by introducing shear forces to the system or through the exposure of additional surfaces. Alternatively, the beads might interfere with the template-catalysed conversion of PrP^{C} into the aggregated prion protein. In a first proof-of-concept experiment, the effect of steel beads on the RT-QuIC reaction mixture was studied. Therefore, Daniel Heinzer and colleagues treated steel beads with 1% non-infectious brain homogenate (NBH) and 1% prion-infected brain homogenate from the Rocky Mountain Laboratory strain (RML), respectively, and washed them thoroughly with PBS to remove unbound infectivity. I then added the beads to the RT-QuIC reaction mixture to investigate their effect on the conversion (**Fig. 3.4**). While both untreated beads as well as NBH-coated beads did not cause any aggregation in the RT-QuIC,

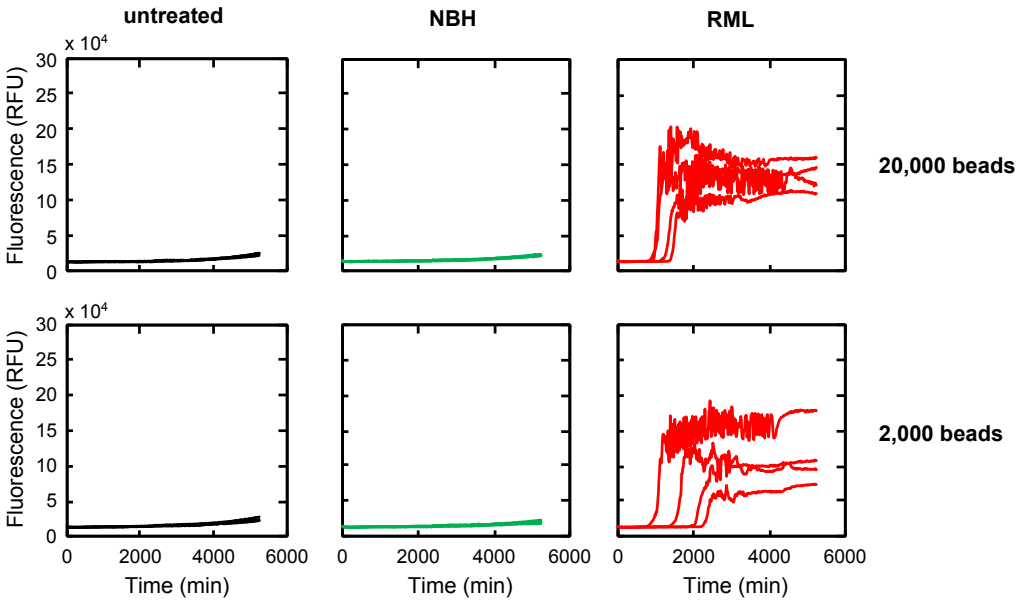

Fig. 3.4.: Proof-of-concept steel beads RT-QuIC. 20,000 (*upper panel*) and 2,000 (*lower panel*) untreated (*black*), NBH-coated (*green*) and RML-coated (*red*) stainless steel beads were used as seeds in the RT-QuIC assay. ThT fluorescence was recorded every 15 min over the course of 90 h. All reactions were performed in quadruplicate.

RML-treated beads were able to seed the conversion of PrP^{C} into PrP^{Sc} efficiently. When seeded with either 20,000 or 2,000 RML-coated steel beads, all four replicate RT-QuIC reactions showed a significant increase in ThT fluorescence, indicating the amplification of protein aggregates through seeding. These results led to the conclusion that introducing steel beads into the RT-QuIC did not interfere with the conversion reaction.

To optimise the number of beads used per well, I tested different bead numbers in the assay. Between 200,000 and 250 NBH- and RML-coated beads were added to the RT-QuIC reaction mixture (**Fig. 3.5**). At bead numbers higher than 50,000 beads, all four replicates of the RT-QuIC reactions seeded with RML-coated beads showed an increase in ThT fluorescence indicating the seeded conversion of prion aggregates. At 1,000 and 500 beads, only 2 and 1 replicate reactions, respectively, were RT-QuIC positive. Seeding with 250 RML-coated steel beads was not efficient, in that it did not show any positive ThT signal. NBH-coated steel beads did not cause any seeded conversion. However, at the highest bead number, a false positive RT-QuIC signal was detected for one out of four replicate reactions. The false positive

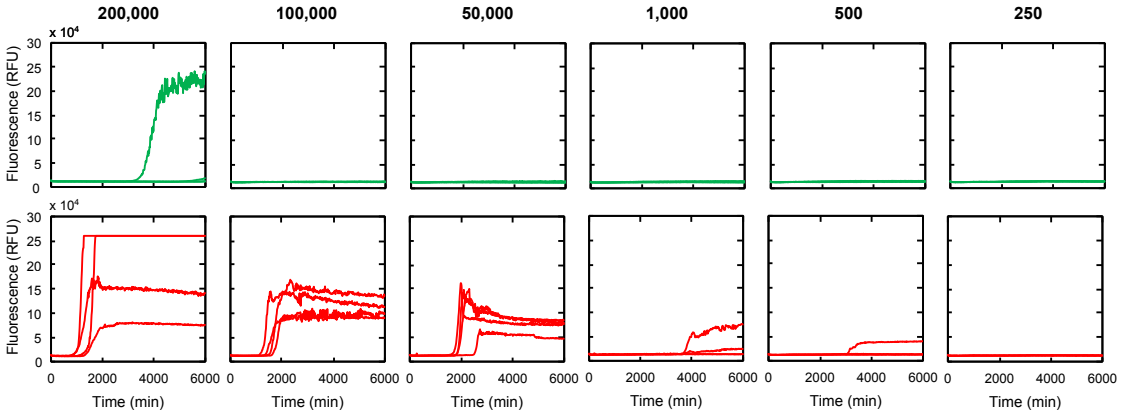

Fig. 3.5.: Steel beads RT-QuIC with different numbers of NBH- (*upper panel, green*) and RML-coated beads (*lower panel, red*). Between 200,000 and 250 NBH- and RML-coated beads were added to the RT-QuIC reaction mixture. ThT fluorescence was recorded every 15 min over the course of 105 h. All reactions were performed in quadruplicate.

signal was most likely caused by seed-independent aggregation initiated by a strictly monomer-dependent primary nucleation event. The spontaneous generation of PrP aggregates through the nucleation of monomeric PrP^C might have been catalysed by the metal surface of the beads as proposed earlier (Edgeworth et al., 2010). To minimise the risk of false positive ThT signals and thus false positive RT-QuIC results, the bead number for further RT-QuIC analyses was set to 100,000 and 10,000 beads per well. These bead numbers should be high enough to detect prions adsorbed to the bead surface, while preventing false positive results provoked by the beads.

In a next step, the steel beads RT-QuIC was validated using standard protocols for prion decontamination. 100,000 and 10,000 RML-coated beads treated with either NaOH (1 M for 2 h at room temperature) or SDS (3% for 10 min at 95 °C) were assessed using the RT-QuIC assay (**Fig. 3.6**). Bead samples decontaminated with NaOH failed to seed the RT-QuIC reaction after treatment, which confirms the prion decontamination efficiency of NaOH. In contrast, samples treated with SDS showed only partial decontamination. While no positive signal was detected in the RT-QuIC reactions seeded with 10,000 steel beads, all four replicate reactions seeded with 100,000 beads were RT-QuIC positive. These results are in agreement with previously published data (Mori et al., 2016), and thus validate the applicability

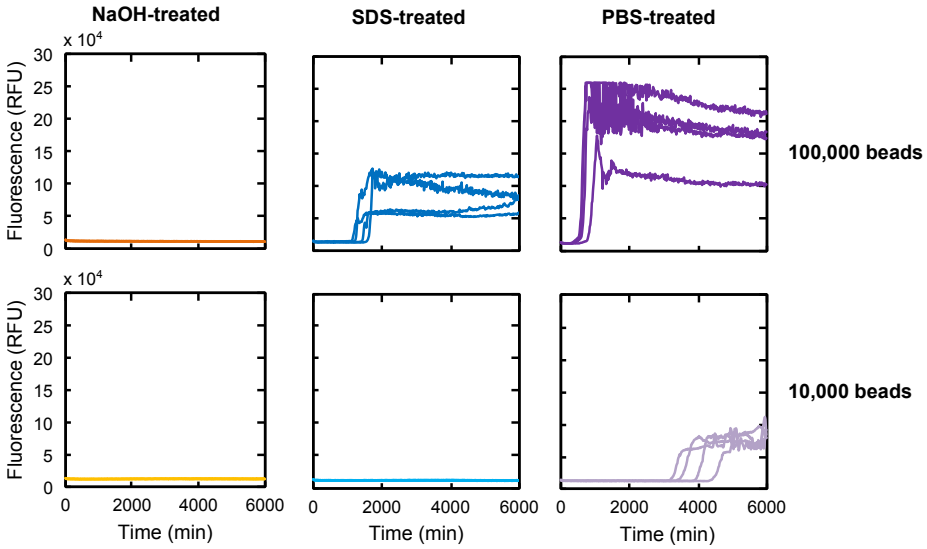

Fig. 3.6.: Validation of steel beads RT-QuIC with standard prion decontamination protocols. 100,000 (*upper panel*) and 10,000 (*lower panel*) RML-coated beads were treated with 1 M NaOH for 2 h at room temperature (*orange*), with 3% SDS for 10 min at 95 °C (*blue*), or with PBS for 10 min at 95 °C (*purple*), and added to the RT-QuIC reaction mixture. ThT fluorescence was recorded every 15 min over the course of 105 h. All reactions were performed in quadruplicate.

of the steel beads RT-QuIC for the study of prion decontamination reagents on steel bead surfaces.

Screening of Prion Decontamination Formulations

In a first test, the decontamination efficiency of seven commercially available products (**Tab. 3.2**) was assessed using the steel beads RT-QuIC. Therefore, the seeding activity of RML-coated steel beads treated with the commercial decontamination formulations was evaluated (**Fig. 3.7**). Only one of the tested products (PR-7, ALKAPHARM ALKA 100) efficiently inactivated prions adsorbed to the steel beads, evident by the complete abolishment of seeding activity in the RT-QuIC. Beads treated with other products either showed a slight reduction in the seeding activity as only a fraction of the four replicate reactions showed a positive ThT signal at late time points (PR-2, PR-4, PR-6) or had no effect on the RT-QuIC reaction (PR-1, PR-3, PR-5). This suggests that the majority of the commercially available cleaning products for prion decontamination show an insufficient prion decontamination activity.

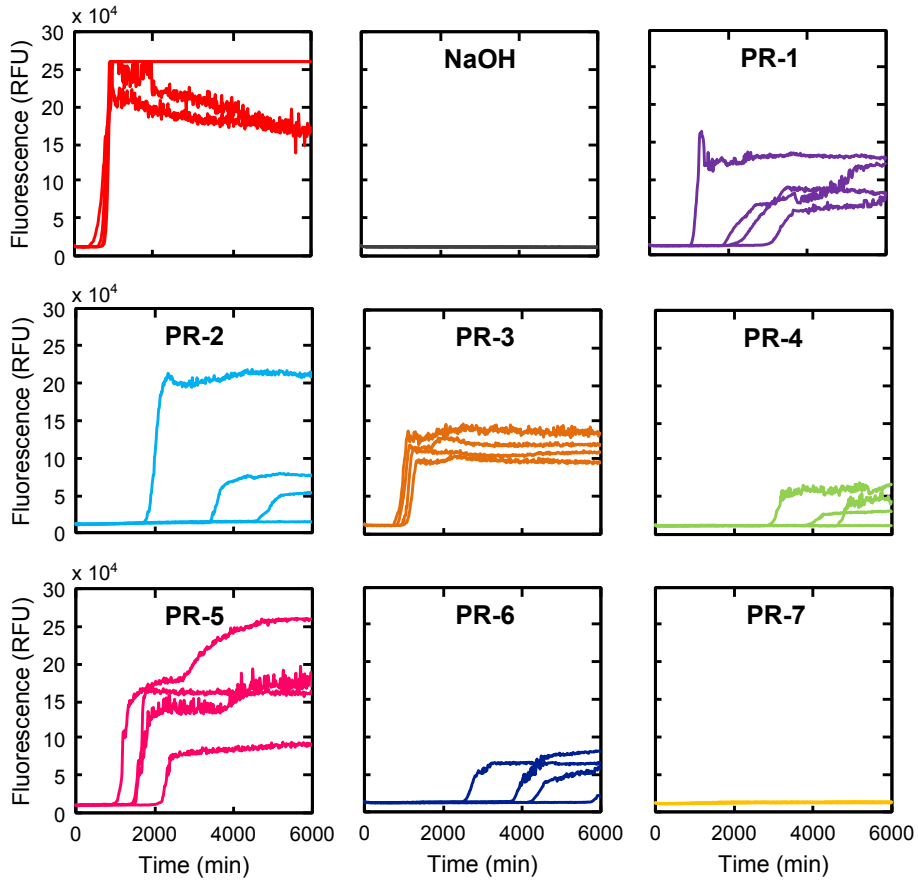

Fig. 3.7.: Steel beads RT-QuIC with prion-coated steel beads inactivated with commercially available decontamination products. 100,000 RML-coated steel beads were treated with seven commercially available prion decontaminants for 10 min at 55 °C, and added to the RT-QuIC reaction. Untreated RML (*red*) and RML treated with NaOH for 2 h at room temperature (*grey*) were used as controls. ThT fluorescence was recorded every 15 min over the course of 105 h. All reactions were performed in quadruplicate.

Product	Product ID	Manufacturer	Concentration
Deconex 28 Alka One-X	PR-1	Borer Chemie AG	0.5%
Deconex Prozyme Alka 2.0	PR-2	Borer Chemie AG	0.5%
Deconex Power Zyme	PR-3	Borer Chemie AG	0.5%
Neodisher Septoclean	PR-4	Dr. Weigert	0.5%
Deconex TWIN PH10 & Zyme	PR-5	Borer Chemie AG	0.3 & 0.2%
ACTANIOS WD	PR-6	Laboratoires ANIOS	0.5%
ALKAPHARM ALKA 100	PR-7	ALKAPHARM	0.5%

Tab. 3.2.: Commercial prion decontamination products, product ID, manufacturer and concentrations. All products were provided by Borer Chemie AG.

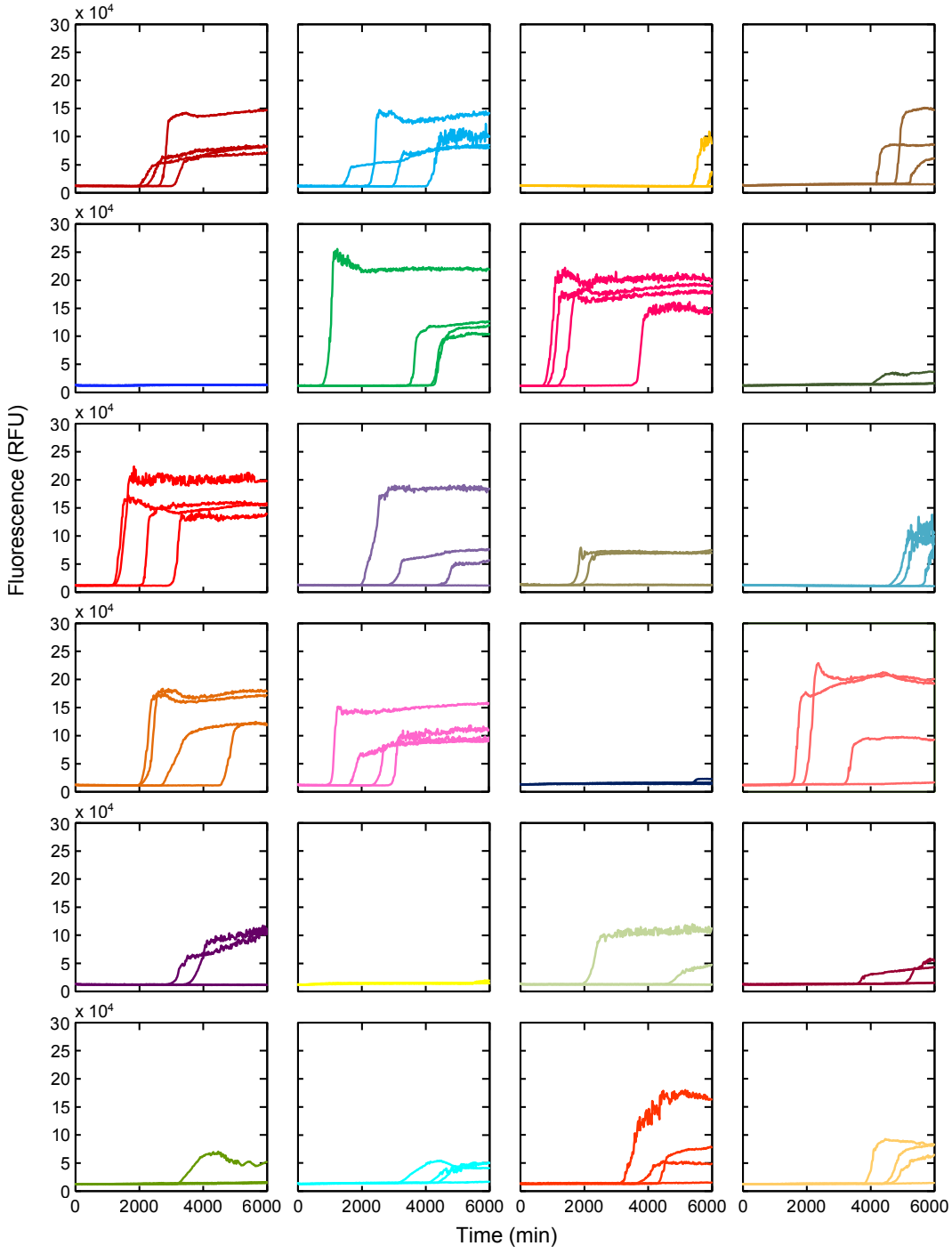

Fig. 3.8.: Example RT-QuIC screening of 24 newly developed prion decontamination formulations. 100,000 RML-coated steel beads were treated with formulations for 10 min at 55 °C, and their efficiency was assessed using RT-QuIC. ThT fluorescence was recorded every 15 min over the course of 105 h. All reactions were performed in quadruplicate. The formulations were synthesised by Borer Chemie AG (Zuchwil).

In a collaborative project, Daniel Heinzer and Borer Chemie AG aimed at developing a practically applicable product for highly efficient prion decontamination of surgical steel surfaces. As part of this project, we used the steel beads RT-QuIC to screen a total of more than 100 different formulations provided by Borer Chemie AG for their efficiency to inactivate prions on metal surfaces (**Fig. 3.8**). The most efficient formulations from every screening round were adapted and improved by Borer Chemie AG and subjected to further screenings. Formulation 10299.70B at a concentration of 0.5% was found to be the most efficient formulation for prion inactivation. It is composed of sodium hypochlorite, tetrapotassium pyrophosphate, dipotassium trioxosilicate and phosphonate. The efficiency of the formulation was further tested using different treatment times ranging from 5 to 30 min (**Fig. 3.9**). A 5 min treatment at 55 °C was sufficient to completely abolish seeding activity of RML-coated beads in the RT-QuIC. This decontamination efficiency was comparable to a 2 h treatment with 1 M NaOH at room temperature, a standard protocol for prion decontamination. The formulation has great potential as a practically applicable decontamination product in surgical steel cleaning. The decontamination efficiency of the lead formulation is further being tested and validated in a cell-based infectivity assay and in a mouse bioassay by Daniel Heinzer and colleagues.

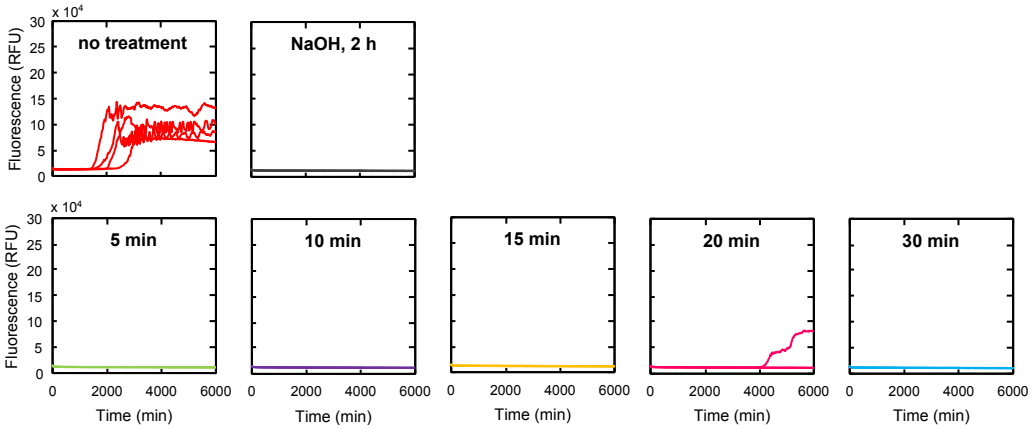

Fig. 3.9.: Efficiency of lead formulation 10299.70B assessed by RT-QuIC. 100,000 RML-coated steel beads were treated with formulation 10299.70B for different treatment times at 55 °C (*lower panel*). Untreated beads coated with RML (*upper panel, red*) and RML-coated beads treated with NaOH for 2 h at room temperature (*upper panel, grey*) were used as controls. The treatment efficiency was assessed using the RT-QuIC assay. ThT fluorescence was recorded every 15 min over the course of 105 h. All reactions were performed in quadruplicate.

3.2.4 RT-QuIC with Cerebellar Organotypic Cultured Slices

Antibodies directed against the globular domain of the cellular prion protein (aa 124-230) exert neurotoxic effects similar to those observed upon prion infection (Sonati et al., 2013; Reimann et al., 2016). The neurotoxic effects are mediated by an effector domain, the flexible tail at the N-terminus (aa 23-123) of PrP^{C} (Sonati et al., 2013). Binding of antibodies to the globular domain is thought to cause a conformational change in the flexible tail region relative to the cell membrane (Sonati et al., 2013), which activates a pathogenic cascade of intracellular processes leading to neurodegeneration (Herrmann et al., 2015). Due to the fact that globular domain binders induce neurodegeneration similar to prion infection, the question arises whether such antibodies activate prion self-replication processes leading to the conversion of cellular PrP^{C} to the scrapie isoform PrP^{Sc}.

Karl Frontzek and colleagues (Institute of Neuropathology, University Hospital Zurich) investigated whether the neurotoxic anti-prion antibody POM1 induces formation of de novo PrP^{Sc} (Frontzek et al., 2016). Karl Frontzek treated cerebellar organotypic cultured slices (COCS) of *tg*a20 mice with POM1 leading to neurodegeneration in brain slices. He then analysed the POM1-treated COCS homogenates for the presence of newly formed, proteinase K (PK) resistant PrP^{Sc}. In his analyses, he did not detect any PK-resistant PrP^{Sc} in Western blot following PK digestion. In addition, no PrP^{Sc} replication was observed in prion-susceptible CNS-derived CAD5 cells treated with POM1 COCS homogenates, and PrP-overexpressing *tga20* inoculated with POM1-treated COCS homogenates did not show any signs of a neurological disease (data published in Frontzek et al., 2016).

To further confirm these findings, we assessed the propagation activity of homogenates of POM1-treated *tg*a20 COCS using the RT-QuIC assay (**Fig. 3.10**). The RT-QuIC reactions were seeded with homogenates of COCS treated with single chain variable fragments of POM1 (scFvPOM1) or scFvPOM1 saturated with recombinant prion protein (recPrP) antigen (scFvPOM1+recPrP). NBH- and RML-treated COCS homogenates were used as controls. Neither the scFvPOM1- nor the (scFvPOM1+recPrP)-treated COCS homogenates showed any positive RT-QuIC

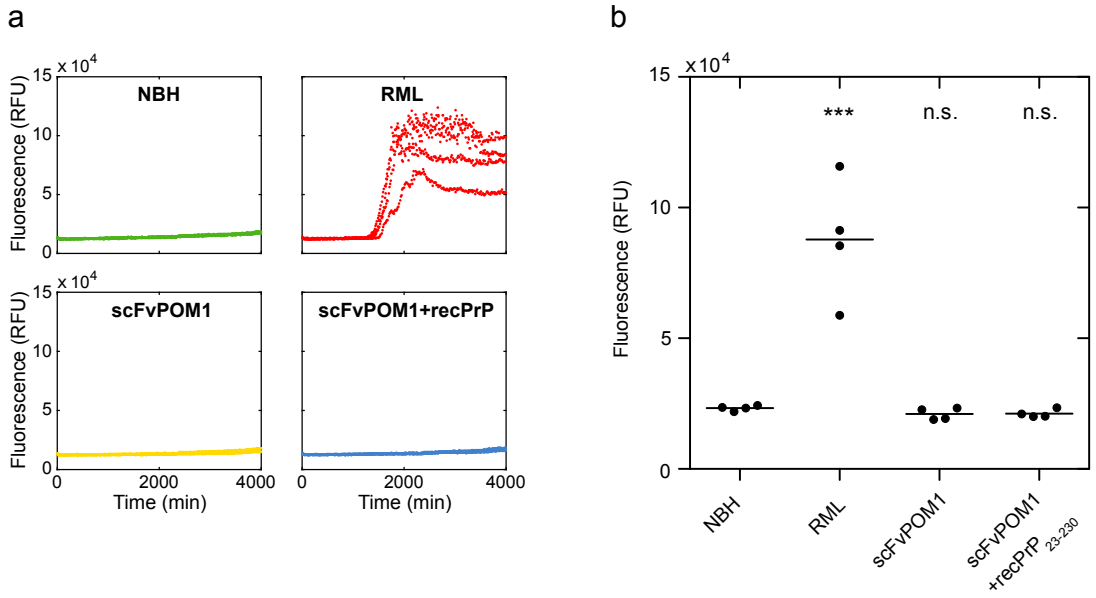

Fig. 3.10.: RT-QuIC analysis of POM1-treated *tg*a20 COCS homogenates. (a) Real-time ThT fluorescence time courses of RT-QuIC reactions seeded with 2 µL of NBH- (*green*), RML- (*red*), scFvPOM1- (*yellow*) or (scFvPOM1+recPrP)-treated (*blue*) COCS homogenates. NBH- and RML-treated homogenates were used as positive and negative controls, respectively. All reactions were performed in quadruplicate. (b) Fluorescence endpoint values of the RT-QuIC reactions. Horizontal lines indicate group means. Data were statistically analysed using a one-way analysis of variance (ANOVA) followed by Dunnett's multiple comparison testing (*** $p < 0.001$, n=4). Panel (a) was adapted from Frontzek et al., 2016 under the terms of the Creative Commons Attribution License.

reaction. In contrast, COCS homogenates treated with RML showed an increase in the ThT fluorescence after approximately 24 h. These findings indicated the absence of propagation-active PrP^{Sc} in POM1-treated COCS homogenates. Along with the results from the PK Western blot, the cell-based assay and the mouse bioassay, these results show that neurotoxic antibodies targeting the globular domain of PrP do not induce self-replication of prions, but rather act downstream of prion self-replication.

3.3 Discussion and Outlook

Diagnostic RT-QuIC

I successfully established the real-time quaking-induced conversion (RT-QuIC) assay for the detection of PrP^{Sc} aggregates in tissue samples. Recombinant hamster PrP was used as substrate for PrP^{Sc}-dependent conversion. Small amounts of pathological aggregates in patient samples induced the conversion of the substrate protein into detectable aggregates, thereby allowing the diagnosis of CJD from CSF samples or brain tissue. After the establishment and validation of the method with CSF samples of known, neuropathologically confirmed diagnostic status, the assay was implemented in the diagnostic analysis of suspected CJD cases.

Diagnostic assays require a high degree of robustness and reliability. Two multicentre studies have assessed the reproducibility of the diagnostic CSF RT-QuIC across different laboratories (Cramm et al., 2016; McGuire et al., 2016). In international, blinded ring trial studies they were able to demonstrate almost complete conformity of the RT-QuIC test results among different laboratories, and calculated a sensitivity of 85–100% and a specificity of 99–100% (Cramm et al., 2016; McGuire et al., 2016). Ring trial samples tested in our laboratory confirmed these findings. All CJD samples were correctly identified, and no false positive RT-QuIC reactions were detected for any of the non-CJD samples. Due to the high diagnostic significance of the assay, many efforts were undertaken recently to further improve and standardise the RT-QuIC assay (Cheng et al., 2014; Orrú et al., 2015; Orrú et al., 2016; Groveman et al., 2017). Faster conversion and enhanced detection of PrP^{Sc} was achieved with an N-terminally truncated PrP substrate, higher assay temperature or altered solution conditions (Orrú et al., 2015; Cheng et al., 2014). Besides that, attempts to apply more practical and less invasive procedures of sample collection resulted in the use of olfactory epithelium samples from nasal brushings (Orrú et al., 2014). Although not yet standardised, this method holds a great potential for future diagnostics, as nasal brushings represent a much less invasive intervention than lumbar puncture or brain biopsies.

One of the practical limitations of the diagnostic CSF RT-QuIC is its low throughput. Working with quadruplicates, a 96-well microplate provides space for 21 CSF samples and 3 control reactions. The long assay duration of 120 h limits the assessment to one assay plate a week. The assay could be further improved by adapting it to a 384-well format to allow higher throughput. A different microplate format would, however, require adaptation of the assay conditions to account for altered reaction volume and surface-volume ratio.

By analogy, the digital amyloid amplification assay described in the previous chapter could be extended to the RT-QuIC. Rather than relative quantification (Takatsuki et al., 2015; Henderson et al., 2015), the RT-QuIC could yield exact numbers of PrP^{Sc} propagons. Relating the propagon numbers to clinical symptoms might reveal interesting aspects of disease progression, and advance our understanding of prion disease spreading.

Steel Beads RT-QuIC

As a further application of the RT-QuIC assay, I adapted the conventional protocol to detect prions adsorbed to stainless steel surfaces. The detection of prions bound to steel beads allowed the assessment of different prion decontaminants in inactivating prions on surgical steel surfaces. Possible side effects of the beads on the RT-QuIC conversion reaction were excluded, and the optimal number of beads used to seed the reaction was determined. At very high bead numbers, false positive RT-QuIC reactions were detected. This effect is likely to be caused by the large metal surface in the assay as was previously reported in a study assessing prions bound to steel wires using a cell-based scrapie assay (Edgeworth et al., 2010). However, at lower bead numbers no false positive RT-QuIC reactions were observed.

As a validation of the steel beads RT-QuIC assay, we assessed the propagation-activity of RML-coated beads treated with two common prion inactivation procedures, 1 M NaOH and 3% SDS. Beads treated with NaOH abolished all propagation activity, while beads treated with SDS showed a reduced propagation activity when compared with untreated beads. These findings are in agreement with a recent study assessing prion decontamination of steel wires using the RT-QuIC method, in which

prions were completely inactivated by NaOH treatment but only partially inactivated by SDS treatment (Mori et al., 2016). In contrast, earlier findings reporting complete inhibition of prion transmissibility upon treatment with SDS (Tateishi et al., 1991) were not confirmed, and corresponding guidelines for decontamination will need to be revisited.

Prior to the screening of newly generated formulations with potential prion decontamination properties, the efficiency of a set of 7 commercially available decontaminants was tested with the steel beads RT-QuIC. Surprisingly, two (ACTANIOS WD, Neodisher Septoclean) of the three strongly alkaline formulations classified as prion inactivating by the french 'Agence nationale de sécurité du médicament et des produits de santé (ANSM, 2015)', did not show any inactivation in the RT-QuIC assay. The only efficient decontaminant was ALKA 100. On the basis of these findings, Borer Chemie AG (Zuchwil) developed new formulations with potential prion decontamination properties, which were assessed using the steel beads RT-QuIC. One efficient lead formulation was identified with RT-QuIC, and will be further validated in a cell-based infectivity assay and in a mouse bioassay.

One of the technical challenges of the steel beads RT-QuIC is the accurate pipetting of beads. The adhesion of the beads to a variety of surfaces is a source of errors, which might affect accuracy of the assay. The loss of beads in every pipetting step leads to an actual number of beads lower than the calculated number. To minimise the error, we used the exact same pipetting steps for every sample thereby reducing the variability between samples. Even though the propagation activity was reproducible for replicate reactions of most experiments, variability in the lag times of the replicates was observed in some experiments. A possible way to account for this technical issue is to perform log reduction experiments in which beads coated with serial dilutions of RML are treated with different formulations. Comparison with the dilution series of untreated beads would reveal the log reduction in propagation activity upon decontamination treatment.

RT-QuIC with Cerebellar Organotypic Cultured Slices

The main scientific application of the RT-QuIC is the investigation of prion propagation activity. Using the RT-QuIC assay with homogenates of cerebellar organotypic cultured slices, we were able to confirm the finding that neurotoxic anti-prion antibodies directed against the globular domain of PrP^{C} did not induce PrP^{Sc} self-replication. A methodologically similar organotypic slice culture assay coupled with RT-QuIC (OSCAR) was published a few month after our report. The publication confirmed that the combination of organotypic slice culture with RT-QuIC represents an efficient way of determining prion propagation activity (Kondru et al., 2017)

Generally, the RT-QuIC assay can be used to assess prion self-propagation in mouse brain homogenate. The effect of various genes on prion replication can be investigated by knocking out the respective gene in a transgenic mouse infected with RML and assessing PrP^{Sc} activity in the brain of the knockout animal. New CRISPR/Cas gene editing tools have drastically facilitated the generation of knockout mouse models. In combination with the assessment of PrP^{Sc} self-replication by RT-QuIC this might become a powerful approach to build our understanding of the basic principles of prion replication.

3.4 Materials and Methods

3.4.1 Construction of Plasmid Encoding the Gene for HaPrP$_{23-231}$

A geneblock encoding full-length (23-231) hamster PrP (Genescript) was cloned into the pRSET A expression vector (Invitrogen) using the NdeI and EcoRI restriction sites. The sequence of the construct was verified by automated Sanger sequencing at Microsynth (Balgach, Switzerland).

3.4.2 Expression and Purification of Hamster Prion Protein

HaPrP$_{23-231}$ was expressed in Rosetta2(DE3)pLysS *E.coli* cells in Overnight Express Instant Terrific Broth (TB) Medium (Merck Novagen) containing 100 µg mL^{-1} carbenicillin and 34 µg mL^{-1} chloramphenicol for 26 h at 30 °C and 90 rpm. Cells were harvested by centrifugation (10,000 *g*, 5 min, 4 °C), and lysed by two freeze-thaw cycles. Cytoplasmic inclusion bodies were then washed twice with 1X and twice with 0.1X BugBuster Protein Extraction Reagent (Novagen) and solubilised in 8 M GdmCl (pH 8.0). After another centrifugation step at 17,000 *g* for 10 min, the supernatant was subjected to an affinity chromatography using Ni^{2+}-nitrilotriacetic acid Superflow resin (QIAGEN). The protein was refolded and purified on column by running a linear gradient from 100 mM NaH_2PO_4, 10 mM Tris-HCl, 6 M GdmCl (pH 8.0) to 100 mM NaH_2PO_4, 10 mM Tris-HCl (pH 8.0) over 3.5 h. After elution with a linear gradient to pre-cooled 500 mM imidazol, 100 mM NaH_2PO_4, 10 mM Tris-HCl (pH 6.0), the protein containing fractions were combined and filtered through a 0.2 µm syringe filter. The purified protein was dialysed against 200 mM NaH_2PO_4 (pH 5.8) and concentrated to a final protein concentration of 0.6-0.8 mg mL^{-1} prior to storage at -80 °C.

3.4.3 Real-Time Quaking-Induced Conversion Assay

RT-QuIC assays were performed using recombinant full-length hamster prion protein ($HaPrP_{23-231}$) as substrate for PrP^{Sc}-catalysed conversion as previously described (Wilham et al., 2010). Recombinant HaPrP was filtered using 100 kDa centrifugal filters (Pall Nanosep OD100C34), and adjusted to a final concentration of 0.1 mg mL^{-1} in PBS (pH 7.4, including 130 mM NaCl) containing 170 mM NaCl, 10 µM EDTA, 10 µM thioflavin T in a total reaction volume of 100 µL per well (including seed volume). RT-QuIC reactions were seeded with 2 µL of brain homogenate or 30 µL of CSF. All RT-QuIC reactions were performed in quadruplicate in black 96-well polystyrene microplates (Nunc, Prod. No. 265301) covered with sealing tape (Nunc, Prod. No. 232702). The reactions were amplified over a time period of 105 hours at 42 °C with alternating cycles of 90 s shaking at 900 rpm in double orbital mode and 30 s resting using a FLUOstar Omega microplate reader (BMG Labtech). The amplification of de novo aggregates was followed in real-time by measuring the increase in thioflavin T fluorescence (ex/em 450/480 nm) every 15 min in bottom read mode.

3.4.4 Ring Trial Materials

Recombinant $HaPrP_{23-231}$ and 10 CSF samples for the ring trial were kindly provided by the National CJD Research & Surveillance Unit, Edinburgh, United Kingdom. Of the 10 CSF samples, 1 was from a patient with confirmed sCJD, 4 were from patients with probable sCJD (diagnosed according to the World Health Organisation criteria), and 5 samples were from non-CJD patients. The samples included 6 males and 4 females within the age range of 44 to 82. The samples were shipped on dry ice, and stored at -80 °C until usage. The CSF RT-QuIC with the ring trial samples was performed as described in the section 'Diagnostic CSF RT-QuIC'.

3.4.5 Diagnostic RT-QuIC

Sample handling and processing of brain tissue and cerebrospinal fluid samples are described below. Experimental details of the assay are given in section 'Real-Time Quaking-Induced Conversion Assay'. The results of the diagnostic RT-QuIC were scored positive if 3 or 4 RT-QuIC responses out of 4 replicate reactions were positive; with 0 or 1 positive RT-QuIC response out of 4 replicate reactions, the RT-QuIC result was scored negative.

Brain Tissue Samples

Human brain tissue was obtained from our brain biobank or from autopsies of suspected CJD cases. Aliquots of 10% (w/v) brain homogenate in 0.32 M sucrose were thawed on ice immediately before the RT-QuIC assay. The brain homogenates were diluted 20,000-fold using PBS containing N2 supplement (Thermo Fisher). 2 µL of the diluted brain homogenates were added to the RT-QuIC reaction mixture adding up to a total reaction volume of 100 µL per well.

Cerebrospinal Fluid Samples

Cerebrospinal fluid was obtained from suspected CJD cases. CSF samples were stored at -80 °C and thawed on ice immediately before the RT-QuIC assay. 30, 15 and 7.5 µL of undiluted CSF were added to the RT-QuIC reaction mixture adding up to a total reaction volume of 100 µL per well.

3.4.6 Steel Beads RT-QuIC

All coatings and decontamination treatments of steel beads were performed by Daniel Heinzer. Details can be found in his Master thesis entitled 'Establishing methods to detect surface-bound scrapie prion protein on surgical steel' (Heinzer, 2016).

Steel beads were dissolved in PBS, diluted to the final bead number and stored at -20 °C until usage. To minimise the error in bead number arising from inaccurate

pipetting (some beads adhered to the pipette tips or to the tube walls), all samples were treated identically and diluted using the same dilution steps. In addition, samples were thoroughly mixed to suspend the beads by vigorous vortexing before every pipetting. RT-QuIC was performed as described in the section 'Real-Time Quaking-Induced Conversion Assay'. RT-QuIC reactions were seeded with 30 µL of the bead samples in a total reaction volume of 100 µL.

3.4.7 COCS RT-QuIC

Preparation and treatment of cerebellar organotypic cultured slices were performed by Karl Frontzek as described previously (Frontzek et al., 2016).

RT-QuIC reactions were seeded with 2 µL of scFvPOM1- or (scFvPOM1+recPrP)-treated *tga20* COCS homogenates (0.5 ng μL^{-1} total protein concentration in N2/PBS, diluted 6000-fold from an initial total protein concentration of 3000 µg mL^{-1} of COCS homogenate) in a total reaction volume of 100 µL. NBH- and RML-treated *tga20* COCS homogenates were used as negative and positive controls, respectively.

4 α-Synuclein Amyloid Amplification Assay

4.1 Introduction

The accumulation and inclusion of misfolded α-synuclein is the main hallmark of Parkinson's disease and other α-synucleinopathies. Despite their high abundance in diseased brains, the detection of pathologic aggregates in easily accessible tissues remains elusive. In this chapter, I describe my work to develop an assay for the sensitive detection and quantification of α-synuclein aggregates. The assay is capable of detecting low abundance amyloid aggregates and therefore allows the biochemical diagnosis of α-synuclein aggregation. Furthermore, I applied the assay to investigate the inactivation of α-synuclein aggregates on steel surfaces using different decontamination reagents.

Parts of this chapter are reproduced or quoted verbatim from the following manuscript in preparation:
α-Synuclein Amyloid Amplification Assay for the Absolute Quantification of α-Synuclein Propagons
Manuela Pfammatter, Daniel Heinzer, Rita Moos, Lisa Caflisch, Adriano Aguzzi, and Simone Hornemann
manuscript in preparation

4.2 Results

4.2.1 Expression and Purification of Human α-Synuclein

The production of large amounts of highly pure human α-synuclein represents an essential prerequisite for the development of an α-synuclein amyloid amplification assay. To improve purity and expression yield of the protein, a codon-optimised version of the *SNCA* gene encoding human α-synuclein was cloned into a pRK172 expression vector, and the purification protocol was optimised based on two previously described protocols (Hoyer et al., 2002; Volpicelli-Daley et al., 2014). To avoid dimerisation due to an erroneously incorporated cysteine residue at position 136, the respective codon was mutated from the triplet TAC to TAT (Cys to Tyr) as suggested previously (Masuda et al., 2006). The mutated expression vector was transformed into *E. coli* BL21(DE3)RIL, and cells were grown overnight to induce protein expression. The overexpressed protein was purified from the cytoplasm using a sequence of heat denaturation of unwanted proteins, DNA precipitation, ammonium sulphate ($(NH_4)_2SO_4$) precipitation, anion exchange chromatography (IEC) and size exclusion chromatography (SEC). The purity of the sample was analysed by SDS-PAGE after each purification step (**Fig. 4.1a**). The identity of the purified protein was confirmed by ESI-MS (**Fig. 4.1b**). A single peak at m/z 14,460 indicated the presence of pure human α-synuclein (expected MW: 14,460 Da). The optimised purification protocol resulted in an average yield of 100 mg of pure protein per litre of bacterial culture, which was used as monomeric substrate in the assay and for the reconstitution of preformed fibrillar seeds.

4.2.2 α-Synuclein Standard Fibril Sample

A stable sample of α-synuclein fibrils with reproducible seeding properties is crucial to establish conditions for the specific, template-catalysed amplification of α-synuclein amyloid fibrils. Therefore, an α-synuclein standard fibril sample was generated from recombinant, monomeric α-synuclein. Highly pure, monomeric α-synuclein was

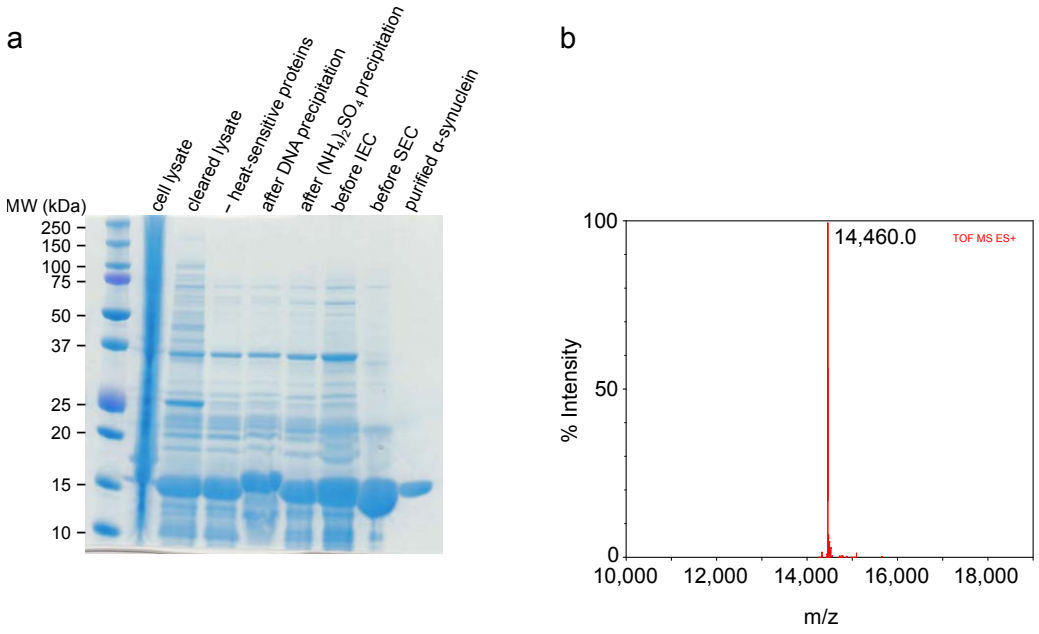

Fig. 4.1.: Purification of recombinantly produced human α-synuclein. (a) SDS-PAGE analysis of samples after every purification step. Highly pure protein obtained after the final purification step is loaded in the rightmost lane. The highly overexpressed protein band indicated by a black arrowhead corresponds to α-synuclein. The gel was stained with Coomassie protein stain (InstantBlue, Expedeon). (b) Electrospray ionisation mass spectrometry of purified α-synuclein (expected molecular weight 14,460 Da).

diluted to 5 mg mL^{-1} using PBS, and incubated at 37 °C, 1000 rpm for 7 days. At the end of the incubation, the sample was visibly turbid, indicative of the formation of fibrils in the sample. To confirm the formation of fibrils and to estimate the fraction of fibrils relative to residual monomeric protein, the sample was analysed using a fibril sedimentation assay as previously described (Volpicelli-Daley et al., 2014). The incubated sample was ultracentrifuged to separate fibrils from soluble protein, and the protein content in the pellet fraction and soluble fraction was estimated by SDS-PAGE analysis (**Fig. 4.2**). α-Synuclein was detected in both the soluble and the insoluble fraction. The majority of the protein was present in the pellet fraction in the form of insoluble fibrillar aggregates. The ratio of fibrillar versus monomeric protein was constant between different preparations of α-synuclein fibril samples. To avoid fibril dissociation, which reduces the propagation activity of the sample, fibril samples were stored in small aliquots at -20 °C.

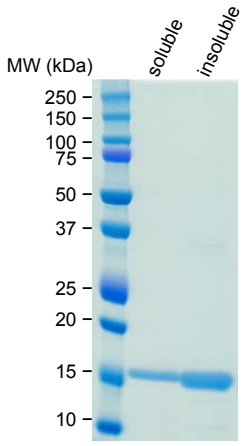

Fig. 4.2.: SDS-PAGE analysis of the fibril sedimentation assay for the confirmation of α-synuclein fibrillar aggregates. After ultracentrifugation, residual monomeric protein appeared in the soluble supernatant fraction, insoluble α-synuclein fibrils in the pellet. The gel was stained with Coomassie protein stain (InstantBlue, Expedeon).

4.2.3 α-Synuclein Amyloid Amplification Assay

To reliably detect minute amounts of α-synuclein aggregates through amplification, it is crucial to perform the amplification reaction under conditions, which selectively enhance template-catalysed conversion of the monomer into fibrils while suppressing spontaneous fibrillation through primary nucleation. Therefore, I studied the effect of different amplification conditions (buffer, pH, salts, monomer concentration, temperature, shaking cycles) on the fibrillation of monomeric α-synuclein into fibrillar aggregates in the presence and absence of preformed α-synuclein fibrils (PFFs). I started with solution conditions that had previously been shown to efficiently promote secondary nucleation events, that is conditions favouring propagon-catalysed fibrillation of α-synuclein (Buell et al., 2014). This allowed me to establish assay conditions for the amplification of α-synuclein aggregates specifically through self-replication. At mildly acidic pH (sodium acetate buffer, NaOAc, pH 5.2), the seeded conversion was highly efficient, while spontaneous nucleation was suppressed over the course of the experiment (24 h). In the reactions seeded with preformed fibrils, aggregation onset was observed after a lag time of less than 4 hours. To determine the detection limit of the assay, I performed serial limiting dilutions of preformed fibrils to generate a standard curve of propagation activity (**Fig. 4.3a**). Aggregates were detectable in

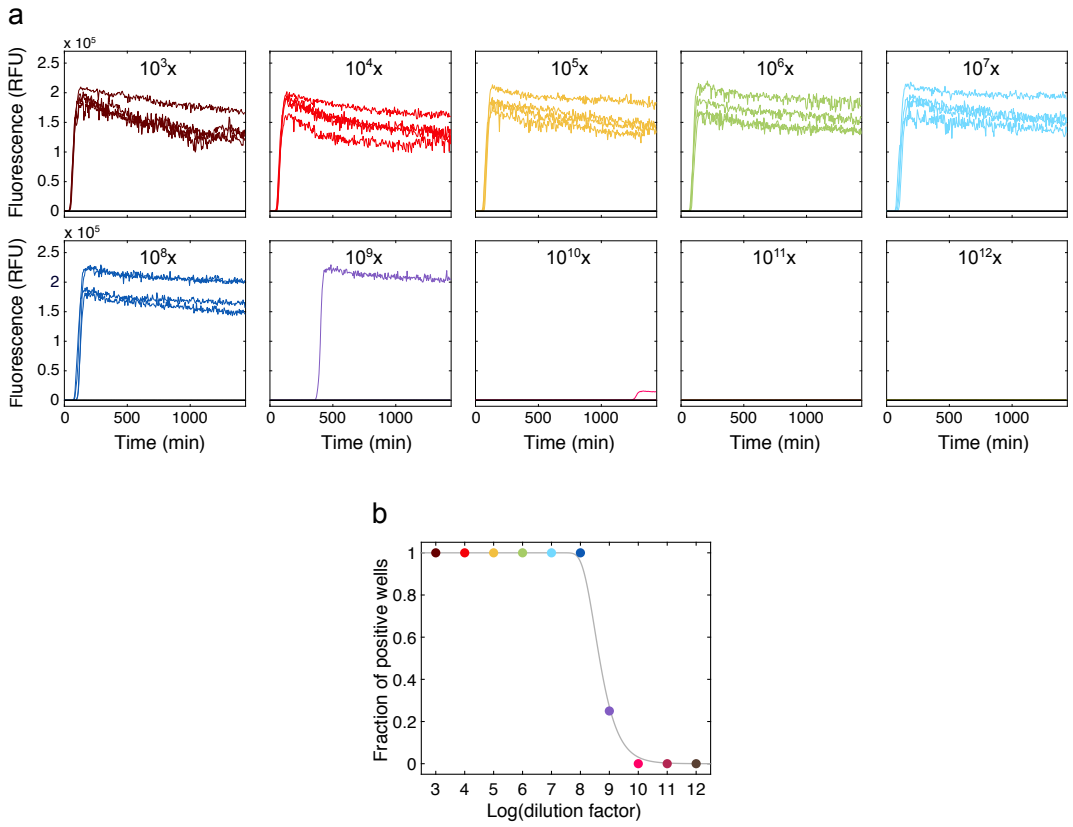

Fig. 4.3.: Standard curve of aggregation of human α-synuclein. (a) Real-time ThT fluorescence time courses of α-synuclein aggregation. Reactions of 10 µM of monomeric α-synuclein in 10 µM Thioflavin T (ThT), 25 mM NaOAc (pH 5.2) were seeded with 10-fold serial dilutions from 10^3 to 10^{12} of preformed fibrils (*coloured*). Only buffer was added to unseeded control reactions (*black*). ThT fluorescence was recorded every 5 min over the course of 24 h. All seeded and control reactions were performed in quadruplicate. (b) Standard curve of α-synuclein aggregation relating the fraction of positive wells to the logarithm of the dilution factor. A Poisson distribution was fitted to the data (*grey line*) to quantify the number of propagons in the original fibril sample.

reactions seeded with as low as femtomolar concentrations (in monomer equivalents) of preformed fibrils, which likely corresponds to single propagons assuming an average fibril is build from several hundred monomers. At higher dilutions ($>10^{10}$-fold dilution), no propagation activity was detected. The fraction of positive wells was related to the logarithm of the dilution factor (**Fig. 4.3b**), and a Poisson distribution was fitted to the data to quantify the number of α-synuclein propagons in the original fibril sample. The best fit yielded an average of $1.6 \cdot 10^{13}$ propagons per µL.

4.2.4 Steel Beads α-Synuclein Amyloid Amplification Assay

Recent reports of prion-like spreading of α-synuclein have raised the question of whether pathological α-synuclein aggregates can be transmitted between individuals (Beekes et al., 2014). This poses the potential risk of iatrogenic transmission through insufficiently decontaminated instruments in medical or surgical procedures. In a collaborative project with Daniel Heinzer (Institute of Neuropathology, University Hospital Zurich), we investigated the potential to deactivate α-synuclein aggregates on steel surfaces using a set of conventional prion decontaminants. Daniel Heinzer coated 316L stainless steel beads with preformed α-synuclein fibrils and applied different decontamination reagents to inactivate the fibrils. Subsequently, I used the α-synuclein amyloid amplification assay to assess the decontamination efficiency of the different decontaminants.

Development of the Steel Beads α-Synuclein Amyloid Amplification Assay

Analogous to the steel beads RT-QuIC (see 3.2.3 Steel Beads RT-QuIC), I modified the α-synuclein amyloid amplification assay to detect α-synuclein aggregates adsorbed to steel beads. To study possible side effects of the steel beads on the aggregation assay, particularly false positive or false negative aggregation, I investigated conversion reactions seeded with non-coated beads as well as with beads coated with monomeric and fibrillar α-synuclein. Steel beads were treated for coating with PBS, monomeric and fibrillar α-synuclein and washed thoroughly to remove unbound material by Daniel Heinzer. The coated beads and the non-coated control beads were added as seeds to the amplification reaction (**Fig. 4.4**). Steel beads treated with preformed α-synuclein fibrils seeded the conversion of monomeric α-synuclein into aggregated α-synuclein efficiently. Amplification reactions seeded with as low as 15 steel beads (calculated bead number) showed monomer-to-aggregate conversion. At high bead numbers (15,000 to 150 beads), all four replicate reactions showed an increase in the ThT fluorescence signal, whereas only half of the replicate reactions were fluorescence positive after 24 h for the reactions seeded with 15 beads. Lower bead numbers and uncoated control beads

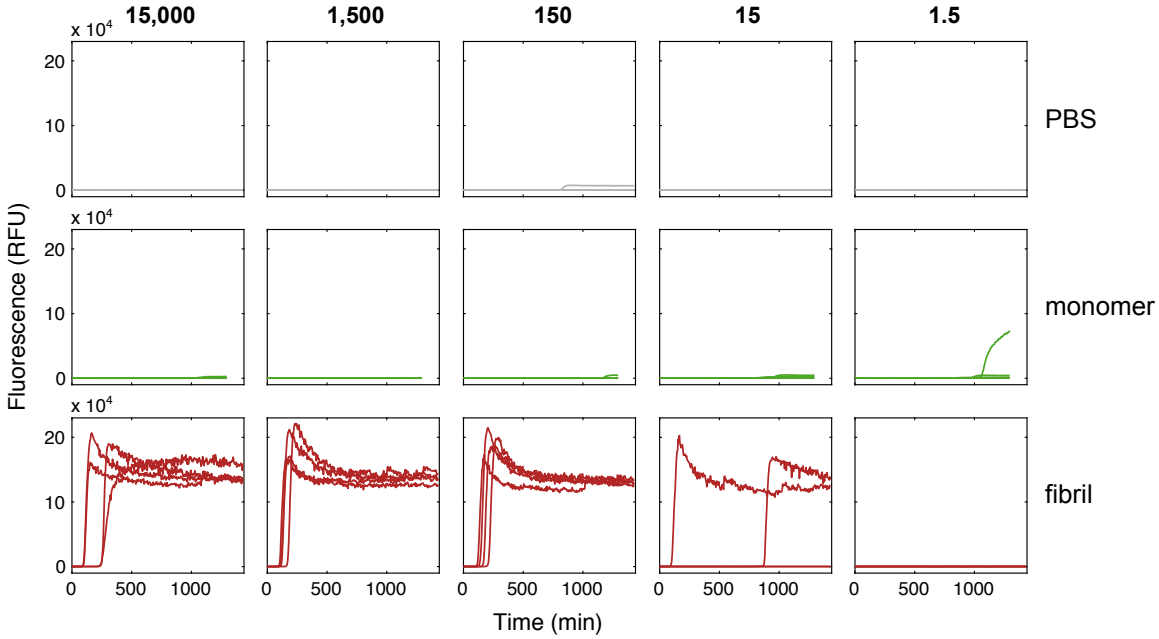

Fig. 4.4.: Steel beads α-synuclein amyloid amplification assay with 316L steel beads coated with monomeric and fibrillar α-synuclein. Between 15,000 and 1.5 non-coated control beads (*grey*), beads coated with monomeric α-synuclein (*green*) and beads coated with preformed α-synuclein fibrils (*red*) were used to seed amplification reactions. ThT fluorescence was recorded every 15 min over the course of 24 h (respectively 22 h for reactions seeded with beads treated with monomeric α-synuclein, which stopped early due to a technical issue). All reactions were performed in quadruplicate.

did not cause aggregation in any of the amplification reactions. Similarly, beads coated with monomeric α-synuclein did not lead to aggregation except for one false positive aggregation signal at the lowest bead number. The long lag time before aggregation onset and the fact that aggregation was observed at the lowest bead number indicate that the aggregation was caused by spontaneous nucleation rather than by the steel beads.

Taken together, the use of steel beads did not affect the conversion in the α-synuclein amyloid amplification assay. The results did not only show the high binding affinity of α-synuclein fibrils to stainless steel beads, but in addition they proved the utility of the amplification assay as a readout for assessing the contamination of steel surfaces with α-synuclein.

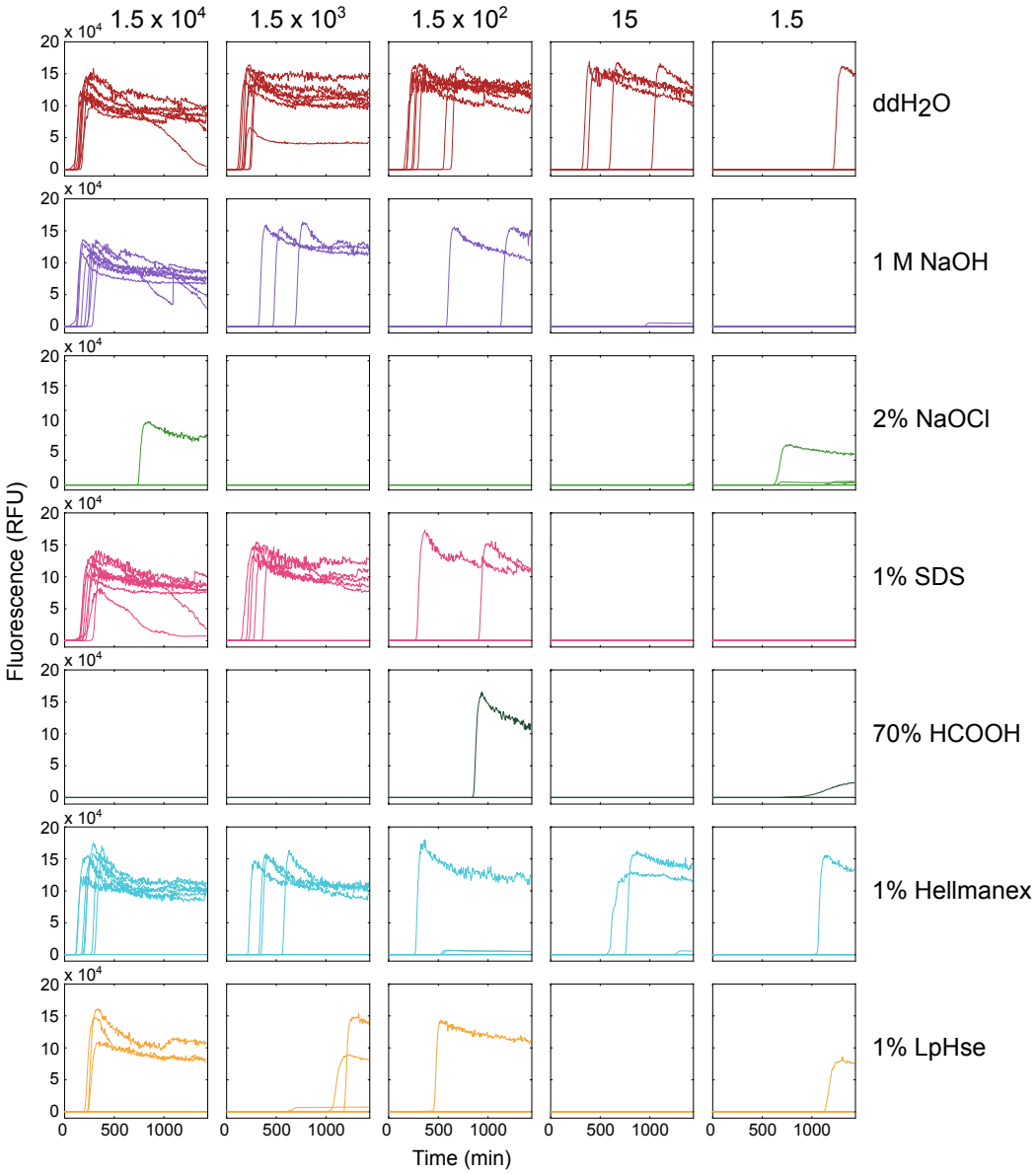

Fig. 4.5.: Decontamination of steel beads coated with α-synuclein fibrils. 316L steel beads coated with α-synuclein fibrils were treated with different decontaminants (1 M NaOH, 2% NaOCl, 1% SDS, 70% HCOOH, 1% Hellmanex, 1% LpHse) for 1 h at room temperature. 15,000 to 1.5 beads were added to the α-synuclein amplification reactions, and the time course of the ThT fluorescence was monitored over 24 h. All reactions were performed in eight technical replicates.

Decontamination of Steel Beads Coated with α-Synuclein Fibrils

The steel beads α-synuclein amyloid amplification assay was used to study the efficiency of six conventional decontaminants:

1 M NaOH, 2% NaOCl, 1% SDS, 70% HCOOH, 1% Hellmanex (Hellma Analytics), 1% LpHse (Steris).

316L steel beads coated with α-synuclein were treated with the decontaminants for 1 h at room temperature, and after treatment, their propagation activity was assessed using the amplification assay (**Fig. 4.5**). Beads incubated in ddH_2O were used as control samples with a high propagation activity. The highly efficient prion decontaminant NaOH (1 M) was not efficient in decontaminating α-synuclein fibrils. At the highest bead number, all replicate reactions were ThT fluorescence positive, and at 150 beads, 25% of the replicate reactions showed ThT positivity at the assay endpoint. Similar propagation activities were observed for beads decontaminated with 1% SDS and 1% Hellmanex. The phenolic, acidic prion decontaminant LpHse showed a slightly better decontamination efficiency. At the highest bead number tested, three out of eight replicate reactions showed a positive ThT signal. Even though the propagation activity of samples treated with LpHse was lower than the activity of the control samples, the overall decontamination activity of LpHse was insufficient. The most efficient inactivation was achieved with 2% NaOCl and 70% HCOOH. Both NaOCl and HCOOH treatment resulted in almost complete inactivation of α-synuclein propagons.

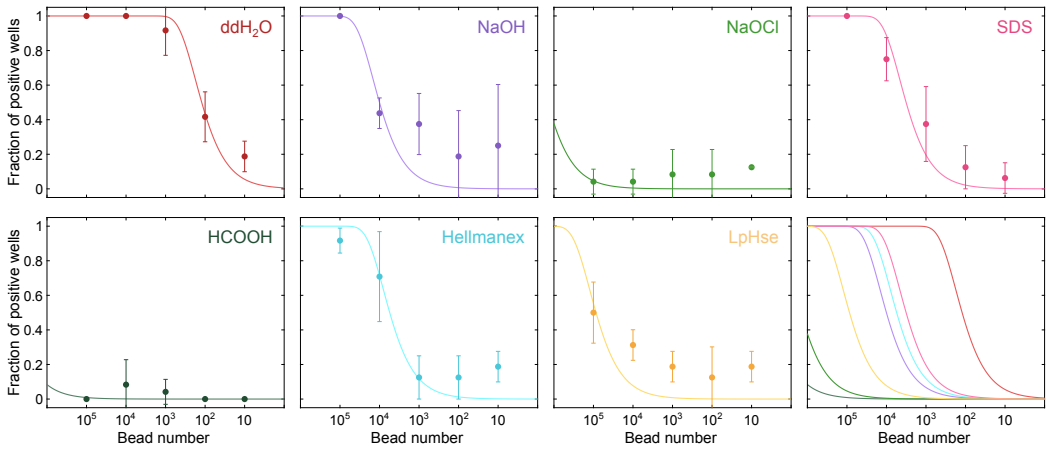

Fig. 4.6.: α-Synuclein amyloid inactivation efficiency of different decontaminants. Propagation activity curves showing the fraction of positive replicates for serial tenfold dilutions of 316L steel beads treated with different decontaminants (1 M NaOH, 2% NaOCl, 1% SDS, 70% HCOOH, 1% Hellmanex, 1% LpHse). Data represent the mean $\pm$ SD from three independent experiments. A Poisson distribution was fitted to the data (*solid lines*) to estimate the propagation activity of the inactivated beads.

4.2.5 Towards a Diagnostic α-Synucleinopathy Blood Assay

The sensitive detection of α-synuclein aggregates in body tissues or fluids enables the biochemical diagnosis of α-synucleinopathies in a minimally-invasive way. After having established conditions for the specific amplification of α-synuclein aggregates, we decided to develop a blood-based assay to detect α-synuclein aggregates in patient samples. The reliable detection of aggregates in such an easily accessible body fluid would take diagnosis of α-synucleinopathies to a new level.

Effect of Blood on the Template-Catalysed Conversion of α-Synuclein

The selective amplification of amyloid propagons in complex mixtures such as blood constitutes a big challenge. Blood proteins and other factors dissolved in blood might interfere with the conversion reaction. To determine the effect of blood on the conversion of α-synuclein, I first performed preliminary experiments of unseeded and seeded conversion reactions of α-synuclein spiked with blood drawn from healthy C57BL/6J mice (**Fig. 4.7**).

In a first step, unseeded reactions were spiked with blood plasma, serum and red blood cells to investigate if blood components cause spontaneous, false positive aggregation of monomeric α-synuclein (**Fig. 4.8**). Unseeded conversion reactions spiked with blood plasma or serum showed a negligibly low level of spontaneously converting, false positive reactions. In contrast, reactions spiked with red blood

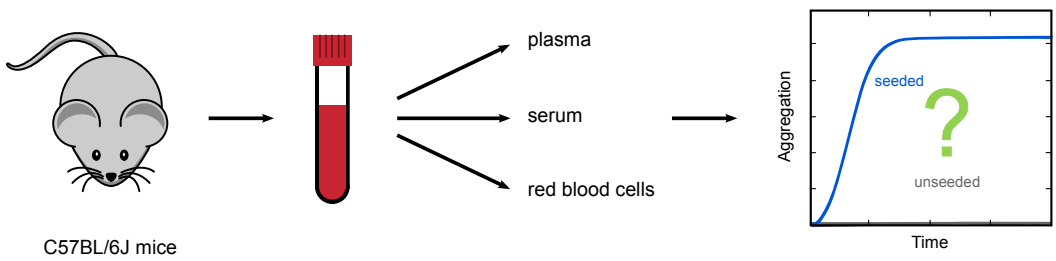

Fig. 4.7.: Schematic of preliminary experiments to investigate the effect of blood on unseeded and seeded conversion of α-synuclein. Blood from healthy C57BL/6J mice was collected into blood collection tubes and processed into plasma, serum and red blood cells. Blood plasma, serum and red blood cells were added to unseeded and seeded α-synuclein conversion reactions to study effects on the conversion.

cells showed a slightly elevated number of false positive reactions. In addition, I found that spontaneous aggregation was triggered by cryoprecipitates that form upon thawing at 4 °C or by fresh, non-hemolysed blood samples. Spontaneous aggregation was prevented by repeated freeze-thaw cycles using a waterbath at 37 °C for thawing.

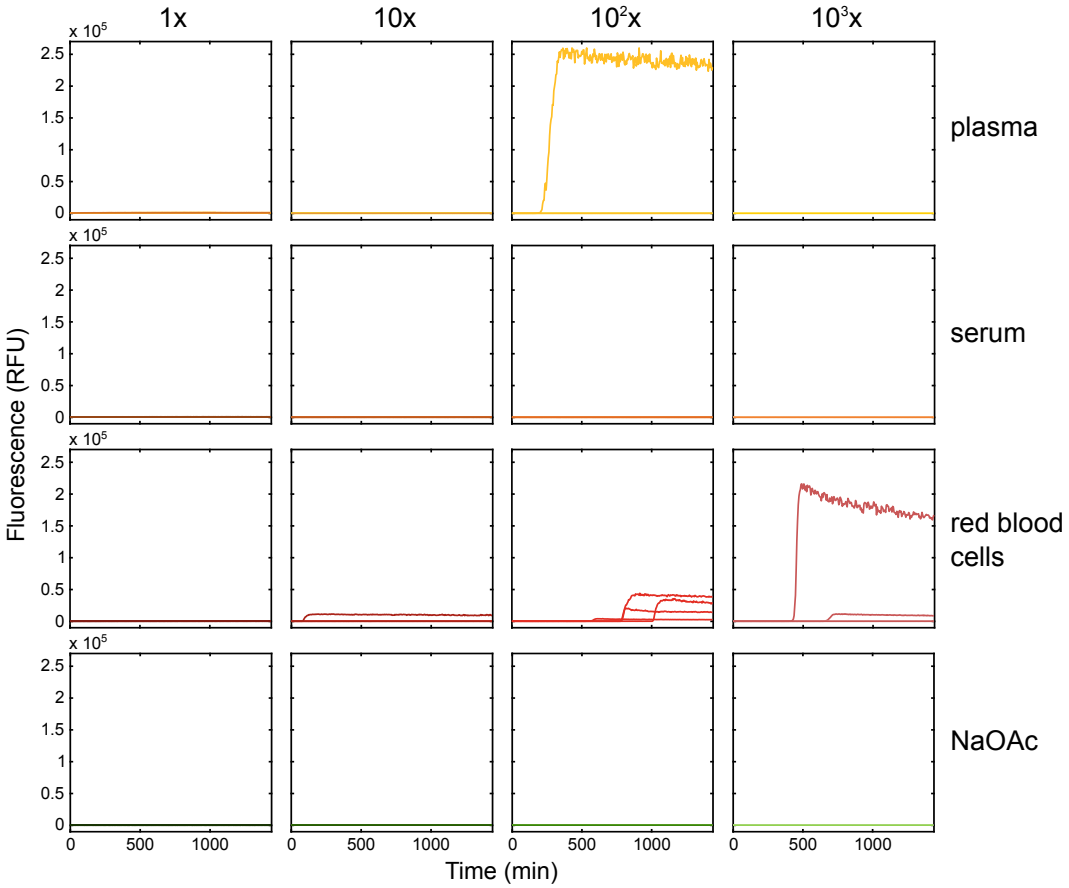

Fig. 4.8.: Effect of blood on unseeded conversion of α-synuclein. Real-time ThT fluorescence time courses of unseeded α-synuclein amyloid amplification reactions spiked with mouse blood. Blood plasma, serum and red blood cells were serially diluted tenfold in assay buffer and added to unseeded α-synuclein amplification reactions containing 10 µM monomeric α-synuclein, 10 µM ThT in 25 mM NaOAc (pH 5.2). Control reactions were spiked with 25 mM NaOAc (pH 5.2). All reactions were performed in quadruplicate.

In a second step, reactions seeded with preformed α-synuclein fibrils were spiked with blood plasma, serum and red blood cells to investigate if blood components might further affect the seeded conversion (**Fig. 4.9**). All blood samples were found

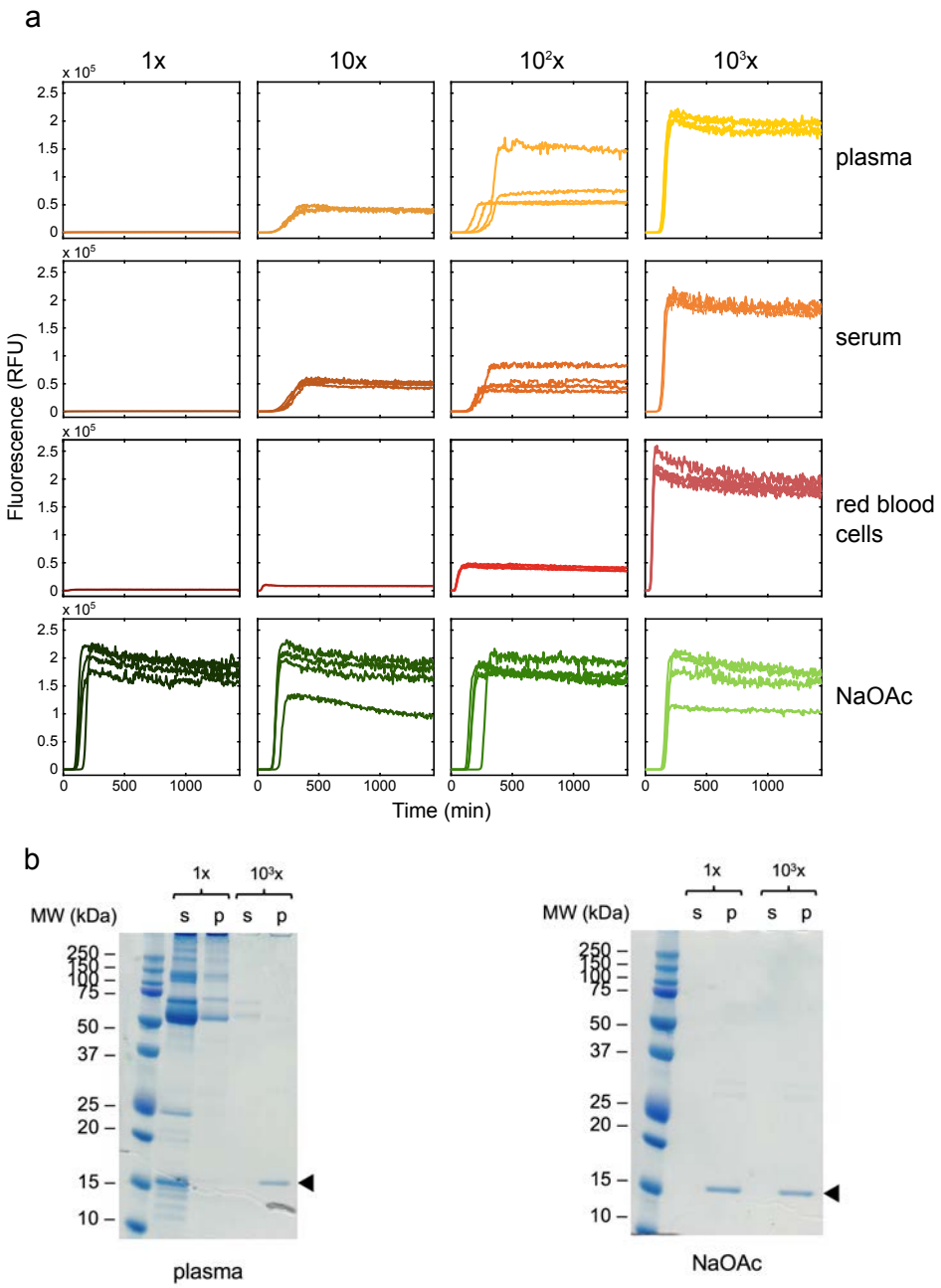

Fig. 4.9.: Effect of blood components on the seeded conversion of α-synuclein. (a) Real-time ThT fluorescence time courses of seeded α-synuclein amyloid amplification reactions spiked with various mouse blood components. Blood plasma, serum and red blood cells were serially diluted tenfold in assay buffer and added to α-synuclein amplification reactions containing 10 µM monomeric α-synuclein, 10 µM ThT, 10 nM preformed α-synuclein fibrils in 25 mM NaOAc (pH 5.2). Control reactions were spiked with 25 mM NaOAc (pH 5.2). All reactions were performed in quadruplicate. (b) SDS-PAGE analysis of soluble (s) and insoluble fractions (p) of conversion reactions spiked with blood plasma and buffer control. The endpoint sample of reactions spiked with undiluted (1x) and 10^3-fold diluted plasma were analysed after ultracentrifugation.

to have an inhibitory effect on the seeded conversion. The addition of 2.5 µL of pure plasma, serum or red blood cells in a total reaction volume of 50 µL was sufficient to completely prevent the template-catalysed amplification of amyloid fibrils. Over the course of 24 h no increase in ThT fluorescence was observed (**Fig. 4.9a**), and ultracentrifugation of the samples at the endpoint showed that all protein remained in the soluble fraction (**Fig. 4.9b**). Dilution of the blood samples prevented the inhibitory effect. At a 10^3-fold dilution of the blood samples the observed propagation activity was comparable to the propagation activity of a control sample not containing any blood components.

Even though diluting blood samples is a possible solution to prevent inhibitory effects of the blood matrix, it lowers the aggregate concentration in the analyte and complicates the sensitive detection of α-synuclein aggregates. Therefore, I suggest an appropriate pretreatment of blood samples to reduce blood matrix effects without lowering the aggregate concentration.

Blood Pretreatment Strategies to Enrich α-Synuclein Aggregates

Sample pretreatment can either involve an enrichment step in which the blood matrix is removed and α-synuclein aggregates are enriched or a capturing step in which aggregates are specifically extracted from the blood. In both approaches the blood matrix is removed, while the amyloid aggregates are accumulated. In prion research, many pretreatment strategies have been used to enrich prion aggregates from body fluids (Orrú et al., 2011; Elder et al., 2015; Concha-Marambio et al., 2016; Bougard et al., 2016). I adapted five pretreatment strategies to enrich α-synuclein aggregates from patient blood samples prior to amplification in the α-synuclein amyloid amplification assay: ultracentrifugation, sarkosyl precipitation, sodium phosphotungstic acid (NaPTA) precipitation, steel beads capturing, and immunoprecipitation.

Sarkosyl solubilisation. A common strategy to purify prion aggregates from blood is the removal of the blood matrix by sarkosyl solubilisation (Concha-Marambio et al., 2016). Sarkosyl (N-laurylsarcosine) is a harsh detergent used to solubilise blood

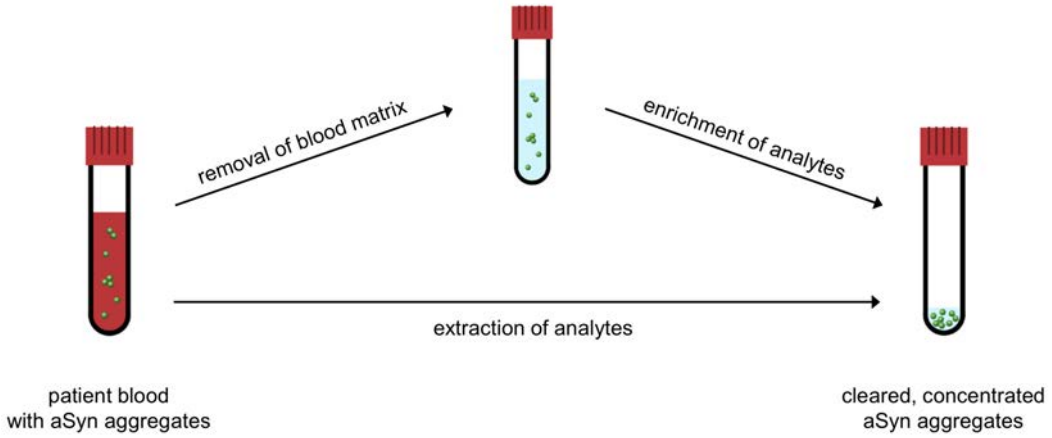

Fig. 4.10.: Sample pretreatment strategies. Amyloid aggregates can either be isolated from blood samples by concentrating the aggregates and removing the blood matrix (*upper strategy*) or by specifically capturing the aggregates from the blood (*lower strategy*).

proteins and other blood components. In contrast, pathologic prion aggregates are sarkosyl insoluble and and can therefore be separated from the sarkosyl-soluble blood fraction.

I tested the stability of synthetic α-synuclein aggregates when solubilising the blood matrix with sarkosyl. I spiked preformed α-synuclein fibrils into the blood of healthy humans and analysed their propagation activity (**Fig. 4.11**). I found that sarkosyl-treated EDTA whole blood spiked with preformed α-synuclein aggregates was propagation active, while sarkosyl-treated blood without fibrils did not show any propagation activity. Accordingly, synthetic α-synuclein fibrils treated with sarkosyl were insoluble and showed normal propagation activity. Furthermore, sarkosyl did not cause any false positive, spontaneous aggregation of monomeric α-synuclein. In a next step, I used blood from both healthy donors and patients suffering from PD to investigate if sarkosyl-solubilisation is adequate for sample pretreatment. EDTA whole blood was solubilised with 15% sarkosyl, and ultracentrifuged to separate insoluble aggregates from solubilised components. Pellets were dissolved in 25 mM NaOAc (pH 5.2) and added to the amyloid amplification assay to analyse the propagation activity (**Fig. 4.12**). Most blood samples from PD patients showed one or more propagation-positive reaction out of four replicate reactions. The observed lag times varied greatly between different patient samples but also within the replicates of a single patient sample. Despite the variability, most samples showed low-level

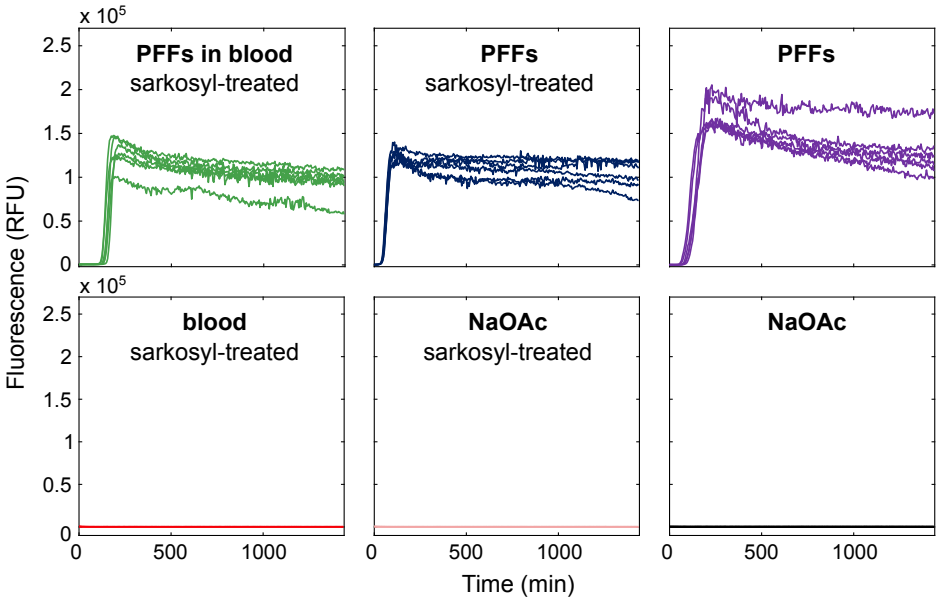

Fig. 4.11.: Sarkosyl solubilisation of human blood spiked with preformed α-synuclein fibrils. Real-time ThT fluorescence time courses of α-synuclein amyloid amplification reactions seeded with preformed α-synuclein fibrils dissolved in sarkosyl-solubilised whole blood. Fibrils were dissolved in healthy human EDTA whole blood, and the mixture was solubilised with 15% sarkosyl before addition to the reaction mastermix (*green*, final fibril concentration of 10 nM). Fibrils solubilised in sarkosyl (*blue*), blood solubilised with sarkosyl (*red*) and pure sarkosyl (*light pink*) were used as controls as well as seeded and unseeded plate control reactions. All reactions were performed in quadruplicate.

propagation activity. In contrast, blood samples from healthy donors were mostly ThT negative, a few false positive reactions were observed. The spontaneously aggregating reactions seeded with healthy patient samples were indicative of incomplete solubilisation of the blood matrix. In light of the false positive reactions from healthy donor samples, the propagation activity observed for the PD samples can not be considered as significant. In order to reliably discriminate between aggregate positive and negative samples, a more rigorous sample pretreatment with more efficient solubilisation and enrichment of aggregates is required.

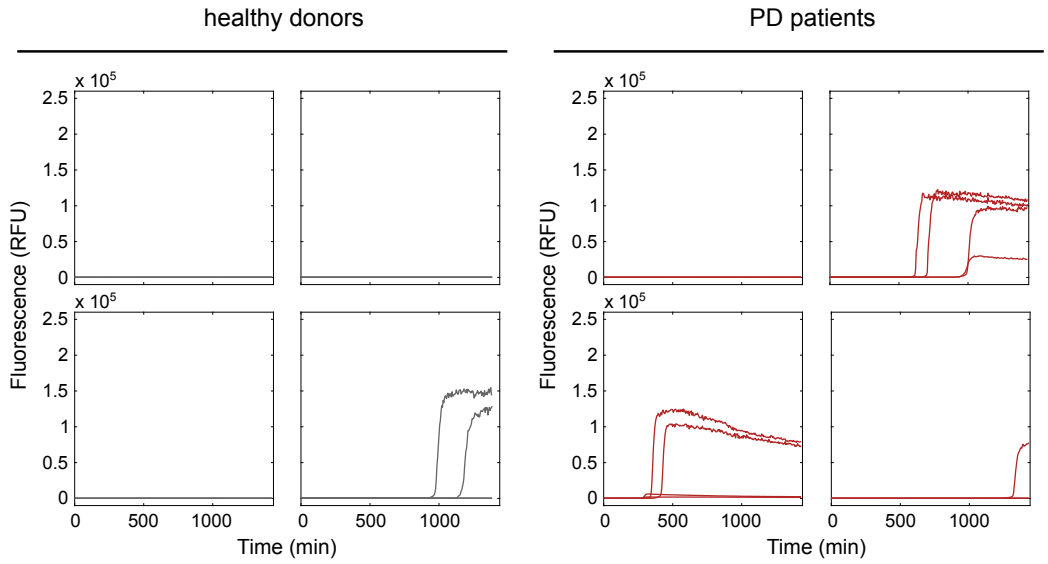

Fig. 4.12.: Sarkosyl solubilisation of human blood samples from healthy donors and PD patients. Real-time ThT fluorescence time courses of α-synuclein amyloid amplification reactions seeded with sarkosyl-solubilised whole blood from healthy donors (*grey*) and PD patients (*red*). Four representative examples of reaction time courses of both healthy donors and PD patients are shown. All reactions were performed in quadruplicate.

NaPTA precipitation. Sodium phosphotungstic acid (NaPTA) precipitation is a method described to specifically enrich insoluble prion aggregates from blood (Elder et al., 2015). Phosphotungstate anions bind prion aggregates and separate them from other factors by facilitating their precipitation (Levine et al., 2015). NaPTA precipitation has also been successfully applied to purify α-synuclein aggregates from brain tissue (Woerman et al., 2015). These findings suggest that NaPTA precipitation could be applied to accumulate α-synuclein aggregates from patient blood. To improve solubilisation, I used harsh sarkosyl conditions (2% sarkosyl for 2 h at 37 °C), which reduced the number of spontaneously aggregating reactions. I applied the improved sarkosyl solubilisation protocol followed by NaPTA precipitation pretreatment to blood samples from PD and healthy control patients (**Fig. 4.13**). The improved sarkosyl solubilisation was efficient in solubilising all blood components from healthy donor samples, resulting in no false positive reactions. However, we detected only a small fraction of propagation-positive reactions in the reactions seeded with PD-positive patient samples. The lag times of the aggregating reactions were comparable among different patient samples with an early aggregation onset (shorter than 5 hours). The short lag times were similar to the lag times of reactions

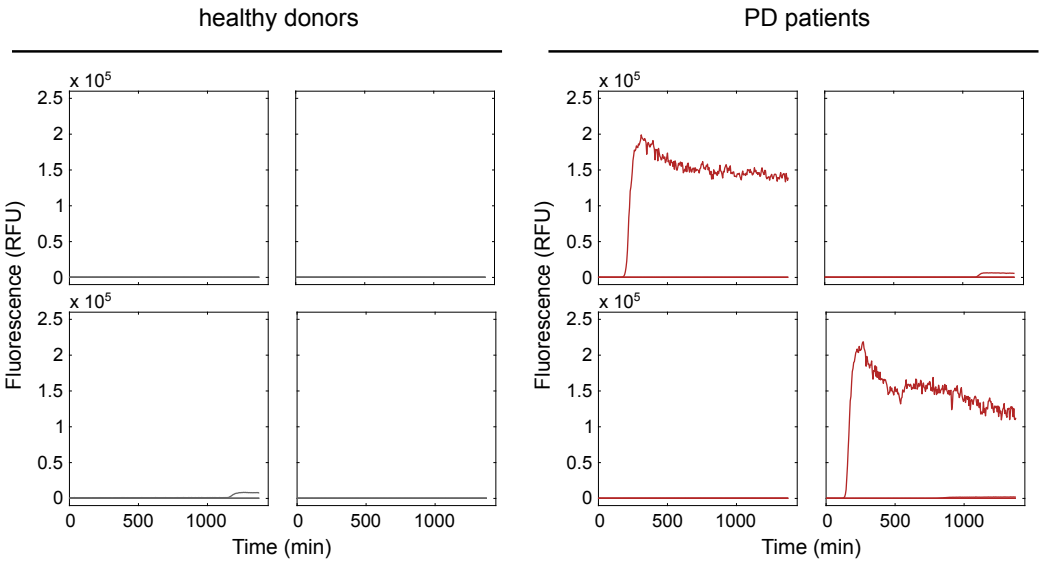

Fig. 4.13.: NaPTA precipitation of human blood samples from healthy donors and PD patients. Real-time ThT fluorescence time courses of α-synuclein amyloid amplification reactions seeded with NaPTA precipitated whole blood from healthy donors (*grey*) and PD patients (*red*). Four representative examples of reaction time courses of both healthy donors and PD patients are shown. Instead of the usual 24 h, the assay stopped after 23 h due to a technical issue. All reactions were performed in quadruplicate.

seeded with synthetic α-synuclein aggregates, which indicates that the observed aggregation was induced through seeds rather than due to spontaneous aggregation events.

Steel beads capturing. Another strategy to enrich amyloid aggregates from blood is specific capturing of the aggregates. Prions and other amyloids have been shown to adsorb to metal surfaces (Zobeley et al., 1999). I found that α-synuclein aggregates also strongly bind to steel beads, and that the beads transmit the propagation activity of the adsorbed α-synuclein aggregates (see section 4.2.4 Steel Beads α-Synuclein Amyloid Amplification Assay). I therefore investigated whether steel beads capturing pathological α-synuclein aggregates from patient blood can be used as a pretreatment of blood samples to enrich aggregates for the α-synuclein amyloid amplification assay.

EDTA whole blood samples from healthy donors and PD patients were incubated overnight with 316L stainless steel beads to capture aggregates. The beads were then used to seed the amplification assay (**Fig. 4.14**). Similar as for the NaPTA precipitation pretreatment, little propagation activity was observed in the reactions

seeded with beads treated with blood from PD patients. No propagation activity was detected in reactions seeded with beads treated with blood from healthy donors. Due to weak signals in the samples from PD patients, no clear discrimination between samples from PD patients and healthy donors was possible.

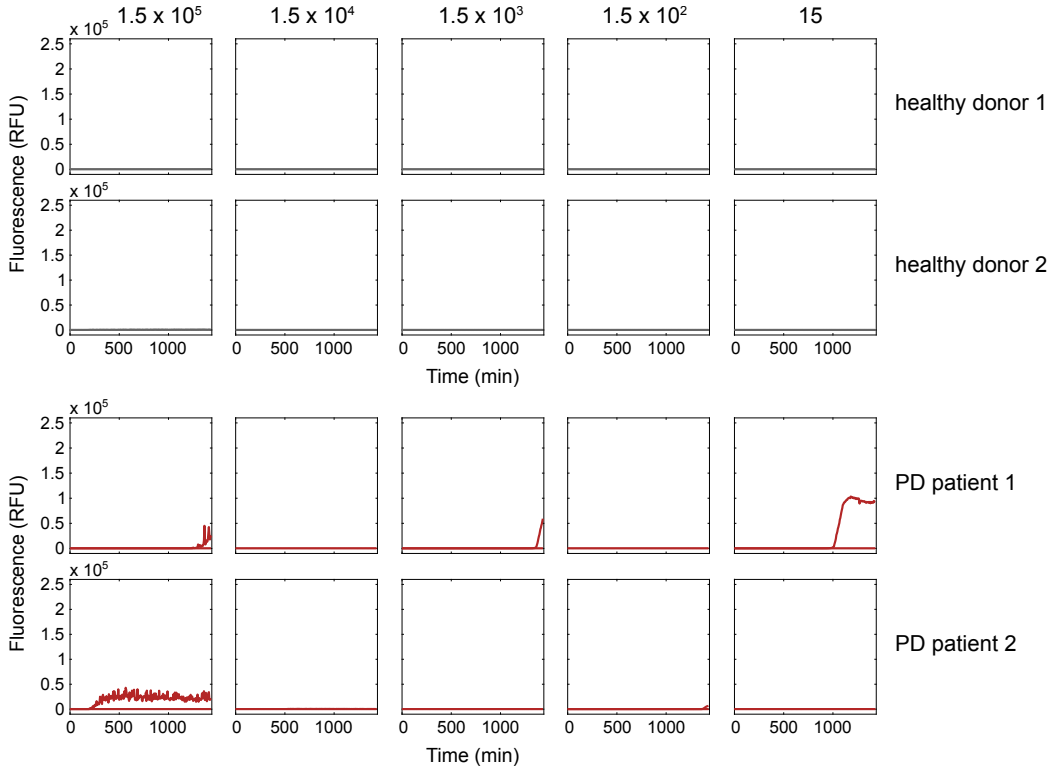

Fig. 4.14.: Steel beads capture of α-synuclein aggregates from human blood samples. Real-time ThT fluorescence time courses of α-synuclein amyloid amplification reactions seeded with steel beads incubated with whole blood from healthy donors (*grey*) and PD patients (*red*). Two representative examples of reaction time courses of both healthy donors and PD patients at different bead numbers are shown. All reactions were performed in quadruplicate.

Immunoprecipitation. In a fourth approach, I used immunoprecipitation to enrich α-synuclein aggregates from patient blood. The combination of amyloid capturing by immunoprecipitation followed by an amplification step has previously been described to detect prions in blood components (Orrú et al., 2011; Bougard et al., 2016). Analogous to these studies, I used magnetic beads coupled to the anti-α-synuclein antibody syn211 (binding to the epitope of aa 120–140 at the C-terminus) to capture α-synuclein from blood samples. After capturing, beads were added to the amplification reactions in the α-synuclein amyloid amplification assay to detect their propagation activity.

As a proof-of-concept experiment, I captured both monomeric and fibrillar α-synuclein that were spiked into the blood of healthy donors, and analysed the propagation activity of the beads (**Fig. 4.15**). To prevent spontaneous aggregation caused by bead-induced shear forces, the shaking cycle was lowered to a short 60 s shaking at low intensity (100 rpm) before each read. Under these conditions, no spontaneous aggregation was observed in the reactions seeded with uncoupled magnetic beads. Similarly, beads treated with monomeric α-synuclein did not show any propagation activity. However, beads treated with synthetic α-synuclein fibrils both pure and spiked in healthy blood showed high propagation activity in the amplification assay.

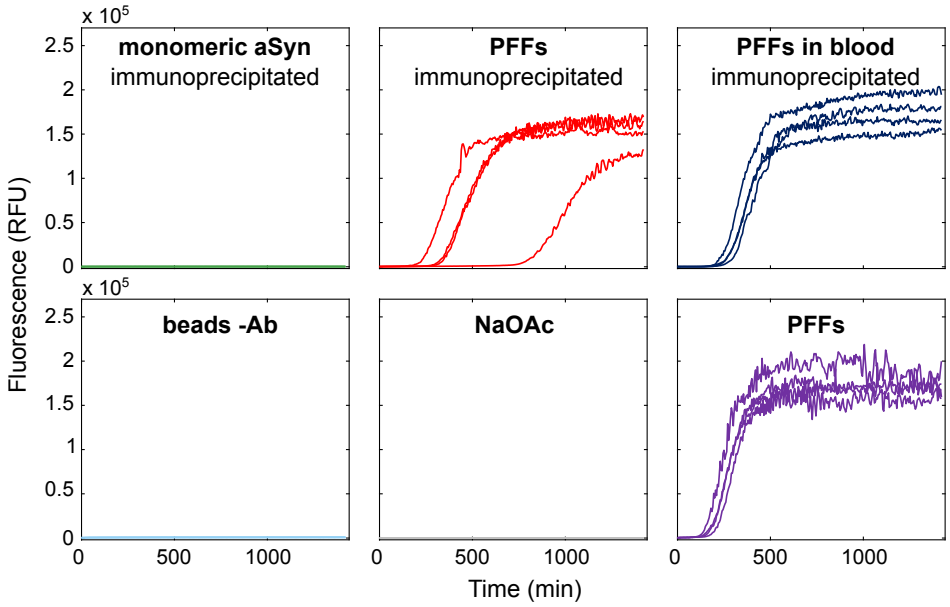

Fig. 4.15.: Immunoprecipitation of human blood spiked with monomeric and fibrillar α-synuclein. Real-time ThT fluorescence time courses of α-synuclein amyloid amplification reactions seeded with magnetic Dynabeads that were treated with monomeric and fibrillar α-synuclein from whole blood. Monomeric protein (*green*) and fibrils (*dark blue*) were dissolved in healthy human EDTA whole blood, and the mixture was incubated with magnetic Dynabeads coated with the anti-α-synuclein antibody syn211 for capturing α-synuclein. Subsequently, beads were added to the reaction mastermix and subjected to amplification. Beads capturing pure fibrils (*red*) and empty beads without anti-α-synuclein antibody (*light blue*) were used as controls as well as seeded (*purple*) and unseeded (*grey*) plate control reactions. All reactions were performed in quadruplicate.

Next, I used immunoprecipitation to capture α-synuclein from human blood samples of PD patients and healthy donors. Magnetic beads coupled to syn211 antibody were mixed with blood samples, and added to the amplification assay to assess their propagation activity (**Fig. 4.15**). While blood samples from healthy donors

did not show any reactivity, most samples from PD patients showed propagation activity in the amplification assay. In the majority of the tested PD-positive blood samples, one or more reactions showed an increase in ThT fluorescence after a lag time of approximately 10–15 hours. These results indicate that there is a low level of propagation-active α-synuclein aggregates specifically in the blood of diseased patients. Yet a clear discrimination between PD-positive and PD-negative samples was not possible. This, however, might reflect a heterogeneity in the aggregate load in PD patients.

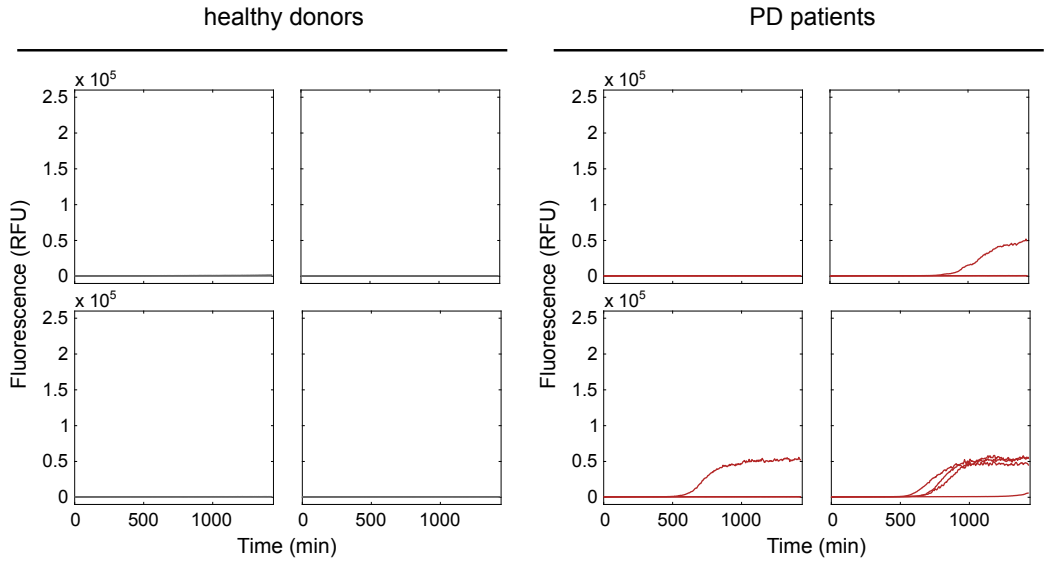

Fig. 4.16.: Immunoprecipitation of α-synuclein from human blood samples of healthy donors and PD patients. Real-time ThT fluorescence time courses of amplification reactions seeded with α-synuclein amyloid amplification reactions seeded with magnetic Dynabeads capturing α-synuclein from whole blood of healthy donors (*grey*) and PD patients (*red*). Four representative examples of reaction time courses of samples from both healthy donors and PD patients are shown. All reactions were performed in quadruplicate.

4.3 Discussion and Outlook

α-Synuclein Amyloid Amplification Assay

In this chapter, I describe the development of an amyloid amplification assay for α-synuclein, the protein involved in Parkinson's disease and other synucleinopathies. Recombinant human α-synuclein expressed from a codon optimised plasmid was used as a substrate for propagon-catalysed conversion. In vitro reconstituted α-synuclein fibrils very efficiently seeded the conversion of monomeric protein after a lag time of less than 4 h, which allowed the detection of single propagating units. Analogous to the digital insulin amyloid amplification assay, digital serial dilution of the analyte sample allowed the quantification of the absolute number of α-synuclein propagons in the analyte. A quantitative assay for α-synuclein propagons based on their propagation activity has not been described to date.

Compared to recently published α-synuclein conversion assays (Fairfoul et al., 2016; Shahnawaz et al., 2017; Sano et al., 2017), our assay is more robust and practical. The observed lag times are highly reproducible and much shorter than the lag times of more than 70 h reported for other α-synuclein conversion assays (Fairfoul et al., 2016; Shahnawaz et al., 2017; Sano et al., 2017). The comparably short lag times resulted in a dramatic decrease in total assay duration. Reactions seeded with synthetic α-synuclein fibrils reached a plateau after approximately 4 h compared to more than 70 h in previously published assays (Shahnawaz et al., 2017). The shorter measurement time allows for a significant increase in the throughput of the assay.

Steel Beads α-Synuclein Amyloid Amplification Assay

Recent studies have provided evidence for prion-like transmission of α-synuclein pathology (Mougenot et al., 2012; Luk et al., 2012a; Masuda-Suzukake et al., 2013). Together with α-synuclein aggregates being remarkably stable and resistant to denaturation (Woerman et al., 2017), these findings have raised the concern of a potential risk of iatrogenic transmission of α-synucleinopathies through contact with

contaminated medical instruments (Beekes et al., 2014). Therefore, the identification of efficient α-synuclein decontamination procedures might be important for the inactivation of potentially hazardous α-synuclein fibrils. I applied the α-synuclein amyloid amplification assay to study the efficiency of potential decontamination reagents for α-synuclein amyloid inactivation. Similar to the steel beads RT-QuIC, I adapted the α-synuclein amyloid amplification assay to detect α-synuclein propagons adsorbed to steel beads. Preliminary validation experiments showed that the steel beads α-synuclein amyloid amplification assay was capable of detecting synthetic α-synuclein fibrils bound to 316L steel beads with a very high affinity. Unspecific reactions due to the beads were not observed, which allowed me to use this modified assay for decontamination studies.

Previous studies reported the successful application of prion-effective decontaminants in α-synuclein inactivation (Thomzig et al., 2014). NaOH and SDS were shown to efficiently reduce α-synuclein aggregates (Thomzig et al., 2014), and other decontaminants such as NaOCl, LpHse or Hellmanex were proposed for α-synuclein decontamination (Bousset et al., 2016). We therefore set out to examine the decontamination potential of the most commonly used prion decontaminants: NaOH, SDS, NaOCl, HCOOH, LpHse and Hellmanex. In contrast to previous findings (Thomzig et al., 2014), both NaOH and SDS treatments did not show any inactivation of α-synuclein propagation activity. Hellmanex and LpHse were found to be equally inefficient. The only efficient decontaminants were NaOCl and HCOOH. α-synuclein coated beads treated with 2% NaOCl or 70% HCOOH showed a significant reduction of propagation activity. The efficiency to inactivate α-synuclein aggregates with hypochlorite was confirmed by two recent publications (Bousset et al., 2016; Hughson et al., 2016). Similar to our findings, Bousset et al., 2016 showed that NaOCl can efficiently remove α-synuclein oligomers and fibrils from stainless steel surfaces, but not from glass and plastic surfaces (Bousset et al., 2016). The same study confirmed our results with respect to NaOH treatment being inefficient. In contrast, the study showed efficient decontamination with SDS and Hellmanex, while in our hands neither SDS nor Hellmanex treatment significantly reduced the propagation activity. The observed discrepancies might be explained

by the different methodologies used to assess decontamination efficiency. While I measured the propagation activity remaining on the surfaces after decontamination treatment, Bousset et al., 2016 determined the amount of α-synuclein aggregates using fluorescence or absorbance measurements.

Further studies are needed to evaluate the efficiency of these and other decontaminants. In light of the increasing evidence suggesting prion-like transmission of α-synuclein pathology, the safety considerations for working with potentially infectious α-synuclein aggregates should be carefully revisited. To ensure patient and researcher safety, proper decontamination procedures should be introduced for the cleaning of surgical and laboratory materials.

Towards a Diagnostic α-Synucleinopathy Blood Assay

The high sensitivity of the α-synuclein amyloid amplification assay makes it a useful tool for the detection of small amounts of α-synuclein aggregates in patient tissues. The detection of α-synuclein aggregates in easily accessible body fluids enables the minimally invasive diagnosis of Parkinson's disease and other α-synucleinopathies. As an extension of previously published assays diagnosing α-synucleinopathies from brain tissue and CSF samples (Fairfoul et al., 2016; Shahnawaz et al., 2017; Sano et al., 2017), we aimed at detecting α-synuclein aggregates in blood. Recent pathophysiologic studies revealed peripheral disease onset in the gastrointestinal system years before first appearance in the central nervous system (Braak et al., 2003a; Hilton et al., 2014; Stokholm et al., 2016). Besides neuron-to-neuron transmission through the vagus nerve (Holmqvist et al., 2014; Ulusoy et al., 2017), the systemic spreading of α-synuclein is hypothesised to occur through the blood stream by crossing the blood-brain-barrier (Peelaerts et al., 2015). Therefore, we decided to adapt the amplification assay to detect α-synuclein aggregates in the blood of patients.

In a first experiment, I investigated the effect of small amounts of blood added to the α-synuclein conversion reactions. The complex blood matrix was found to have a strong inhibitory effect on the propagon-catalysed conversion of α-synuclein. Therefore, I investigated pretreatment strategies aimed at minimising the inhibitory effect

of the blood matrix enriching α-synuclein aggregates at the same time. A harsh sarkosyl treatment solubilised most components of blood, and subsequent precipitation of insoluble aggregates with NaPTA enriched α-synuclein aggregates, similar to previously shown studies purifying prion aggregates from blood (Concha-Marambio et al., 2016; Elder et al., 2015). In the α-synuclein amyloid amplification assay, most PD patient samples showed partial reactivity with one or more (out of four) replicate reactions being positive. In contrast, samples from healthy donors mainly lacked propagation activity. Similar results were achieved with pretreatments for more specific accumulation of α-synuclein aggregates from blood samples. α-Synuclein aggregates were captured and enriched from blood with steel beads, similar to the enrichment of blood prions with steel wires before RT-QuIC (Edgeworth et al., 2011). Beads incubated with blood from healthy donors did not show any reactivity, while beads incubated with PD patient blood showed little reactivity. A slightly higher propagation reactivity of the PD blood samples was achieved by specifically enriching α-synuclein aggregates through immunoprecipitation with anti-α-synuclein coupled magnetic beads.

Taken together, this study provides evidence that we can specifically detect α-synuclein aggregates in PD patient blood samples. However, the reliable detection of the aggregates remains challenging. One possible explanation for the uncertain diagnosis is the fact that the tests were performed with blood samples of patients with unknown disease stage. The aggregate load in such samples might vary widely and therefore cause inconsistent results. The use of samples with a known, high amyloid content from patients with advanced synucleinopathy might lead to more consistent results. Moreover, the detection sensitivity could potentially be improved by further optimisation of pretreatment strategies. An increase in blood analyte volume would possibly raise the number of propagating α-synuclein aggregates. Combined with enrichment by immunoprecipitation this might lead to more sensitive detection.

With improved reliability and robustness, the assay could serve as a tool for the diagnosis of α-synucleinopathies similar to the RT-QuIC assay for CJD diagnostics. The capability to use blood samples for diagnosis would present a major advance

compared to the use of brain biopsies and CSF samples (Fairfoul et al., 2016; Shahnawaz et al., 2017; Sano et al., 2017). An easy-to-use and minimally invasive blood test would present a very powerful biochemical diagnostic tool that could complement current clinical diagnostic tests.

4.4 Materials and Methods

4.4.1 Expression and Purification of Human α-Synuclein

Construction of Plasmid Encoding the *SNCA* Gene

The pRK172 plasmid harbouring the human α-synuclein gene (*SNCA*), kindly provided by Prof. Kelvin Luk (University of Pennsylvania, Perelman School of Medicine), was used as the template for mutagenesis. To avoid misincorporation of cysteine for tyrosine at codon 136 (Masuda et al., 2006), codon 136 was mutated from Y136-TAC to Y136-TAT by site-directed mutagenesis using the QuikChange II Site-Directed Mutagenesis Kit (Agilent) with primers aSyn_c408t_for and aSyn_c408t_rev (see Appendix) following the instruction manual. The sequence of the construct was verified by automated Sanger sequencing at Microsynth (Balgach, Switzerland).

Expression and Purification of Human α-Synuclein

E. coli BL21(DE3)RIL harbouring the pRK172 plasmid encoding the human α-synuclein gene (codon Y136-TAT) were grown overnight at 37 °C in TB medium containing 100 µg mL^{-1} ampicillin. Cells were harvested by centrifugation, resuspended in 10 mM Tris-HCl (pH 7.6), 750 mM NaCl, 1 mM EDTA, 1 mM PMSF, complete EDTA-free protease inhibitor tablet (Roche), and lysed by five freeze-thaw cycles using liquid nitrogen and tap warm water. Cell debris were removed by centrifugation (12,000 g, 30 min, 4 °C), and the supernatant was boiled for 15 min at 99 °C to heat-denature and precipitate unwanted proteins. Precipitates were removed by centrifugation (12,000 g, 30 min, 4 °C). Nucleic acids were removed with streptomycin sulphate (10 mg mL^{-1}) precipitation followed by centrifugation (12,000 g, 30 min, 4 °C). For further purification, α-synuclein was salted out using ammonium sulphate (361 mg mL^{-1}) precipitation, and enriched by centrifugation (12,000 g, 30 min, 4 °C). Pellets containing precipitated α-synuclein were resuspended in 10 mM Tris-HCl (pH 7.6), and dialysed overnight against 10 mM Tris-HCl (pH 7.6) to remove remaining salts. The dialysed sample was loaded onto a Hi-Trap Q HP

anion-exchange chromatography column (GE Healthcare) equilibrated with 10 mM Tris-HCl (pH 7.6). After washing unbound materials with 5 column volumes of 10 mM Tris-HCl (pH 7.6), the protein was eluted with a linear salt gradient from 0 to 1 M of NaCl over 20 column volumes. Protein containing fractions were collected, and analysed by SDS-PAGE. Fractions containing α-synuclein were pooled and dialysed overnight against 25 mM Tris-HCl (pH 7.4), 100 mM NaCl. The dialysed sample was loaded onto a HiLoad 26/60 Superdex75 size exclusion column (GE Healthcare), and eluted with 25 mM Tris-HCl (pH 7.4), 100 mM NaCl at a flow rate of 2 mL min^{-1}. Protein containing fractions were analysed by SDS-PAGE, and fractions containing α-synuclein were pooled. The purification yields were 90–120 mg L^{-1} of bacterial culture. The purity of the protein was verified by SDS-PAGE and ESI-MS (Functional Genomics Center Zurich). Protein concentrations were measured by absorbance at 280 nm using a molar extinction coefficient (ε_{280}) of 5960 $M^{-1}cm^{-1}$.

4.4.2 Preparation of Preformed α-Synuclein Fibrils

Highly pure, monomeric α-synuclein was thawed, adjusted to 5 mg mL^{-1} in a final volume of 500 µL using PBS in a Protein LoBind tube (Eppendorf). To reconstitute the protein into amyloid fibrils, the protein was incubated at 37 °C under vigorous shaking at 1000 rpm for 7 d inside a thermomixer with heatable lid (Volpicelli-Daley et al., 2014). The fibrils were aliquoted and stored at -20 °C. Low temperature storage is crucial to prevent the dissociation of fibrils and thus the loss in propagation activity as described earlier (Bousset et al., 2013; Volpicelli-Daley et al., 2014).

4.4.3 Fibril Sedimentation Assay

Pelletable, active α-synuclein fibrils were confirmed as previously published (Volpicelli-Daley et al., 2014). Briefly, 20 µL of fibrils were centrifuged at 100,000 g for 60 min at room temperature. The supernatant was removed and mixed with 2X Laemmli buffer for SDS-PAGE analysis. The pellet was resuspended in 20 µL PBS, and again centrifuged at 100,000 g for 60 min at room temperature. After centrifugation

the supernatant was discarded, and the pellet was resuspended in 20 µL PBS and mixed with 2X Laemmli buffer. Both collected supernatant and pellet fractions were analysed by SDS-PAGE.

4.4.4 α-Synuclein Amyloid Amplification Assay

The α-synuclein amyloid amplification assay was performed using recombinant human α-synuclein as substrate. Recombinant human α-synuclein was thawed and filtered using 50 kDa Amicon Ultra centrifugal filters (Millipore, Prod. No. UFC505096) to remove potential aggregated protein. The protein was adjusted to a final concentration of 10 µM in 25 mM NaOAc (pH 5.2) containing 10 µM thioflavin T in a total reaction volume of 30 µL (including seed volume). Amplification reactions were seeded with 2.5 µL of preformed α-synuclein fibrils, patient samples or with buffer for the unseeded control reaction. All amplification reactions were performed in quadruplicate in black 96-well half area polystyrene microplates (Corning, Prod. No. 3880) covered with a sealing tape (Sarstedt, Prod. No. 95.1999). The reactions were amplified over 24 h at 60 °C with alternating cycles of 150 s shaking at 1100 rpm in double orbital mode and 150 s resting using a FLUOstar Omega microplate reader (BMG Labtech). A low intensity shaking of 60 s shaking at 100 rpm was used for blood samples pretreated by immunoprecipitation to prevent spontaneous aggregation caused by the magnetic beads. The formation of new aggregates was followed real-time by measuring thioflavin T fluorescence (ex/em filters 450/480 nm) every 5 min in bottom read mode.

4.4.5 Steel Beads α-Synuclein Amyloid Amplification Assay

All coatings and decontamination treatments of steel beads were performed by Daniel Heinzer. Steel beads were dissolved in PBS, diluted to the final bead number and stored at -20 °C until usage. All samples were treated identically and diluted using the same dilution steps to minimise the error in bead number arising from inaccurate pipetting. In addition, samples were thoroughly vortexed before every

pipetting to suspend the beads. Amplification was performed as described in the section 'α-Synuclein Amyloid Amplification Assay'. Amplification reactions were seeded with 2.5 µL of the bead samples in a total reaction volume of 30 µL.

4.4.6 Mouse Blood Samples

Mouse blood was collected from adult C57BL/6J mice, and processed to plasma, serum and red blood cells.

Preparation of Blood Plasma

Mouse blood was collected into tubes containing 17 IU mL^{-1} sodium heparin (Braun), and mixed by inverting the tube 8–10 times. Blood plasma was separated immediately after collection (at latest 1 h after sample collection) by centrifugation at 2000 g for 10 min at 4 °C. The supernatant (blood plasma) was collected, aliquoted and stored at -20 °C until usage.

Preparation of Blood Serum

Mouse blood was collected, and allowed to clot for 30–40 min at room temperature. The clot was removed by centrifugation at 2000 g for 10 min at 4 °C. The supernatant (blood serum) was collected, aliquoted and stored at -20 °C until usage.

Preparation of Red Blood Cells

Mouse blood was collected into tubes containing 17 IU mL^{-1} sodium heparin (Braun), and mixed by inverting the tube 8–10 times. Red blood cells were separated from blood plasma immediately after collection (at latest 1 h after sample collection) by centrifugation at 2000 g for 10 min at 4 °C. The red blood cells collected in the pellet fraction were washed three times in PBS (pH 7.4, Ca^{2+}- and Mg^{2+}-free), aliquoted and stored at -20 °C until usage.

4.4.7 Patient Samples

Ethics Statement and Patient Population

Ethics approval for the use of patient samples was given by the cantonal ethics commission Zurich under the project number 2017-00760. According to the ethics approval, patient blood drawn for diagnostic purposes can be further reused for research purposes after diagnostic application. All patients have given written informed consent for the reuse of their biological specimens.

Blood samples from patients suffering from Parkinson's disease were provided by the Institute of Neurology at the University Hospital Zurich (Dr. med. Evdokia Efthymiou, Prof. Dr. med. Christian Baumann). Patients were diagnosed by the clinicians of the Institute of Neurology according to standard clinical diagnostic criteria, and most of them were in the hospital to undergo deep brain stimulation surgery.

Blood samples from healthy donors were obtained from the Swiss Transfusion SRC Zurich.

Blood Samples

Blood was collected into Vacutainer® blood collection tubes (Becton Dickinson, Prod. No. 366643) containing 1.8 mg mL^{-1} EDTA, and stored at -20 °C until usage. Samples were thawed at 37 °C directly before analysis.

4.4.8 Blood Pretreatment of Patient Samples

Sarkosyl Solubilisation

To solubilise patient blood samples, 600 µL of EDTA whole blood was mixed with 600 µL of a 30% sarkosyl (N-lauroylsarcosine sodium salt) stock solution (Sigma, Prod. No. 61747), and the mixture was incubated for 10 min at room temperature, 650 rpm. To collect insoluble particles, the mixture was ultracentrifuged at 100,000 g for 1 h at 4 °C. The pelleted fraction was resuspended in 1 mL of 50 mM NaOAc (pH 5.2) for washing, and centrifuged again at 100,000 g, 25 min, 4 °C). The supernatant was

discarded, and the pellet was resuspended in 50 µL of 50 mM NaOAc (pH 5.2). The resuspended pellets were vortexed vigorously before addition to the amplification reaction.

NaPTA Precipitation

To solubilise blood samples before precipitation with sodium phosphotungstic acid (NaPTA), 600 µL of EDTA whole blood was mixed with 200 µL of a 8% sarkosyl (Sigma, Prod. No. 61747) stock solution to a final sarkosyl concentration 2%, and solubilised for 2 h at 37 °C, 1200 rpm. After solubilisation, 800 µL of a 4% NaPTA (Sigma, Prod. No. P6395) were added for precipitation with a final NaPTA concentration of 2% overnight at 37 °C, 1200 rpm. To collect precipitates, the mixture was centrifuged at 15,000 g for 30 min at 25 °C. The supernatant was removed and the pellet resuspended in 2% sarkosyl, 2% NaPTA and incubated for another 1 h at 37 °C, 1200 rpm. Precipitates were collected by centrifugation at 15,000 g for 30 min at 25 °C. The pelleted precipitates were washed with 1 mL of PBS, centrifuged (15,000 g, 30 min, 25 °C), and resuspended in 50 µL of PBS. The resuspended pellets were used to seed the amplification reactions.

Steel beads capturing

316L grade stainless steel beads (ThyssenKrupp) with an average bead diameter of <20 µm were used for capturing of α-synuclein aggregates from human blood. Beads were autoclaved at 121 °C for 20 min before use. For capturing, 250 µg of autoclaved beads were mixed with 1 mL of EDTA whole blood, and the mixture was incubated overnight on a rotating wheel at room temperature. After incubation, the beads were collected with a magnet, and the blood supernatant was removed. The beads were resuspended in 500 µL of PBS and used to seed the amplification reactions.

Immunoprecipitation

Supramagnetic, 2.8 µm diameter sheep anti mouse IgG Dynabeads coupled to the anti-α-synuclein antibody syn211 (Thermo Fisher Scientific, Prod. No. 11202D) were used to specifically capture α-synuclein from human blood. For the coating, beads were resuspended by vortexing for 30 s, and 2 x 200 µL of beads were transferred to two tubes to prepare beads for four different samples. The beads were collected with a magnet, and the bead storage buffer was discarded. The beads were washed twice with 0.1% BSA in PBS, before addition of the primary anti-α-synuclein antibody syn211 (8 µg of Ab in 0.1% BSA in PBS per 200 µg of beads) into one of the two tubes and incubation for 2 h on a rotating wheel at 4 °C. The other tube with beads was incubated with 0.1% BSA in PBS (no primary Ab) for 2 h on a rotating wheel at 4 °C. After incubation, the beads in both tubes were collected with a magnet, and washed 3x with 1 mL of 0.1% BSA in PBS. After the last washing step, the beads were resuspended in 2 x 200 µL of 0.1% BSA in PBS. For the immunoprecipitation, 500 µL of EDTA whole blood was incubated for 30 min at room temperature on a rotating wheel with 500 µL of 50 mM Tris-HCl (pH 7.4), 1% NP-40, 150 mM NaCl and protease inhibitor (Roche). Following this preincubation, BSA was added to a final concentration of 0.5%, and 50 µL of uncoated Dynabeads were added for preclearing of the blood for 45 min on a rotating wheel at room temperature. After preclearing, beads with unspecifically bound material were removed with a magnet, and the supernatant was added to 50 µL of Dynabeads coated with syn211 anti-α-synuclein antibodies for immunoprecipitation. The samples were incubated overnight at room temperature on a rotating wheel. The next day, the beads were collected with a magnet, washed 2x with 1 mL of 50 mM Tris-HCl (pH 7.4), 0.5% NP-40, 150 mM NaCl containing 0.5% BSA, then 3x with 1 mL of the same buffer without BSA, and finally 2x with 1 mL of PBS. After the last washing step, the supernatant was discarded, an the beads were resuspended in 50 µL of PBS for propagation analysis with the α-synuclein amyloid amplification assay.

5 Conclusions and Perspectives

Amyloid amplification assays recapitulate the self-replicating properties of amyloid proteins. In the framework of this PhD study, I was able to advance amyloid amplification assays in different amyloid systems. By combining the power of digital microfluidics with the concept of amyloid self-propagation, I developed a quantitative assay to determine absolute numbers of amyloid propagons in a test sample. The assay is capable of detecting single propagation units, and precisely quantifying propagons at low concentrations. Further work included amplification of the disease-related proteins, prion protein and α-synuclein. I implemented the RT-QuIC, a prion amplification assay, and applied it for diagnostic and scientific applications. Moreover, I established an amplification assay for α-synuclein fibrils. The α-synuclein assay was used to study potential decontaminants for the inactivation of α-synuclein aggregates. In addition, different strategies were tested to develop a diagnostic blood test for α-synucleinopathies using the α-synuclein assay. Both, the prion and the α-synuclein amplification assays provide powerful tools to study diagnostic and scientific aspects of amyloid propagation.

The digitisation of amyloid amplification assays for pathologic proteins might represent the next step towards a new era of molecular diagnostics of neurodegenerative disorders. The absolute quantification of disease-related amyloid propagons holds great potential for applications in preclinical point-of-care diagnostics and for studying disease progression. Moreover, the ability to diagnose neurodegenerative disorders in patient blood samples at presymptomatic stages would represent a major breakthrough in the diagnosis of protein misfolding and aggregation diseases. More fundamentally, the further advancement of digital amyloid amplification assays will help us to develop a more complete understanding of the molecular mechanisms underlying self-propagation and infectivity in neurodegenerative diseases.

A Appendix

A.1 Protein Parameters

Protein	**MW** (Da)	ε_{280} $M^{-1}cm^{-1}$	**isoelectric point**	**#aa**
human insulin	5,808	5,270	5.39	51
insulin glargine	6,063	4,930	6.88	53
human α-synuclein	14,460	5,960	4.67	140
mouse PrP	23,019	63,370	9.56	209
hamster PrP	22,973	61,880	9.58	209

A.2 Primer Sequences

aSyn_c408t_for: `5'-ggaagggtatcaagactatgaacctgaagcctaagaa-3'`

37 bp, T_m: 78.28 C.

aSyn_c408t_rev: `5'-ttcttaggcttcaggttcatagtcttgatacccttcc-3'`

37 bp, T_m: 78.28 C.

All primers were synthesised by Microsynth (Balgach, Switzerland).

A.3 Gene and Protein Sequences of Human α-Synuclein

DNA Sequence of aSyn TAC136TAT

```
1          11         21         31         41
atggatgtat tcatgaaagg actttcaaag gccaaggagg gagttgtggc

51         61         71         81         91
tgctgctgag aaaaccaaac agggtgtagc agaagcagca ggaaagacaa

101        111        121        131        141
aagagggtgt tctctatgta ggctccaaaa ccaaggaggg agtggtgcat

151        161        171        181        191
ggtgtggcaa cagtggctga gaagaccaaa gagcaagtga ctaatgttgg

201        211        221        231        241
aggagcagtg gtgacgggtg tgacagcagt agcccagaag acagtggagg

251        261        271        281        291
gagcagggag cattgcagca gccactggct ttgtcaaaaa ggaccagttg

301        311        321        331        341
ggcaagaatg aagaaggagc cccacaggaa ggaattctgg aagatatgcc

351        361        371        381        391
tgtggatcct gacaatgagg cttatgaaat gccttctgag gaagggtatc

401        411
aagactatga acctgaagcc
```

Amino Acid Sequence of aSyn

```
1          11         21         31         41
MDVFMKGLSK AKEGVVAAAE KTKQGVAEAA GKTKEGVLYV GSKTKEGVVH

51         61         71         81         91
GVATVAEKTK EQVTNVGGAV VTGVTAVAQK TVEGAGSIAA ATGFVKKDQL

101        111        121        131
GKNEEGAPQE GILEDMPVDP DNEAYEMPSE EGYQDYEPEA
```

List of Figures

List of Tables

Bibliography

ADA (2010). „Diagnosis and classification of diabetes mellitus“. In: *American Diabetes Association: Diabetes Care* 33, pp. 62–69 (cit. on p. 18).

Aguzzi, A. (2009). „Cell biology: Beyond the prion principle“. In: *Nature* 459, pp. 924–925 (cit. on p. 14).

Aguzzi, A. and L. Rajendran (2009). „The transcellular spread of cytosolic amyloids, prions, and prionoids“. In: *Neuron* 64, pp. 783–790 (cit. on pp. 14, 16).

Aguzzi, A. and C. Zhu (2017). „Microglia in prion diseases“. In: *The Journal of Clinical Investigation* 127, pp. 3230–3239 (cit. on p. 8).

Aguzzi, A., C. Sigurdson, and M. Heikenwaelder (2008). „Molecular mechanisms of prion pathogenesis“. In: *Annual Review of Pathology Mechanisms of Disease* 3, pp. 11–40 (cit. on p. 8).

Aguzzi, A., M. Nuvolone, and C. Zhu (2013). „The immunobiology of prion diseases“. In: *Nature Reviews Immunology* 13, pp. 888–902 (cit. on p. 6).

Ahmad, A., I. S. Millett, S. Doniach, V. N. Uversky, and A. L. Fink (2003). „Partially folded intermediates in insulin fibrillation“. In: *Biochemistry* 42, pp. 11404–11416 (cit. on p. 35).

Anfinsen, C. B. (1973). „Principles that govern the folding of protein chains“. In: *Science* 181, pp. 223–230 (cit. on p. 3).

Arosio, P., T. C. Michaels, S. Linse, et al. (2016). „Kinetic analysis reveals the diversity of microscopic mechanisms through which molecular chaperones suppress amyloid formation“. In: *Nature Communications* 7, ncomms10948 (cit. on p. 6).

Atarashi, R., R. A. Moore, V. L. Sim, et al. (2007). „Ultrasensitive detection of scrapie prion protein using seeded conversion of recombinant prion protein.“ In: *Nature Methods* 4, pp. 645–650 (cit. on p. 22).

Atarashi, R., J. M. Wilham, L. Christensen, et al. (2008). „Simplified ultrasensitive prion detection by recombinant PrP conversion with shaking“. In: *Nature Methods* 5, pp. 211–212 (cit. on p. 22).

Atarashi, R., K. Satoh, K. Sano, et al. (2011). „Ultrasensitive human prion detection in cerebrospinal fluid by real-time quaking-induced conversion“. In: *Nature Medicine* 17, pp. 175–178 (cit. on p. 23).

Baba, M., S. Nakajo, P.-H. Tu, et al. (1998). „Aggregation of alpha-synuclein in Lewy bodies of sporadic Parkinson’s disease and dementia with Lewy bodies.“ In: *The American Journal of Pathology* 152, pp. 879–884 (cit. on p. 10).

Baldwin, A. J., T. P. Knowles, G. G. Tartaglia, et al. (2011). „Metastability of native proteins and the phenomenon of amyloid formation“. In: *Journal of the American Chemical Society* 133, pp. 14160–14163 (cit. on p. 3).

Baskakov, I. V. (2009). „Switching in amyloid structure within individual fibrils: implication for strain adaptation, species barrier and strain classification“. In: *FEBS Letters* 583, pp. 2618–2622 (cit. on p. 19).

Basler, K, B Oesch, M Scott, et al. (1986). „Scrapie and cellular PrP isoforms are encoded by the same chromosomal gene“. In: *Cell* 46, pp. 417–428 (cit. on p. 13).

Basova, E. Y. and F. Foret (2015). „Droplet microfluidics in (bio) chemical analysis“. In: *Analyst* 140, pp. 22–38 (cit. on p. 27).

Beekes, M., A. Thomzig, W. J. Schulz-Schaeffer, and R. Burger (2014). „Is there a risk of prion-like disease transmission by Alzheimer- or Parkinson-associated protein particles?“ In: *Acta Neuropathologica* 128, pp. 463–476 (cit. on pp. 78, 94).

Beer, N. R., B. J. Hindson, E. K. Wheeler, et al. (2007). „On-chip, real-time, single-copy polymerase chain reaction in picoliter droplets“. In: *Analytical Chemistry* 79, pp. 8471–8475 (cit. on p. 27).

Béland, M. and X. Roucou (2012). „The prion protein unstructured N-terminal region is a broad-spectrum molecular sensor with diverse and contrasting potential functions“. In: *Journal of Neurochemistry* 120, pp. 853–868 (cit. on p. 13).

Bennhold, H (1922). „Specific staining of amyloid by Congo red“. In: *Munchener Medizinische Wochenschrift* 69, pp. 1537–1538 (cit. on p. 1).

Bishop, M. F. and F. A. Ferrone (1984). „Kinetics of nucleation-controlled polymerization. A perturbation treatment for use with a secondary pathway“. In: *Biophysical Journal* 46, pp. 631–644 (cit. on p. 4).

Bolton, D. C., M. P. McKinley, and S. B. Prusiner (1982). „Identification of a protein that purifies with the scrapie prion“. In: *Science* 218, pp. 1309–1311 (cit. on p. 13).

Bouchard, M., J. Zurdo, E. J. Nettleton, C. M. Dobson, and C. V. Robinson (2000). „Formation of insulin amyloid fibrils followed by FTIR simultaneously with CD and electron microscopy“. In: *Protein Science* 9, pp. 1960–1967 (cit. on p. 34).

Bougard, D., J.-P. Brandel, M. Bélondrade, et al. (2016). „Detection of prions in the plasma of presymptomatic and symptomatic patients with variant Creutzfeldt-Jakob disease“. In: *Science Translational Medicine* 8, 370ra182 (cit. on pp. 21, 85, 90).

Bousset, L., L. Pieri, G. Ruiz-Arlandis, et al. (2013). „Structural and functional characterization of two alpha-synuclein strains“. In: *Nature Communications* 4, ncomms2575 (cit. on p. 99).

Bousset, L., P. Brundin, A. Böckmann, B. Meier, and R. Melki (2016). „An efficient procedure for removal and inactivation of alpha-synuclein assemblies from laboratory materials“. In: *Journal of Parkinson's Disease* 6, pp. 143–151 (cit. on pp. 94, 95).

Braak, H., U Rüb, W. Gai, and K. Del Tredici (2003a). „Idiopathic Parkinson's disease: possible routes by which vulnerable neuronal types may be subject to neuroinvasion by an unknown pathogen“. In: *Journal of Neural Transmission* 110, pp. 517–536 (cit. on p. 95).

Braak, H., K. Del Tredici, U. Rüb, et al. (2003b). „Staging of brain pathology related to sporadic Parkinson's disease“. In: *Neurobiology of Aging* 24, pp. 197–211 (cit. on p. 9).

Brange, J., L. Andersen, E. D. Laursen, G. Meyn, and E. Rasmussen (1997). „Toward understanding insulin fibrillation“. In: *Journal of Pharmaceutical Sciences* 86, pp. 517–525 (cit. on pp. 37, 42).

Bremer, J., F. Baumann, C. Tiberi, et al. (2010). „Axonal prion protein is required for peripheral myelin maintenance“. In: *Nature Neuroscience* 13, pp. 310–318 (cit. on p. 12).

Budka, H., A. Aguzzi, P. Brown, et al. (1995). „Neuropathological diagnostic criteria for Creutzfeldt-Jakob disease (CJD) and other human spongiform encephalopathies (Prion diseases)“. In: *Brain Pathology* 5, pp. 459–466 (cit. on p. 8).

Büeler, H., A. Aguzzi, A Sailer, et al. (1993). „Mice devoid of PrP are resistant to scrapie“. In: *Cell* 73, pp. 1339–1347 (cit. on p. 14).

Buell, A. K., C. Galvagnion, R. Gaspar, et al. (2014). „Solution conditions determine the relative importance of nucleation and growth processes in α-synuclein aggregation“. In: *Proceedings of the National Academy of Sciences* 111, pp. 7671–7676 (cit. on p. 76).

Burke, M. J. and M. A. Rougvie (1972). „Cross-β protein structures. I. Insulin fibrils“. In: *Biochemistry* 11, pp. 2435–2439 (cit. on p. 17).

Burré, J., M. Sharma, T. Tsetsenis, et al. (2010). „α-Synuclein promotes SNARE-complex assembly in vivo and in vitro“. In: *Science* 329, pp. 1663–1667 (cit. on p. 15).

Castilla, J., P. Saá, and C. Soto (2005a). „Detection of prions in blood“. In: *Nature Medicine* 11, pp. 982–985 (cit. on pp. 21, 22).

Castilla, J., P. Saá, C. Hetz, and C. Soto (2005b). „In vitro generation of infectious scrapie prions“. In: *Cell* 121, pp. 195–206 (cit. on pp. 14, 21).

Caughey, B., D. A. Kocisko, G. J. Raymond, and P. T. Lansbury (1995). „Aggregates of scrapie-associated prion protein induce the cell-free conversion of protease-sensitive prion protein to the protease-resistant state“. In: *Chemistry & Biology* 2, pp. 807–817 (cit. on p. 20).

Chan, S. J., P. Keim, and D. F. Steiner (1976). „Cell-free synthesis of rat preproinsulins: characterization and partial amino acid sequence determination“. In: *Proceedings of the National Academy of Sciences* 73, pp. 1964–1968 (cit. on p. 17).

Chen, B., R. Morales, M. A. Barria, and C. Soto (2010). „Estimating prion concentration in fluids and tissues by quantitative PMCA“. In: *Nature Methods* 7, pp. 519–520 (cit. on pp. 21, 42).

Cheng, K., A. Sloan, K. M. Avery, et al. (2014). „Exploring physical and chemical factors influencing the properties of recombinant prion protein and the real-time quaking-induced conversion (RT-QuIC) assay“. In: *PLoS One* 9, e84812 (cit. on p. 65).

Chiti, F. and C. M. Dobson (2006). „Protein misfolding, functional amyloid, and human disease“. In: *Annual Review of Biochemistry* 75, pp. 333–366 (cit. on pp. 1, 7, 8).

Cohen, A. S. and E. Calkins (1959). „Electron microscopic observations on a fibrous component in amyloid of diverse origins“. In: *Nature* 183, pp. 1202–1203 (cit. on p. 1).

Cohen, S. I., M. Vendruscolo, M. E. Welland, et al. (2011). „Nucleated polymerization with secondary pathways. I. Time evolution of the principal moments“. In: *The Journal of Chemical Physics* 135, jcp065105 (cit. on p. 5).

Cohen, S. I., M. Vendruscolo, C. M. Dobson, and T. P. Knowles (2012). „From macroscopic measurements to microscopic mechanisms of protein aggregation“. In: *Journal of Molecular Biology* 421, pp. 160–171 (cit. on p. 5).

Cohen, S. I., S. Linse, L. M. Luheshi, et al. (2013). „Proliferation of amyloid-β42 aggregates occurs through a secondary nucleation mechanism“. In: *Proceedings of the National Academy of Sciences* 110, pp. 9758–9763 (cit. on p. 6).

Cohen, S. I., P. Arosio, J. Presto, et al. (2015). „A molecular chaperone breaks the catalytic cycle that generates toxic Aβ oligomers“. In: *Nature Structural & Molecular Biology* 22, pp. 207–213 (cit. on p. 6).

Colby, D. W., Q. Zhang, S. Wang, et al. (2007). „Prion detection by an amyloid seeding assay“. In: *Proceedings of the National Academy of Sciences* 104, pp. 20914–20919 (cit. on pp. 20, 23).

Collinge, J. (2001). „Prion diseases of humans and animals: their causes and molecular basis“. In: *Annual Review of Neuroscience* 24, pp. 519–550 (cit. on p. 8).

Collins, D. J., A. Neild, A.-Q. Liu, Y. Ai, et al. (2015). „The Poisson distribution and beyond: methods for microfluidic droplet production and single cell encapsulation“. In: *Lab on a Chip* 15, pp. 3439–3459 (cit. on p. 27).

Collins, S, A Boyd, A Fletcher, et al. (2000). „Creutzfeldt-Jakob disease: diagnostic utility of 14–3–3 protein immunodetection in cerebrospinal fluid“. In: *Journal of Clinical Neuroscience* 7, pp. 203–208 (cit. on pp. 9, 55).

Collins, S. R., A. Douglass, R. D. Vale, and J. S. Weissman (2004). „Mechanism of prion propagation: amyloid growth occurs by monomer addition“. In: *PLoS Biology* 2, e321 (cit. on p. 5).

Concha-Marambio, L, S Pritzkow, F Moda, F Tagliavini, J. Ironside, et al. (2016). „Detection of prions in blood from patients with variant Creutzfeldt-Jakob disease.“ In: *Science Translational Medicine* 8, 370ra183 (cit. on pp. 21, 85, 96).

Cox, B., F. Ness, and M. Tuite (2003). „Analysis of the generation and segregation of propagons: entities that propagate the [PSI+] prion in yeast“. In: *Genetics* 165, pp. 23–33 (cit. on p. 6).

Cramm, M., M. Schmitz, A. Karch, et al. (2016). „Stability and reproducibility underscore utility of RT-QuIC for diagnosis of Creutzfeldt-Jakob disease“. In: *Molecular Neurobiology* 53, pp. 1896–1904 (cit. on pp. 23, 65).

Davidson, W. S., A. Jonas, D. F. Clayton, and J. M. George (1998). „Stabilization of α-synuclein secondary structure upon binding to synthetic membranes“. In: *Journal of Biological Chemistry* 273, pp. 9443–9449 (cit. on p. 14).

Diaz-Espinoza, R. and C. Soto (2010). „Generation of prions in vitro and the protein-only hypothesis“. In: *Prion* 4, pp. 53–59 (cit. on p. 14).

Dische, F., C Wernstedt, G. Westermark, et al. (1988). „Insulin as an amyloid-fibril protein at sites of repeated insulin injections in a diabetic patient“. In: *Diabetologia* 31, pp. 158–161 (cit. on p. 11).

Du, D., A. N. Murray, E. Cohen, et al. (2011). „A kinetic aggregation assay allowing selective and sensitive amyloid-β quantification in cells and tissues“. In: *Biochemistry* 50, pp. 1607–1617 (cit. on p. 25).

Eanes, E. and G. Glenner (1968). „X-ray diffraction studies on amyloid filaments“. In: *Journal of Histochemistry & Cytochemistry* 16, pp. 673–677 (cit. on p. 1).

Edgeworth, J. A., N. Gros, J. Alden, et al. (2010). „Spontaneous generation of mammalian prions“. In: *Proceedings of the National Academy of Sciences* 107, pp. 14402–14406 (cit. on pp. 58, 66).

Edgeworth, J. A., M. Farmer, A. Sicilia, et al. (2011). „Detection of prion infection in variant Creutzfeldt-Jakob disease: a blood-based assay“. In: *The Lancet* 377, pp. 487–493 (cit. on p. 96).

Eisenberg, D. and M. Jucker (2012). „The amyloid state of proteins in human diseases“. In: *Cell* 148, pp. 1188–1203 (cit. on pp. 1, 2).

Elder, A. M., D. M. Henderson, A. V. Nalls, et al. (2013). „In vitro detection of prionemia in TSE-infected cervids and hamsters“. In: *PLoS One* 8, e80203 (cit. on p. 23).

Elder, A. M., D. M. Henderson, A. V. Nalls, et al. (2015). „Immediate and ongoing detection of prions in the blood of hamsters and deer following oral, nasal, or blood inoculations“. In: *Journal of Virology* 89, pp. 7421–7424 (cit. on pp. 85, 88, 96).

Eliezer, D., E. Kutluay, R. Bussell, and G. Browne (2001). „Conformational properties of α-synuclein in its free and lipid-associated states“. In: *Journal of Molecular Biology* 307, pp. 1061–1073 (cit. on p. 14).

Estrada, L. D., D. Chamorro, M. J. Yañez, et al. (2016). „Reduction of blood amyloid-β oligomers in Alzheimer's disease transgenic mice by c-Abl kinase inhibition“. In: *Journal of Alzheimer's Disease* 54, pp. 1193–1205 (cit. on p. 26).

Fairfoul, G., L. I. McGuire, S. Pal, et al. (2016). „Alpha-synuclein RT-QuIC in the CSF of patients with alpha-synucleinopathies“. In: *Annals of Clinical and Translational Neurology* 3, pp. 812–818 (cit. on pp. 10, 26, 93, 95, 97).

Ferrone, F. (1999). „[17] Analysis of protein aggregation kinetics“. In: *Methods in Enzymology* 309, pp. 256–274 (cit. on p. 5).

Ferrone, F. A., J. Hofrichter, H. R. Sunshine, and W. A. Eaton (1980). „Kinetic studies on photolysis-induced gelation of sickle cell hemoglobin suggest a new mechanism“. In: *Biophysical Journal* 32, pp. 361–380 (cit. on p. 4).

Ferrone, F. A., J. Hofrichter, and W. A. Eaton (1985). „Kinetics of sickle hemoglobin polymerization: II. A double nucleation mechanism“. In: *Journal of Molecular Biology* 183, pp. 611–631 (cit. on p. 4).

Flagmeier, P., G. Meisl, M. Vendruscolo, et al. (2016). „Mutations associated with familial Parkinson's disease alter the initiation and amplification steps of α-synuclein aggregation“. In: *Proceedings of the National Academy of Sciences* 113, pp. 10328–10333 (cit. on p. 6).

Flechsig, E., I. Hegyi, M. Enari, et al. (2001). „Transmission of scrapie by steel-surface-bound prions“. In: *Molecular Medicine* 7, pp. 679–684 (cit. on p. 56).

Friedreich, N and A Kekule (1859). „Zur Amyloidfrage“. In: *Virchows Archive for Pathological Anatomy and Physiology* 16, pp. 50–65 (cit. on p. 1).

Frontzek, K., M. Pfammatter, S. Sorce, et al. (2016). „Neurotoxic antibodies against the prion protein do not trigger prion replication“. In: *PLoS One* 11, e0163601 (cit. on pp. 63, 64, 72).

Galvagnion, C., A. K. Buell, G. Meisl, et al. (2015). „Lipid vesicles trigger α-synuclein aggregation by stimulating primary nucleation“. In: *Nature Chemical Biology* 11, pp. 229–234 (cit. on p. 6).

Gazit, E. (2002). „The "correctly folded" state of proteins: is it a metastable state?“ In: *Angewandte Chemie International Edition* 41, pp. 257–259 (cit. on p. 3).

Geddes, A., K. Parker, E. Atkins, and E Beighton (1968). „"Cross-β" conformation in proteins“. In: *Journal of Molecular Biology* 32, pp. 343–358 (cit. on p. 1).

Gelb, D. J., E. Oliver, and S. Gilman (1999). „Diagnostic criteria for Parkinson disease“. In: *Archives of Neurology* 56, pp. 33–39 (cit. on p. 10).

Giasson, B. I., I. V. Murray, J. Q. Trojanowski, and V. M.-Y. Lee (2001). „A hydrophobic stretch of 12 amino acid residues in the middle of α-synuclein is essential for filament assembly“. In: *Journal of Biological Chemistry* 276, pp. 2380–2386 (cit. on p. 14).

Gilman, S, P. A. Low, N Quinn, et al. (1999). „Consensus statement on the diagnosis of multiple system atrophy“. In: *Journal of the Neurological Sciences* 163, pp. 94–98 (cit. on p. 10).

Gomez-Tortosa, E, K Newell, M. Irizarry, et al. (1999). „Clinical and quantitative pathologic correlates of dementia with Lewy bodies“. In: *Neurology* 53, pp. 1284–1284 (cit. on p. 10).

Gonzalez-Montalban, N., N. Makarava, V. G. Ostapchenko, et al. (2011). „Highly efficient protein misfolding cyclic amplification“. In: *PLoS Pathogens* 7, e1001277 (cit. on p. 22).

Gonzalez-Romero, D., M. A. Barria, P. Leon, R. Morales, and C. Soto (2008). „Detection of infectious prions in urine“. In: *FEBS Letters* 582, pp. 3161–3166 (cit. on p. 21).

Groveman, B. R., C. D. Orrú, A. G. Hughson, et al. (2017). „Extended and direct evaluation of RT-QuIC assays for Creutzfeldt-Jakob disease diagnosis“. In: *Annals of Clinical and Translational Neurology* 4, pp. 139–144 (cit. on pp. 9, 25, 65).

Guo, M. T., A. Rotem, J. A. Heyman, and D. A. Weitz (2012). „Droplet microfluidics for high-throughput biological assays“. In: *Lab on a Chip* 12, pp. 2146–2155 (cit. on pp. 27, 39).

Gupta, Y., G. Singla, and R. Singla (2015). „Insulin-derived amyloidosis“. In: *Indian Journal of Endocrinology and Metabolism* 19, pp. 174–177 (cit. on p. 11).

Heinzer, D. (2016). „Establishing methods to detect surface-bound scrapie prion protein on surgical steel“. In: *University of Zurich,* Master Thesis, pp. 1–73 (cit. on p. 71).

Henderson, D. M., K. A. Davenport, N. J. Haley, et al. (2015). „Quantitative assessment of prion infectivity in tissues and body fluids by real-time quaking-induced conversion“. In: *Journal of General Virology* 96, pp. 210–219 (cit. on pp. 29, 42, 66).

Herrmann, U. S., T. Sonati, J. Falsig, et al. (2015). „Prion infections and anti-PrP antibodies trigger converging neurotoxic pathways“. In: *PLoS Pathogens* 11, e1004662 (cit. on p. 63).

Herva, M. E., S. Zibaee, G. Fraser, et al. (2014). „Anti-amyloid compounds inhibit α-synuclein aggregation induced by protein misfolding cyclic amplification (PMCA)“. In: *Journal of Biological Chemistry* 289, pp. 11897–11905 (cit. on p. 26).

Hill, A. F., M. Antoniou, and J. Collinge (1999). „Protease-resistant prion protein produced in vitro lacks detectable infectivity.“ In: *Journal of General Virology* 80, pp. 11–14 (cit. on p. 20).

Hilton, D., M. Stephens, L. Kirk, et al. (2014). „Accumulation of α-synuclein in the bowel of patients in the pre-clinical phase of Parkinson’s disease“. In: *Acta Neuropathologica* 127, pp. 235–241 (cit. on p. 95).

Hindson, B. J., K. D. Ness, D. A. Masquelier, et al. (2011). „High-throughput droplet digital PCR system for absolute quantitation of DNA copy number“. In: *Analytical Chemistry* 83, pp. 8604–8610 (cit. on p. 27).

Holmqvist, S., O. Chutna, L. Bousset, et al. (2014). „Direct evidence of Parkinson pathology spread from the gastrointestinal tract to the brain in rats“. In: *Acta Neuropathologica* 128, pp. 805–820 (cit. on p. 95).

Holtze, C, A. Rowat, J. Agresti, et al. (2008). „Biocompatible surfactants for water-in-fluorocarbon emulsions“. In: *Lab on a Chip* 8, pp. 1632–1639 (cit. on p. 47).

Hoyer, W., T. Antony, D. Cherny, et al. (2002). „Dependence of α-synuclein aggregate morphology on solution conditions“. In: *Journal of Molecular Biology* 322, pp. 383–393 (cit. on p. 74).

Hua, Q.-X., S. N. Gozani, R. E. Chance, et al. (1995). „Structure of a protein in a kinetic trap“. In: *Nature Structural & Molecular Biology* 2, pp. 129–138 (cit. on p. 17).

Huang, S. and M. P. Czech (2007). „The GLUT4 glucose transporter“. In: *Cell Metabolism* 5, pp. 237–252 (cit. on p. 18).

Huggett, J. F., S. Cowen, and C. A. Foy (2015). „Considerations for digital PCR as an accurate molecular diagnostic tool“. In: *Clinical Chemistry* 61, pp. 79–88 (cit. on p. 28).

Hughson, A. G., B. Race, A. Kraus, et al. (2016). „Inactivation of prions and amyloid seeds with hypochlorous acid“. In: *PLoS Pathogens* 12, e1005914 (cit. on p. 94).

Ivanova, M. I., S. A. Sievers, M. R. Sawaya, J. S. Wall, and D. Eisenberg (2009). „Molecular basis for insulin fibril assembly“. In: *Proceedings of the National Academy of Sciences* 106, pp. 18990–18995 (cit. on p. 34).

Jankovic, J. (2008). „Parkinson's disease: clinical features and diagnosis“. In: *Journal of Neurology, Neurosurgery & Psychiatry* 79, pp. 368–376 (cit. on p. 9).

Jeffrey, P. and J. Coates (1966). „An equilibrium ultracentrifuge study of the self-association of bovine insulin“. In: *Biochemistry* 5, pp. 489–498 (cit. on p. 17).

Jellinger, K. A., K. Seppi, and G. K. Wenning (2005). „Grading of neuropathology in multiple system atrophy: proposal for a novel scale“. In: *Movement Disorders* 20, pp. 29–36 (cit. on p. 10).

Jiménez, J. L., E. J. Nettleton, M. Bouchard, et al. (2002). „The protofilament structure of insulin amyloid fibrils“. In: *Proceedings of the National Academy of Sciences* 99, pp. 9196–9201 (cit. on pp. 2, 34).

Johnson, I. S. (1983). „Human insulin from recombinant DNA technology“. In: *Science* 219, pp. 632–637 (cit. on p. 18).

Jung, B. C., Y.-J. Lim, E.-J. Bae, et al. (2017). „Amplification of distinct α-synuclein fibril conformers through protein misfolding cyclic amplification“. In: *Experimental & Molecular Medicine* 49, e314 (cit. on p. 26).

Kiss, M. M., L. Ortoleva-Donnelly, N. R. Beer, et al. (2008). „High-throughput quantitative polymerase chain reaction in picoliter droplets“. In: *Analytical Chemistry* 80, pp. 8975–8981 (cit. on p. 27).

Knowles, T. P., A. W. Fitzpatrick, S. Meehan, et al. (2007). „Role of intermolecular forces in defining material properties of protein nanofibrils“. In: *Science* 318, pp. 1900–1903 (cit. on p. 3).

Knowles, T. P., C. A. Waudby, G. L. Devlin, et al. (2009). „An analytical solution to the kinetics of breakable filament assembly“. In: *Science* 326, pp. 1533–1537 (cit. on p. 5).

Knowles, T. P., D. A. White, A. R. Abate, et al. (2011). „Observation of spatial propagation of amyloid assembly from single nuclei“. In: *Proceedings of the National Academy of Sciences* 108, pp. 14746–14751 (cit. on p. 27).

Knowles, T. P., M. Vendruscolo, and C. M. Dobson (2014). „The amyloid state and its association with protein misfolding diseases“. In: *Nature Reviews Molecular Cell Biology* 15, pp. 384–396 (cit. on pp. 3, 7).

Kocisko, D. A., J. H. Come, S. A. Priola, et al. (1994). „Cell-free formation of protease-resistant prion protein“. In: *Nature* 370, pp. 471–474 (cit. on p. 20).

Kondru, N., S. Manne, J. Greenlee, et al. (2017). „Integrated organotypic slice cultures and RT-QuIC (OSCAR) assay: implications for translational discovery in protein misfolding diseases“. In: *Scientific Reports* 7, srep43155 (cit. on p. 68).

Kretzschmar, H. A., L. E. Stowring, D. Westaway, et al. (1986). „Molecular cloning of a human prion protein cDNA“. In: *DNA* 5, pp. 315–324 (cit. on p. 12).

Küffer, A., A. K. Lakkaraju, A. Mogha, et al. (2016). „The prion protein is an agonistic ligand of the G protein-coupled receptor Adgrg6“. In: *Nature* 536, pp. 464–468 (cit. on p. 12).

Lacroux, C., E. Comoy, M. Moudjou, et al. (2014). „Preclinical detection of variant CJD and BSE prions in blood“. In: *PLoS Pathogens* 10, e1004202 (cit. on p. 21).

Lan, F., J. R. Haliburton, A. Yuan, and A. R. Abate (2016). „Droplet barcoding for massively parallel single-molecule deep sequencing“. In: *Nature Communications* 7, ncomms11784 (cit. on p. 27).

Legname, G., I. V. Baskakov, H.-O. B. Nguyen, et al. (2004). „Synthetic mammalian prions“. In: *Science* 305, pp. 673–676 (cit. on p. 14).

Levine, D. J., J. Stoehr, L. E. Falese, et al. (2015). „Mechanism of scrapie prion precipitation with phosphotungstate anions“. In: *ACS Chemical Biology* 10, pp. 1269–1277 (cit. on p. 88).

Logan, T., J. Bendor, C. Toupin, K. Thorn, and R. H. Edwards (2017). „[alpha]-Synuclein promotes dilation of the exocytotic fusion pore“. In: *Nature Neuroscience* 20, pp. 681–689 (cit. on p. 16).

Luk, K. C., V. M. Kehm, B. Zhang, et al. (2012a). „Intracerebral inoculation of pathological α-synuclein initiates a rapidly progressive neurodegenerative α-synucleinopathy in mice“. In: *Journal of Experimental Medicine*, jem20112457 (cit. on pp. 16, 93).

Luk, K. C., V. Kehm, J. Carroll, et al. (2012b). „Pathological α-synuclein transmission initiates Parkinson-like neurodegeneration in nontransgenic mice“. In: *Science* 338, pp. 949–953 (cit. on pp. 16, 30).

Makin, O. S., E. Atkins, P. Sikorski, J. Johansson, and L. C. Serpell (2005). „Molecular basis for amyloid fibril formation and stability“. In: *Proceedings of the National Academy of Sciences* 102, pp. 315–320 (cit. on p. 3).

Mao, X., M. T. Ou, S. S. Karuppagounder, et al. (2016). „Pathological α-synuclein transmission initiated by binding lymphocyte-activation gene 3“. In: *Science* 353, aah3374 (cit. on p. 16).

Maroteaux, L., J. T. Campanelli, and R. H. Scheller (1988). „Synuclein: a neuron-specific protein localized to the nucleus and presynaptic nerve terminal“. In: *Journal of Neuroscience* 8, pp. 2804–2815 (cit. on pp. 14, 15).

Martí, M. J., E. Tolosa, and J. Campdelacreu (2003). „Clinical overview of the synucleinopathies“. In: *Movement Disorders* 18, pp. 21–27 (cit. on p. 9).

Masuda, M., N. Dohmae, T. Nonaka, et al. (2006). „Cysteine misincorporation in bacterially expressed human α-synuclein“. In: *FEBS Letters* 580, pp. 1775–1779 (cit. on pp. 74, 98).

Masuda-Suzukake, M., T. Nonaka, M. Hosokawa, et al. (2013). „Prion-like spreading of pathological α-synuclein in brain“. In: *Brain* 136, pp. 1128–1138 (cit. on pp. 16, 30, 93).

Matteucci, E., O. Giampietro, V. Covolan, et al. (2015). „Insulin administration: present strategies and future directions for a noninvasive (possibly more physiological) delivery“. In: *Drug Design, Development and Therapy* 9, pp. 3109–3118 (cit. on p. 11).

McDonald, J. C., D. Duffy, J. Anderson, et al. (2000). „Fabrication of microfluidic systems in poly(dimethylsiloxane)“. In: *Electrophoresis* 21, pp. 27–40 (cit. on p. 46).

McGuire, L. I., A. H. Peden, C. D. Orrú, et al. (2012). „Real time quaking-induced conversion analysis of cerebrospinal fluid in sporadic Creutzfeldt–Jakob disease“. In: *Annals of Neurology* 72, pp. 278–285 (cit. on p. 23).

McGuire, L. I., A. Poleggi, I. Poggiolini, et al. (2016). „Cerebrospinal fluid real-time quaking-induced conversion is a robust and reliable test for sporadic Creutzfeldt–Jakob disease: An international study“. In: *Annals of Neurology* 80, pp. 160–165 (cit. on pp. 23, 37, 53, 65).

McKeith, I. G., D. W. Dickson, J Lowe, et al. (2005). „Diagnosis and management of dementia with Lewy bodies third report of the DLB consortium“. In: *Neurology* 65, pp. 1863–1872 (cit. on p. 10).

Meisl, G., X. Yang, E. Hellstrand, et al. (2014). „Differences in nucleation behavior underlie the contrasting aggregation kinetics of the Aβ40 and Aβ42 peptides“. In: *Proceedings of the National Academy of Sciences* 111, pp. 9384–9389 (cit. on p. 6).

Meisl, G., L. Rajah, S. A. Cohen, et al. (2017). „Scaling behaviour and rate-determining steps in filamentous self-assembly“. In: *Chemical Science* 8, pp. 7087–7097 (cit. on pp. 5, 6).

Meyer, V., P. D. Dinkel, E. Rickman Hager, and M. Margittai (2014). „Amplification of Tau fibrils from minute quantities of seeds“. In: *Biochemistry* 53, pp. 5804–5809 (cit. on p. 26).

Miller, M. B. and S. Supattapone (2011). „Superparamagnetic nanoparticle capture of prions for amplification“. In: *Journal of Virology* 85, pp. 2813–2817 (cit. on p. 22).

Mok, J., M. N. Mindrinos, R. W. Davis, and M. Javanmard (2014). „Digital microfluidic assay for protein detection“. In: *Proceedings of the National Academy of Sciences* 111, pp. 2110–2115 (cit. on p. 27).

Mori, T., R. Atarashi, K. Furukawa, et al. (2016). „A direct assessment of human prion adhered to steel wire using real-time quaking-induced conversion“. In: *Scientific Reports* 6, srep24993 (cit. on pp. 58, 67).

Mougenot, A.-L., S. Nicot, A. Bencsik, et al. (2012). „Prion-like acceleration of a synucleinopathy in a transgenic mouse model“. In: *Neurobiology of Aging* 33, pp. 2225–2228 (cit. on pp. 16, 93).

Nagase, T., K. Iwaya, Y. Iwaki, et al. (2014). „Insulin-derived amyloidosis and poor glycemic control: a case series“. In: *The American Journal of Medicine* 127, pp. 450–454 (cit. on p. 11).

Nelson, R., M. R. Sawaya, M. Balbirnie, et al. (2005). „Structure of the cross-β spine of amyloid-like fibrils“. In: *Nature* 435, pp. 773–778 (cit. on pp. 2, 3, 34).

Nettleton, E. J., P. Tito, M. Sunde, et al. (2000). „Characterization of the oligomeric states of insulin in self-assembly and amyloid fibril formation by mass spectrometry“. In: *Biophysical Journal* 79, pp. 1053–1065 (cit. on p. 34).

Nielsen, L., S. Frokjaer, J. Brange, V. N. Uversky, and A. L. Fink (2001). „Probing the mechanism of insulin fibril formation with insulin mutants“. In: *Biochemistry* 40, pp. 8397–8409 (cit. on p. 17).

Nilsson, M. R. (2016). „Insulin amyloid at injection sites of patients with diabetes“. In: *Amyloid* 23, pp. 139–147 (cit. on p. 11).

Nilsson, M. R. and C. M. Dobson (2003). „Chemical modification of insulin in amyloid fibrils“. In: *Protein Science* 12, pp. 2637–2641 (cit. on pp. 34, 44).

Oosawa, F. and M. Kasai (1962). „A theory of linear and helical aggregations of macromolecules“. In: *Journal of Molecular Biology* 4, pp. 10–21 (cit. on p. 4).

Orrú, C. D., J. M. Wilham, L. D. Raymond, et al. (2011). „Prion disease blood test using immunoprecipitation and improved quaking-induced conversion“. In: *MBio* 2, e00078–11 (cit. on pp. 85, 90).

Orru, C. D., J. M. Wilham, S. Vascellari, A. G. Hughson, and B. Caughey (2012). „New generation QuIC assays for prion seeding activity“. In: *Prion* 6, pp. 147–152 (cit. on p. 41).

Orrú, C. D., M. Bongianni, G. Tonoli, et al. (2014). „A test for Creutzfeldt–Jakob disease using nasal brushings“. In: *New England Journal of Medicine* 371, pp. 519–529 (cit. on pp. 25, 65).

Orrú, C. D., B. R. Groveman, A. G. Hughson, et al. (2015). „Rapid and sensitive RT-QuIC detection of human Creutzfeldt-Jakob disease using cerebrospinal fluid“. In: *MBio* 6, e02451–14 (cit. on pp. 23, 25, 65).

Orrú, C. D., A. G. Hughson, B. R. Groveman, et al. (2016). „Factors that improve RT-QuIC detection of prion seeding activity“. In: *Viruses* 8, p. v140 (cit. on p. 65).

Osterberg, V. R., K. J. Spinelli, L. J. Weston, et al. (2015). „Progressive aggregation of alpha-synuclein and selective degeneration of Lewy inclusion-bearing neurons in a mouse model of parkinsonism“. In: *Cell Reports* 10, pp. 1252–1260 (cit. on p. 16).

Park, J.-H., Y.-G. Choi, Y.-J. Lee, et al. (2016). „Real-time quaking-induced conversion analysis for the diagnosis of sporadic Creutzfeldt-Jakob disease in Korea“. In: *Journal of Clinical Neurology* 12, pp. 101–106 (cit. on p. 23).

Peelaerts, W., L. Bousset, A. Van der Perren, et al. (2015). „α-Synuclein strains cause distinct synucleinopathies after local and systemic administration“. In: *Nature* 522, pp. 340–344 (cit. on p. 95).

Pfammatter, M., M. Andreasen, G. Meisl, et al. (2017). „Absolute Quantification of Amyloid Propagons by Digital Microfluidics“. In: *Analytical chemistry* 89, pp. 12306–12313 (cit. on pp. 32–36, 38–40, 42).

Provencher, S. W. (1982). „A constrained regularization method for inverting data represented by linear algebraic or integral equations“. In: *Computer Physics Communications* 27, pp. 213–227 (cit. on p. 45).

Prusiner, S. B. et al. (1982). „Novel proteinaceous infectious particles cause scrapie“. In: *Science* 216, pp. 136–144 (cit. on pp. 12, 14).

Prusiner, S. B., M. P. McKinley, K. A. Bowman, et al. (1983). „Scrapie prions aggregate to form amyloid-like birefringent rods“. In: *Cell* 35, pp. 349–358 (cit. on p. 13).

Prusiner, S. B., M. Scott, D. Foster, et al. (1990). „Transgenetic studies implicate interactions between homologous PrP isoforms in scrapie prion replication“. In: *Cell* 63, pp. 673–686 (cit. on p. 13).

Pyatigorskaya, N., C. Gallea, D. Garcia-Lorenzo, M. Vidailhet, and S. Lehericy (2014). „A review of the use of magnetic resonance imaging in Parkinson's disease“. In: *Therapeutic Advances in Neurological Disorders* 7, pp. 206–220 (cit. on p. 10).

Raeber, A., D. Borchelt, M Scott, and S. Prusiner (1992). „Attempts to convert the cellular prion protein into the scrapie isoform in cell-free systems.“ In: *Journal of Virology* 66, pp. 6155–6163 (cit. on p. 20).

Reimann, R. R., T. Sonati, S. Hornemann, et al. (2016). „Differential toxicity of antibodies to the prion protein“. In: *PLoS Pathogens* 12, e1005401 (cit. on p. 63).

Riek, R., S. Hornemann, G. Wider, et al. (1996). „NMR structure of the mouse prion protein domain PrP (121–231)“. In: *Nature* 382, pp. 180–182 (cit. on p. 12).

Riek, R., S. Hornemann, G. Wider, R. Glockshuber, and K. Wüthrich (1997). „NMR characterization of the full-length recombinant murine prion protein, mPrP (23–231)“. In: *FEBS Letters* 413, pp. 282–288 (cit. on p. 12).

Roberts, C. J. (2014). „Protein aggregation and its impact on product quality“. In: *Current Opinion in Biotechnology* 30, pp. 211–217 (cit. on p. 43).

Ross, C. A. and M. A. Poirier (2004). „Protein aggregation and neurodegenerative disease“. In: *Nature Medicine* 10, pp. 10–17 (cit. on p. 7).

Rubenstein, R., B. Chang, P. Gray, et al. (2010). „A novel method for preclinical detection of PrPSc in blood“. In: *Journal of General Virology* 91, pp. 1883–1892 (cit. on p. 22).

Saá, P., J. Castilla, and C. Soto (2006a). „Presymptomatic detection of prions in blood“. In: *Science* 313, pp. 92–94 (cit. on p. 21).

– (2006b). „Ultra-efficient replication of infectious prions by automated protein misfolding cyclic amplification“. In: *Journal of Biological Chemistry* 281, pp. 35245–35252 (cit. on p. 22).

Saborio, G. P., B. Permanne, and C. Soto (2001). „Sensitive detection of pathological prion protein by cyclic amplification of protein misfolding“. In: *Nature* 411, pp. 810–813 (cit. on pp. 20, 21, 41).

Saha, S., A. Sharma, and S. Deep (2016). „Differential influence of additives on the various stages of insulin aggregation“. In: *RSC Advances* 6, pp. 28640–28652 (cit. on p. 37).

Saijo, E., B. Ghetti, G. Zanusso, et al. (2017). „Ultrasensitive and selective detection of 3-repeat tau seeding activity in Pick disease brain and cerebrospinal fluid“. In: *Acta Neuropathologica* 133, pp. 751–765 (cit. on p. 26).

Saltiel, A. R. and C. R. Kahn (2001). „Insulin signalling and the regulation of glucose and lipid metabolism“. In: *Nature* 414, pp. 799–806 (cit. on p. 18).

Salvadores, N., M. Shahnawaz, E. Scarpini, F. Tagliavini, and C. Soto (2014). „Detection of misfolded Aβ oligomers for sensitive biochemical diagnosis of Alzheimer's disease". In: *Cell Reports* 7, pp. 261–268 (cit. on pp. 26, 37).

Sano, K., R. Atarashi, K. Satoh, et al. (2017). „Prion-Like Seeding of Misfolded α-Synuclein in the Brains of Dementia with Lewy Body Patients in RT-QUIC". In: *Molecular Neurobiology*, pp. 1–15 (cit. on pp. 10, 26, 93, 95, 97).

Serpell, L. (2014). „Amyloid structure". In: *Essays in Biochemistry* 56, pp. 1–10 (cit. on p. 2).

Shahnawaz, M., T. Tokuda, M. Waragai, et al. (2017). „Development of a biochemical diagnosis of Parkinson disease by detection of α-synuclein misfolded aggregates in cerebrospinal fluid". In: *Jama Neurology* 74, pp. 163–172 (cit. on pp. 10, 26, 37, 93, 95, 97).

Shi, S., G. Mitteregger-Kretzschmar, A. Giese, and H. A. Kretzschmar (2013). „Establishing quantitative real-time quaking-induced conversion (qRT-QuIC) for highly sensitive detection and quantification of PrPSc in prion-infected tissues". In: *Acta Neuropathologica Communications* 1, actaneurocomms44 (cit. on pp. 29, 42).

Sipe, J. D., M. D. Benson, J. N. Buxbaum, et al. (2016). „Amyloid fibril proteins and amyloidosis: chemical identification and clinical classification International Society of Amyloidosis 2016 Nomenclature Guidelines". In: *Amyloid* 23, pp. 209–213 (cit. on p. 7).

Situma, C., M. Hashimoto, and S. A. Soper (2006). „Merging microfluidics with microarray-based bioassays". In: *Biomolecular Engineering* 23, pp. 213–231 (cit. on p. 27).

Sonati, T., R. R. Reimann, J. Falsig, et al. (2013). „The toxicity of antiprion antibodies is mediated by the flexible tail of the prion protein". In: *Nature* 501, pp. 102–106 (cit. on p. 63).

Soto, C., L. Anderes, S. Suardi, et al. (2005). „Pre-symptomatic detection of prions by cyclic amplification of protein misfolding". In: *FEBS Letters* 579, pp. 638–642 (cit. on p. 21).

Souza, J. M., B. I. Giasson, V. M.-Y. Lee, and H. Ischiropoulos (2000). „Chaperone-like activity of synucleins". In: *FEBS Letters* 474, pp. 116–119 (cit. on p. 15).

Sparkes, R. S., M. Simon, V. H. Cohn, et al. (1986). „Assignment of the human and mouse prion protein genes to homologous chromosomes". In: *Proceedings of the National Academy of Sciences* 83, pp. 7358–7362 (cit. on p. 12).

Spillantini, M. G., A. Divane, and M. Goedert (1995). „Assignment of human α-synuclein (SNCA) and β-synuclein (SNCB) genes to chromosomes 4q21 and 5q35". In: *Genomics* 27, pp. 379–381 (cit. on p. 14).

Spillantini, M. G., R. A. Crowther, R. Jakes, et al. (1998). „Filamentous α-synuclein inclusions link multiple system atrophy with Parkinson's disease and dementia with Lewy bodies". In: *Neuroscience Letters* 251, pp. 205–208 (cit. on p. 10).

Steiner, D. F., D. Cunningham, L. Spigelman, and B. Aten (1967). „Insulin biosynthesis: evidence for a precursor". In: *Science* 157, pp. 697–700 (cit. on p. 17).

Steinhoff, B. J., I. Zerr, M. Glatting, et al. (2004). „Diagnostic value of periodic complexes in Creutzfeldt–Jakob disease". In: *Annals of Neurology* 56, pp. 702–708 (cit. on p. 9).

Stokholm, M. G., E. H. Danielsen, S. J. Hamilton-Dutoit, and P. Borghammer (2016). „Pathological α-synuclein in gastrointestinal tissues from prodromal Parkinson disease patients". In: *Annals of Neurology* 79, pp. 940–949 (cit. on p. 95).

Störkel, S, H. Schneider, H Müntefering, and S Kashiwagi (1983). „Iatrogenic, insulin-dependent, local amyloidosis.“ In: *Laboratory Investigation; a Journal of Technical Methods and Pathology* 48, pp. 108–111 (cit. on p. 11).

Takatsuki, H., K. Satoh, K. Sano, et al. (2015). „Rapid and quantitative assay of amyloid-seeding activity in human brains affected with prion diseases“. In: *PLoS One* 10, e0126930 (cit. on pp. 29, 42, 66).

Tanaka, M., S. R. Collins, B. H. Toyama, and J. S. Weissman (2006). „The physical basis of how prion conformations determine strain phenotypes“. In: *Nature* 442, pp. 585–589 (cit. on p. 5).

Tateishi, J., T. Tashima, and T. Kitamoto (1991). „Practical methods for chemical inactivation of Creutzfeldt-Jakob disease pathogen“. In: *Microbiology and Immunology* 35, pp. 163–166 (cit. on p. 67).

Tattum, M. H., S. Jones, S. Pal, J. Collinge, and G. S. Jackson (2010). „Discrimination between prion-infected and normal blood samples by protein misfolding cyclic amplification“. In: *Transfusion* 50, pp. 996–1002 (cit. on p. 21).

Taylor, D. (2000). „Inactivation of transmissible degenerative encephalopathy agents: a review“. In: *The Veterinary Journal* 159, pp. 10–17 (cit. on p. 56).

Thomzig, A., K. Wagenführ, M. L. Daus, et al. (2014). „Decontamination of medical devices from pathological amyloid-β-, tau-and α-synuclein aggregates“. In: *Acta Neuropathologica Communications* 2, actaneurocomms151 (cit. on p. 94).

Tolosa, E., G. Wenning, and W. Poewe (2006). „The diagnosis of Parkinson's disease“. In: *The Lancet Neurology* 5, pp. 75–86 (cit. on p. 10).

Uéda, K., H. Fukushima, E. Masliah, et al. (1993). „Molecular cloning of cDNA encoding an unrecognized component of amyloid in Alzheimer disease“. In: *Proceedings of the National Academy of Sciences* 90, pp. 11282–11286 (cit. on p. 14).

Ulmer, T. S., A. Bax, N. B. Cole, and R. L. Nussbaum (2005). „Structure and dynamics of micelle-bound human α-synuclein“. In: *Journal of Biological Chemistry* 280, pp. 9595–9603 (cit. on p. 15).

Ulusoy, A., R. J. Phillips, M. Helwig, et al. (2017). „Brain-to-stomach transfer of α-synuclein via vagal preganglionic projections“. In: *Acta Neuropathologica* 133, pp. 381–393 (cit. on p. 95).

Usov, I. and R. Mezzenga (2015). „FiberApp: an open-source software for tracking and analyzing polymers, filaments, biomacromolecules, and fibrous objects“. In: *Macromolecules* 48, pp. 1269–1280 (cit. on p. 44).

Virchow, R. (1854). „Ueber eine im Gehirn und Rückenmark des Menschen aufgefundene Substanz mit der chemischen Reaction der Cellulose“. In: *Virchows Archiv* 6, pp. 135–138 (cit. on p. 1).

Volpicelli-Daley, L. A., K. C. Luk, and V. M. Lee (2014). „Addition of exogenous α-synuclein preformed fibrils to primary neuronal cultures to seed recruitment of endogenous α-synuclein to Lewy body and Lewy neurite–like aggregates“. In: *Nature Protocols* 9, pp. 2135–2146 (cit. on pp. 74, 75, 99).

Wang, Y., B. Vaidya, H. D. Farquar, et al. (2003). „Microarrays assembled in microfluidic chips fabricated from poly (methyl methacrylate) for the detection of low-abundant DNA mutations“. In: *Analytical Chemistry* 75, pp. 1130–1140 (cit. on p. 27).

Waugh, D. F. (1944). „The linkage of corpuscular protein molecules. I. A fibrous modification of insulin“. In: *Journal of the American Chemical Society* 66, pp. 663–663 (cit. on pp. 17, 42).

– (1946). „A fibrous modification of insulin. I. The heat precipitate of insulin“. In: *Journal of the American Chemical Society* 68, pp. 247–250 (cit. on pp. 17, 42).

Wegner, A. (1982). „Spontaneous fragmentation of actin filaments in physiological conditions“. In: *Nature* 296, pp. 266–267 (cit. on p. 4).

Whitesides, G. M. (2006). „The origins and the future of microfluidics“. In: *Nature* 442, pp. 368–373 (cit. on p. 27).

WHO (1998). „Report of a WHO consultation on global surveillance, diagnosis and therapy of human transmissible spongiform encephalopathies“. In: *WHO, Geneva*, pp. 8–11 (cit. on p. 9).

– (2013). „Diabetes fact sheet No. 312“. In: *WHO, Geneva* (cit. on p. 18).

Wilham, J. M., C. D. Orrú, R. A. Bessen, et al. (2010). „Rapid end-point quantitation of prion seeding activity with sensitivity comparable to bioassays“. In: *PLoS Pathogens* 6, e1001217 (cit. on pp. 20, 23, 41, 42, 70).

Will, R. G. (2003). „Acquired prion disease: iatrogenic CJD, variant CJD, kuru“. In: *British Medical Bulletin* 66, pp. 255–265 (cit. on p. 8).

Woerman, A. L., J. Stöhr, A. Aoyagi, et al. (2015). „Propagation of prions causing synucleinopathies in cultured cells“. In: *Proceedings of the National Academy of Sciences* 112, pp. 4949–4958 (cit. on p. 88).

Woerman, A. L., S. A. Kazmi, S. Patel, et al. (2017). „MSA prions exhibit remarkable stability and resistance to inactivation“. In: *Acta Neuropathologica*, pp. 1–15 (cit. on p. 93).

Wulf, M.-A., A. Senatore, and A. Aguzzi (2017). „The biological function of the cellular prion protein: an update“. In: *BMC Biology* 15, bmcbiol34 (cit. on p. 12).

Zahn, R., A. Liu, T. Lührs, et al. (2000). „NMR solution structure of the human prion protein“. In: *Proceedings of the National Academy of Sciences* 97, pp. 145–150 (cit. on pp. 12, 13).

Zerr, I., K Kallenberg, D. Summers, et al. (2009). „Updated clinical diagnostic criteria for sporadic Creutzfeldt-Jakob disease“. In: *Brain* 132, pp. 2659–2668 (cit. on pp. 9, 55).

Zhu, Y., L.-N. Zhu, R. Guo, et al. (2014). „Nanoliter-scale protein crystallization and screening with a microfluidic droplet robot“. In: *Scientific Reports* 4, srep5046 (cit. on p. 27).

Zobeley, E., E. Flechsig, A. Cozzio, M. Enari, and C. Weissmann (1999). „Infectivity of scrapie prions bound to a stainless steel surface.“ In: *Molecular Medicine* 5, pp. 240–243 (cit. on pp. 56, 89).

Acknowledgements

During the last four years, I have met many people along the way. Every one of them has inspired me in some way, and I am very grateful for that.

First and foremost, I would like to express my gratitude to my thesis supervisors Prof. Adriano Aguzzi and PD Dr. Simone Hornemann for giving me the opportunity to conduct this research under their supervision. I am grateful for their scientific advice, inspiration and support, as well as for their confidence in me and the freedom they gave me to develop this research.

I extend my gratitude to the members of my PhD committee Prof. Ben Schuler and Prof. Tuomas Knowles for their guidance, constructive criticism and support throughout my studies.

I would like to thank the current and former members of the Institute of Neuropathology for their generous help, stimulating discussions, and for creating a pleasant and positive working atmosphere: Kristina Airich, Merve Avar, Alexandra Bentrup, Manfredi Carta, Dr. Andra Chincisan, Dr. Alessandro Crimi, Valeria Eckhardt, Marc Emmenegger, Dr. Katrin Frauenknecht, Dr. Karl Frontzek, Daniel Heinzer, Anna Henzi, Dr. Uli Herrmann, Dr. Eleanna Kara, Daniel Kirschenbaum, Dr. Alexander Küffer, Dr. Asvin Lakkaraju, Dr. Yingjun Liu, Marco Losa, Andreia Magalhaes, Dr. Mario Nuvolone, Daniel Pease, Dr. Regina Reimann, Dr. Elisabeth Rushing, Dr. Claudia Scheckel, Carmen Schiavi, Dr. Assunta Senatore, Dr. Tiziana Sonati, Dr. Silvia Sorce, Flavio Vasella, Marie-Angela Wulf, Dr. Caihong Zhu. It has been a great pleasure to work with every one of them.
I thank Rita Moos, Lisa Caflisch, Petra Schwarz, Cinzia Tiberi, Yvonne Fuhrer, Musa Hadzere and the technical staff for technical help; as well as Isabella Gianella, Meike Nau Lüber and Jacqueline Wiedler for administrative help.

Furthermore, I greatly appreciate the support received through the collaboration with the groups of Prof. Tuomas Knowles and Prof. Christopher Dobson at the University of Cambridge. In particular, I would like to thank Dr. Georg Meisl, Dr. Maria Andreasen, Itzel Condado Morales and Dr. Christopher Taylor.
I would also like to thank my collaborators at ETH Zurich, Prof. Raffaele Mezzenga and his coworkers Dr. Jozef Adamcik, Dr. Sreenath Bolisetty and Dr. Antoni Sanchez-Ferrer.
I would like to thank Prof. Dr. med. Christian Baumann and Dr. med. Evdokia Efthymiou from the Institute of Neurology, University Hospital Zurich for collaborating and providing α-synucleinopathy patient samples.
Many thanks to Prof. Kelvin Luk (Perelman School of Medicine, University of Pennsylvania) for providing the plasmid harbouring the α-synuclein gene, anti-α-synuclein antibodies and for helpful discussions.

I would like to acknowledge the institutions that provided financial support for my PhD thesis: University of Zurich (career development award 'Forschungskredit Candoc'), European Molecular Biology Organization (EMBO Short-Term Fellowship).

And finally, I owe special thanks to my boyfriend and my family, for their endless support, encouragement and confidence in me. This accomplishment would not have been possible without them.

Curriculum Vitae

Personal Information

Family Name	**Pfammatter**
Given Names	**Manuela Christine**
Date of Birth	**09.01.1990**
Place of Origin	**Naters VS**

Education and Academic Degrees

04/2014 – 04/2018 **Dr. sc. nat. UZH in Molecular Life Sciences**
Institute of Neuropathology, University Hospital Zurich

Thesis: 'Amyloid Amplification Assays for the Sensitive Detection of Protein Aggregates'
Supervision: Prof. Adriano Aguzzi

09/2012 – 02/2014 **Master of Science ETH in Structural Biology and Biophysics**
Institute of Molecular Biology and Biophysics, ETH Zurich
Department of Chemistry, University of Cambridge (UK)

Thesis: 'Biophysical Characterisation of the Stability and Specificity of the Semliki Forest Virus Capsid Protein'
Supervision: Prof. Rudi Glockshuber

09/2009 – 05/2012 **Bachelor of Science ETH in Biology**
Department of Biology, ETH Zurich

08/2004 – 06/2009 **Gymnasiale Maturität**
Kollegium Spiritus Sanctus, Brig
major subject music, minor subject biology

Honours & Grants

2016 Forschungskredit Grant, University of Zurich
2016 EMBO Short-Term Fellowship, EMBO
2013 Erasmus Scholarship, Erasmus Foundation
2012 Finalist Excellence Scholarship Program (ESOP), ETH Zurich
2010 Top 10% Ranking of all biology 1^{st} year examinations, ETH Zurich

Publications

Gang H, Galvagnion C, Meisl G, Muller T, **Pfammatter M**, Buell AK, Levin A, Dobson CM, Mu BZ, and Knowles TPJ. A microfluidic diffusion platform for characterizing the size of lipid vesicles and the thermodynamics of protein-lipid interactions. *Analytical Chemistry*, 2018.

Pfammatter M, Andreasen M, Meisl G, Taylor CG, Adamcik J, Bolisetty S, Sanchez-Ferrer A, Klenerman D, Dobson CM, Mezzenga R, Knowles TPJ, Aguzzi A, and Hornemann S. Absolute Quantification of Amyloid Propagons by Digital Microfluidics. *Analytical Chemistry*, 2017.

Meisl G, Rajah L, Cohen SAI, **Pfammatter M**, Saric A, Hellstrand E, Buell AK, Aguzzi A, Linse S, Vendruscolo M, Dobson CM, and Knowles TPJ. Scaling behaviour and rate-determining steps in filamentous self-assembly. *Chemical Science*, 2017.

Frontzek K, **Pfammatter M**, Sorce S, Senatore A, Schwarz P, Moos R, Frauenknecht K, Hornemann S, and Aguzzi A. Neurotoxic antibodies against the prion protein do not trigger prion replication. *PLOS One*, 2016.